

## PUBLISHER :



### Address of Publisher & Editor's Office :

GDAŃSK UNIVERSITY  
OF TECHNOLOGY

Faculty  
of Ocean Engineering  
& Ship Technology

ul. Narutowicza 11/12  
80-952 Gdańsk, POLAND  
tel.: +48 58 347 13 66  
fax : +48 58 341 13 66  
e-mail : office.pmr@pg.gda.pl

### Account number :

**BANK ZACHODNI WBK S.A.**

I Oddział w Gdańsku  
41 1090 1098 0000 0000 0901 5569

### Editorial Staff :

**Tadeusz Borzęcki** Editor in Chief

e-mail : tadbtor@pg.gda.pl

**Przemysław Wierzchowski** Scientific Editor

e-mail : e.wierzchowski@chello.pl

**Jan Michalski** Editor for review matters

e-mail : janmi@pg.gda.pl

**Aleksander Kniat** Editor for international relations

e-mail : olek@pg.gda.pl

**Kazimierz Kempa** Technical Editor

e-mail : kkempa@pg.gda.pl

**Piotr Bzura** Managing Editor

e-mail : pbzura@pg.gda.pl

**Cezary Spigarski** Computer Design

e-mail : biuro@oficynamorska.pl

### Domestic price :

single issue : 20 zł

### Prices for abroad :

single issue :

- in Europe EURO 15

- overseas US\$ 20

ISSN 1233-2585



**POLISH  
MARITIME  
RESEARCH**

*in internet*

[www.bg.pg.gda.pl/pmr/pmr.php](http://www.bg.pg.gda.pl/pmr/pmr.php)



## POLISH MARITIME RESEARCH

No 3(70) 2011 Vol 18

## CONTENTS

- 3 **ZBIGNIEW SEKULSKI**  
*Multi-objective optimization of high speed vehicle-passenger catamaran by genetic algorithm. Part II*
- 31 **JERZY GIRTLER**  
*A method for evaluating theoretical and real operation of diesel engines in energy conversion formulation taking into account their operating indices*
- 37 **ZBIGNIEW KORCZEWSKI**  
*Exhaust gas temperature measurements in diagnostic examination of naval gas turbine engines. Part II*
- 43 **WOJCIECH HOMIK**  
*Damping of torsional vibrations of ship engine crankshafts – general selection methods of viscous vibration damper*
- 48 **ANDRZEJ BŁASZCZYK, JERZY GŁUCH, ANDRZEJ GARDZILEWICZ**  
*Operating and economic conditions of cooling water control for marine steam turbine condensers*
- 55 **JAN KORALEWSKI**  
*Influence of hydraulic oil viscosity on the volumetric losses in a variable capacity piston pump*
- 66 **H. MEHDIGHOLI, H. MIRZAEI RAFSANJANI, BEHZAD, MEHDI**  
*Estimation of rolling bearing life with damage curve approach*

# Editorial

---

POLISH MARITIME RESEARCH is a scientific journal of worldwide circulation. The journal appears as a quarterly four times a year. The first issue of it was published in September 1994. Its main aim is to present original, innovative scientific ideas and Research & Development achievements in the field of :

## **Engineering, Computing & Technology, Mechanical Engineering,**

which could find applications in the broad domain of maritime economy. Hence there are published papers which concern methods of the designing, manufacturing and operating processes of such technical objects and devices as : ships, port equipment, ocean engineering units, underwater vehicles and equipment as well as harbour facilities, with accounting for marine environment protection.

The Editors of POLISH MARITIME RESEARCH make also efforts to present problems dealing with education of engineers and scientific and teaching personnel. As a rule, the basic papers are supplemented by information on conferences , important scientific events as well as cooperation in carrying out international scientific research projects.

## Scientific Board

---

Chairman : Prof. **JERZY GIRTLE**R - Gdańsk University of Technology, Poland

Vice-chairman : Prof. **ANTONI JANKOWSKI** - Institute of Aeronautics, Poland

Vice-chairman : Prof. **MIROSLAW L. WYSZYŃSKI** - University of Birmingham, United Kingdom

---

Dr **POUL ANDERSEN**  
Technical University  
of Denmark  
Denmark

Prof. **STANISŁAW GUCMA**  
Maritime University of Szczecin  
Poland

Dr **YOSHIO SATO**  
National Traffic Safety  
and Environment Laboratory  
Japan

Dr **MEHMET ATLAR**  
University of Newcastle  
United Kingdom

Prof. **ANTONI ISKRA**  
Poznań University  
of Technology  
Poland

Prof. **KLAUS SCHIER**  
University of Applied Sciences  
Germany

Prof. **GÖRAN BARK**  
Chalmers University  
of Technology  
Sweden

Prof. **JAN KICIŃSKI**  
Institute of Fluid-Flow Machinery  
of PASci  
Poland

Prof. **FREDERICK STERN**  
University of Iowa,  
IA, USA

Prof. **SERGEY BARSUKOV**  
Army Institute of Odessa  
Ukraine

Prof. **ZYGMUNT KITOWSKI**  
Naval University  
Poland

Prof. **JÓZEF SZALA**  
Bydgoszcz University  
of Technology and Agriculture  
Poland

Prof. **MUSTAFA BAYHAN**  
Süleyman Demirel University  
Turkey

Prof. **JAN KULCZYK**  
Wrocław University of Technology  
Poland

Prof. **TADEUSZ SZELANGIEWICZ**  
Technical University  
of Szczecin  
Poland

Prof. **MAREK DZIDA**  
Gdańsk University  
of Technology  
Poland

Prof. **NICOS LADOMMATOS**  
University College London  
United Kingdom

Prof. **WITALIJ SZCZAGIN**  
State Technical University  
of Kaliningrad  
Russia

Prof. **ODD M. FALTINSEN**  
Norwegian University  
of Science and Technology  
Norway

Prof. **JÓZEF LISOWSKI**  
Gdynia Maritime University  
Poland

Prof. **BORIS TIKHOMIROV**  
State Marine University  
of St. Petersburg  
Russia

Prof. **PATRICK V. FARRELL**  
University of Wisconsin  
Madison, WI  
USA

Prof. **JERZY MATUSIAK**  
Helsinki University  
of Technology  
Finland

Prof. **DRACOS VASSALOS**  
University of Glasgow  
and Strathclyde  
United Kingdom

Prof. **WOLFGANG FRICKE**  
Technical University  
Hamburg-Harburg  
Germany

Prof. **EUGEN NEGRUS**  
University of Bucharest  
Romania

Prof. **YASUHIKO OHTA**  
Nagoya Institute of Technology  
Japan

# Multi-objective optimization of high speed vehicle-passenger catamaran by genetic algorithm

## Part II Computational simulations

Zbigniew Sekulski, Ph. D.  
West Pomeranian University of Technology in Szczecin

### ABSTRACT



*Real ship structural design problems are usually characterized by presence of many conflicting objectives. Simultaneously, a complete definition of the optimum structural design requires a formulation of size-topology-shape-material optimization task unifying the optimization problems of the four areas and giving an effective solution of the problem. So far, a significant progress towards the solution of the problem has not been obtained. An objective of the present paper was to develop an evolutionary algorithm for multi-objective optimization of structural elements of large spatial sections of ships. Selected elements of the multi-criteria optimization theory have been presented in detail. Methods for solution of the multi-criteria optimization problems have been discussed with the focus on the evolutionary optimization algorithms. In the paper an evolutionary algorithm where selection takes place based on the aggregated objective function combined with domination attributes as well as distance to the asymptotic solution, is proposed and applied to solve the problem of optimizing structural elements with respect to their weight and surface area on a high speed vehicle-passenger catamaran structure, with several design variables, such as plate thickness, scantlings of longitudinal stiffeners and transverse frames, and spacing between longitudinal and transversal members, taken into account. Details of the computational models were at the level typical for conceptual design. Scantlings were analyzed by using selected rules of a classification society. The results of numerical experiments with the use of the developed algorithm, are presented. They show that the proposed genetic algorithm can be an efficient tool for multi-objective optimization of ship structures.*

*The paper is published in three parts: Part I: Theoretical background on evolutionary multi-objective optimization, Part II: Computational investigations, and Part III: Analysis of the results.*

**Keywords:** ship structure; multi-objective optimization; evolutionary algorithm; genetic algorithm; Pareto domination, set of non-dominated solutions

### SEAGOING SHIP HULL STRUCTURE MODEL FOR MULTI-OBJECTIVE OPTIMIZATION

#### *General*

Effectiveness of the developed evolutionary algorithm for the multi-objective optimization of seagoing ship structures has been verified by solving the multi-objective optimization problem for the midship segment of the passenger-car catamaran ferry, based on the Austal Auto Express 82 design developed by Austal [HANSA (1997)], [Significant Ships (1997)], Figure 14. Models developed for the multi-objective optimization are: (1) ship structural model, (2) optimization model and (3) genetic model.



**Fig. 14.** The Auto Express 82 high speed vehicle-passenger catamaran "Boomerang"

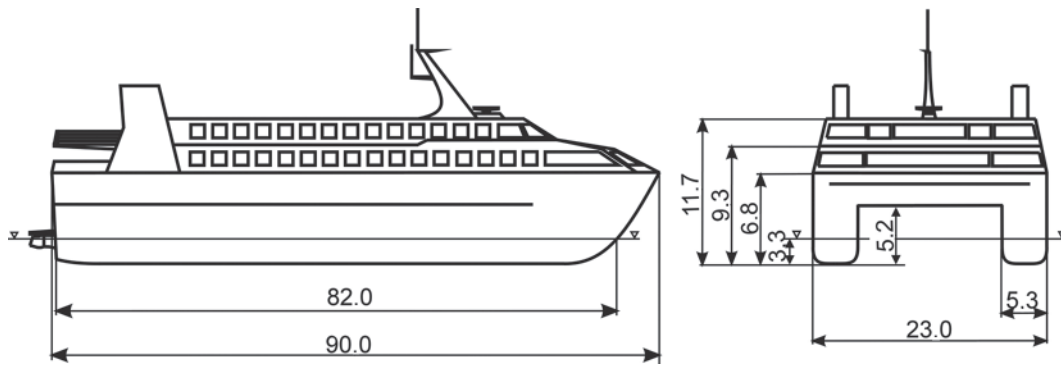


Fig. 15. Main particulars of the Auto Express 82 high-speed vehicle-passenger catamaran

### Structural model of the ship hull structure

Main particulars of the Austal Auto Express 82 vessel are given in Fig. 15. The general arrangement of the ship and her corresponding cross- and longitudinal sections are shown in Fig. 16. For seagoing ships structural design in its initial stage concerns the cylindrical and prismatic zone amidships. For this reason the analysis of the midship block-section (17.5 x 23.0 x 11.7 m) was assumed. Bulkheads form boundaries of the block in the longitudinal direction. In the block nine structural regions can be distinguished. All regions are longitudinally stiffened with stiffeners; their spacing being different in each structural region. The transverse web frame spacing is common for all the regions. Both types of spacing, i.e. of stiffeners and transverse frames, are considered the design variables. The transverse bulkheads were disregarded to minimize the number of design variables.

The structural materials are aluminium alloys of the properties given in Tab. 1. The 5083-H111 aluminium alloys are used for plate elements while 6082-T6 aluminium alloys are used for bulb extrusions. The plate thicknesses and the bulb and T-bulb extruded stiffener sections are assumed according to the commercial standards and given in Tab. 2, 3 and 4. The bulb extrusions are used as longitudinal stiffeners while the T-bulb extrusions are used as web frame profiles. Practically, the web frames are produced by welding the elements cut out of the metal sheets. Dimensions of the prefabricated T-bar elements are described by the four following design variables: web height and thickness as well as and flange breadth and thickness. In the case of extruded bulb a single variable is sufficient to identify the profile, its dimensions and geometric properties. It reduces the computational problem and accelerates analysis.

Tab. 1. Properties of structural material – aluminium alloys

No.	Property	Value
1	Yield stress $R_{0.2}$	125 (for 5083-H111 alloy) [N/mm <sup>2</sup> ] 250 (for 6082-T6 alloy) [N/mm <sup>2</sup> ]
2	Young modulus E	70,000 N/mm <sup>2</sup>
3	Poisson ratio $\nu$	0.33
4	Density $\rho$	26.1 kN/m <sup>3</sup>

The strength criteria for calculation of plate thicknesses and section moduli of stiffeners and web frames are taken in accordance to the classification rules [UNITAS (1995)]. It was assumed that bottom, wet deck, outer side and superstructure I and II are subject to the pressure of water depending on the speed and the navigation region. The main deck was loaded by the weight of the trucks transmitted through the tires, the mezzanine deck the – weight of the cars, while the upper deck

– the weight of equipment and passengers. Values of pressure were calculated according to the procedures taken from the classification rules.

In the study a minimum structural weight (volume of structure) and total outer area of structural elements intended for maintenance (cleaning, painting, etc.) were taken as the criteria and introduced to the definition of the objective functions and constraints defined on the basis of the classification rules. When structural weight and surface area are chosen as the objective functions, their values depend only on the geometrical properties of the structure (if structural material is fixed). The assumed optimization task is rather simple but the main objective of the study was to build the computational method, verify the computer code and prove its application to the multi-objective optimization of a ship hull.

Tab. 2. Thickness of plates

No.	Thickness t [mm]
1	3.00
2	4.00
3	5.00
4	6.00
5	7.00
6	8.00
7	10.00
8	12.00
9	15.00
10	20.00
11	30.00
12	40.00
13	50.00
14	60.00

Tab. 3. Dimensions of bulb extrusions

No.	Dimensions (h, b, s, s <sub>1</sub> ) <sup>1)</sup> [mm]	Cross-sectional area [cm <sup>2</sup> ]
1	80 x 19 x 5 x 7.5	5.05
2	100 x 20.5 x 5 x 7.5	6.16
3	120 x 25 x 8 x 12	11.64
4	140 x 27 x 8 x 12	13.64
5	150 x 25 x 6 x 9	10.71
6	160 x 29 x 7 x 10.5	13.51
7	200 x 38 x 10 x 15	24.20

<sup>1)</sup> h – cross-section height; b - flange width; s - web thickness; s<sub>1</sub> - flange thickness.

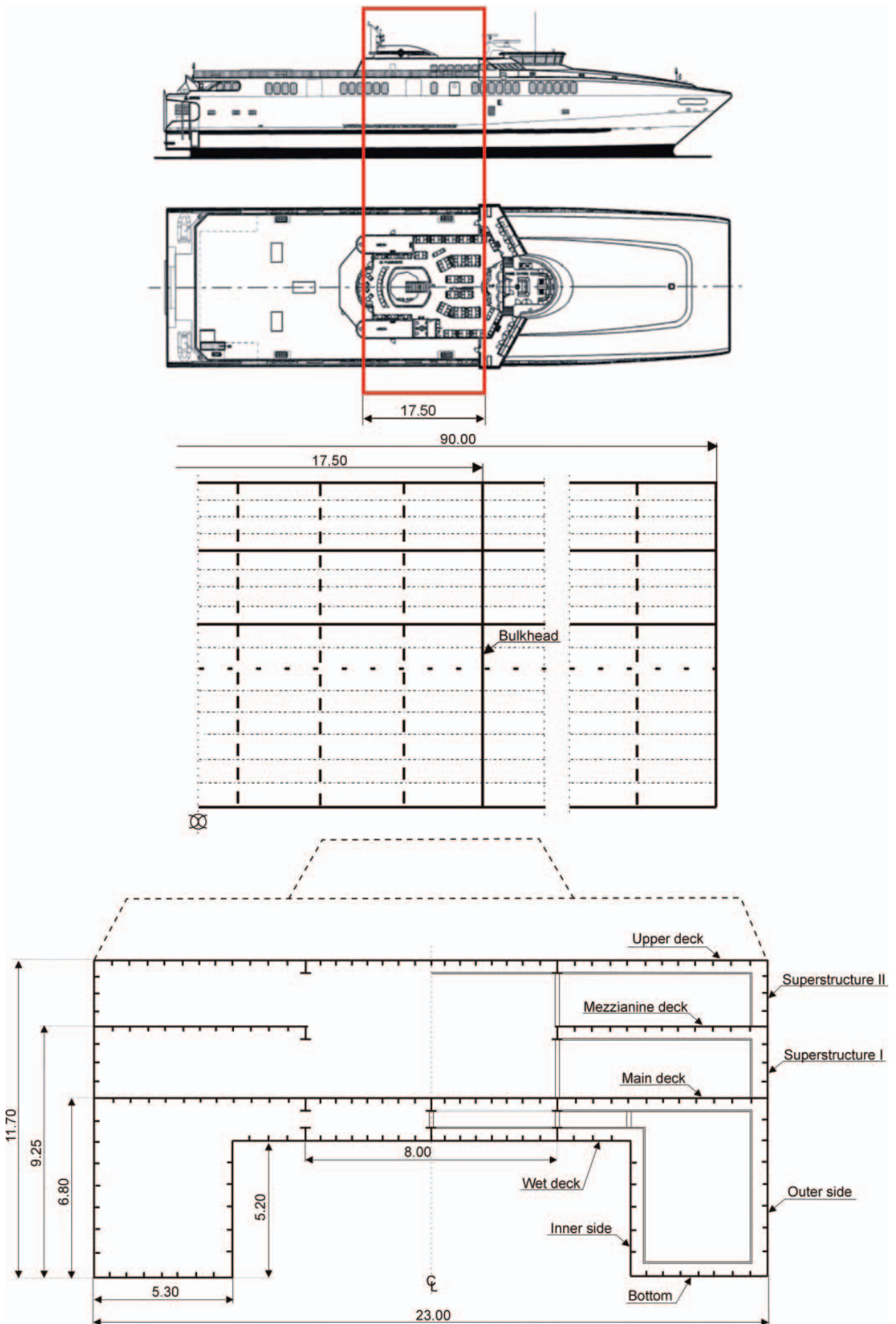


Fig. 16. Assumed model of craft structure – midship block-section, frame system and structural regions

Tab. 4. Dimensions of T-bulb extrusions

No.	Dimensions (h, b, s, s <sub>1</sub> ) <sup>2)</sup> [mm]	Cross-sectional area [cm <sup>2</sup> ]
1	200 x 100 x 8 x 15	29.80
2	200 x 140 x 8 x 5	35.80
3	200 x 60 x 10 x 12	22.50
4	200 x 50 x 8 x 9.5	21.04
5	210 x 50 x 5 x 16	14.78
6	216 x 140 x 7.6 x 8	37.60
7	220 x 80 x 5 x 8	17.00
8	230 x 80 x 10 x 8	28.60
9	230 x 80 x 5.8 x 8	19.28
10	235 x 170 x 8 x 10	35.00
11	240 x 140 x 6 x 10	27.80
12	260 x 90 x 5 x 9.5	21.08
13	275 x 150 x 9 x 12	41.67
14	280 x 100 x 5 x 8	21.60
15	280 x 100 x 8 x 10	31.60
16	300 x 60 x 15 x 15	51.75
17	310 x 100 x 7 x 16	36.58
18	310 x 123 x 5 x 8	24.94
19	350 x 100 x 8 x 10	37.20
20	350 x 100 x 5 x 8	25.10
21	390 x 150 x 6 x 8	34.92
22	390 x 150 x 6 x 12	40.68
23	400 x 140 x 5 x 8	30.80
24	410 x 100 x 6 x 8	32.12
25	420 x 15 x 5 x 10	35.10
26	420 x 15 x 8 x 10	47.80
27	450 x 100 x 9 x 10	49.60
28	450 x 150 x 10 x 12	61.80

<sup>2)</sup> h – cross-section height, b - flange width,  
s - web thickness, s<sub>1</sub> - flange thickness.

### Multi-objective optimization model of the ship hull structure

In the most general formulation to solve ship structural multi-objective optimization problem means to find a combination of values of the vector of design variables  $\mathbf{x} = [x_1 \ x_2 \ \dots \ x_n]^T$  defining the structure which optimizes vector of the objective function  $\mathbf{f}(\mathbf{x})$ . The design variables should also meet complex set of constraints imposed on their values. The constraints formulate the set of feasible solutions. It is assumed that all functions of the multi-objective optimization problem are real and a number of constraints is finite. When considering computational costs an additional requirement may also be formulated that they should be as small as possible.

For the multi-objective optimization problem a substitute scalar objective function may be formulated, on the basis of components of vector objective function, in the following form:

$$F(\mathbf{x}) = F(f_1(\mathbf{x}), f_2(\mathbf{x})) = w_1 f_1(\mathbf{x}) + w_2 f_2(\mathbf{x}) \rightarrow \min! \quad (15)$$

where:

- $f_1(\mathbf{x})$  – a structural weight of midship block-section taken to optimization,

- $f_2(\mathbf{x})$  – an area of the outer surface of structural members subjected to cleaning and painting operations (surface area for maintenance) in the section,
- $w_1$  and  $w_2$  – weight coefficients used for partial optimization criteria.

Taking into consideration the operational loads as well as the constraints imposed on the design variables especially those resulting from conditions of local and global strength formulated in the approved rules of a classification society the substitute scalar objective function can be expressed as augmented objective function of unconstrained minimization problem:

$$\begin{aligned} f(\mathbf{x}) &= F(\mathbf{x}) + \sum_{k=1}^{n_c} w_k P_k(\mathbf{x}) = \\ &= w_1 f_1(\mathbf{x}) + w_2 f_2(\mathbf{x}) + \sum_{k=1}^{n_c} w_k P_k(\mathbf{x}) \rightarrow \min! \end{aligned} \quad (16)$$

where all symbols are described before.

The augmented objective function expression (Eq. 16) has been extended by components corresponding to dominance attributes and distance to the asymptotic solution. As a consequence the following form of combined objective function has been adopted:

$$\begin{aligned} f(\mathbf{x}) &= w_1 u_1(\mathbf{x}) + w_2 u_2(\mathbf{x}) + \\ &w_{\text{rank}} R_{\text{fi}}(\mathbf{x}) + w_{\text{count}} C_{\text{fi}}(\mathbf{x}) + \\ &+ w_{\text{distance}} [1 - d_{\text{fi}}(\mathbf{x})] + \sum_{k=1}^{n_c} w_k P_k(\mathbf{x}) \end{aligned} \quad (17)$$

where:

- $w_1$  and  $w_2$  – weight coefficients used for partial optimization criteria,
- $w_{\text{rank}}$  – dominance rank coefficient,
- $w_{\text{count}}$  – dominance count weight coefficient,
- $w_{\text{distance}}$  – distance from asymptotic solution weight coefficient,
- $u_1$  – utility function for structural weight:

$$u_1(\mathbf{x}) = \left( \frac{f_{1,\text{max}} - f_1(\mathbf{x})}{f_{1,\text{max}}} \right) \rightarrow \max! \quad (18a)$$

- $u_2$  – an utility function for area of the outer surface of structural members subjected to cleaning and painting operations:

$$u_2(\mathbf{x}) = \left( \frac{f_{2,\text{max}} - f_2(\mathbf{x})}{f_{2,\text{max}}} \right) \rightarrow \max! \quad (18b)$$

where:

- $f_1(\mathbf{x})$  – current value of the first optimization criterion,
- $f_{1,\text{max}}$  – maximum value of the first criterion,
- $f_2(\mathbf{x})$  – current value of the second optimization criterion,
- $f_{2,\text{max}}$  – maximum value of the second criterion and all the remaining symbols are as outlined before.

As it has already been stated earlier, three aggregation-based multi-objective evolutionary strategies for taking account of the partial optimization criteria  $f_1(\mathbf{x})$  and  $f_2(\mathbf{x})$  are used in the scalar objective function (Eq. 4) calculation, and therefore also in the fitness function value calculation (Eq. 16):

- selection of variants by using the scalar objective function (Eq. 16) with the values of weight coefficients  $w_1$  and  $w_2$  set by the user ( $w\_strategy = 2$ ),
- selection of variants by using the scalar objective function (Eq. 16) with the values of weight coefficients  $w_1$  and  $w_2$  randomly and independently generated in the range  $[0, 1]$  ( $w\_strategy = 4$ ),
- selection of variants by using the randomly selected single partial optimization criterion  $F(\mathbf{x}) = w_1 f_1(\mathbf{x})$  or  $F(\mathbf{x}) = w_2 f_2(\mathbf{x})$  ( $w\_strategy = 3$ ) which is implemented by the random selection of a single nonzero weight criterion. Additionally, it is also possible to have:
- selection of variants without ( $w_{rank} = 0$ ) or with ( $w_{rank} \neq 0$ ) (Eq. 17) by taking into account the dominance rank of feasible solutions,
- selection of variants without ( $w_{count} = 0$ ) or with ( $w_{count} \neq 0$ ) (Eq. 17) by taking into account the dominance count of feasible solutions,
- selection of variants without ( $w_{distance} = 0$ ) or with ( $w_{distance} \neq 0$ ) (Eq. 17) taking into account the distance of feasible solutions to the asymptotic solution.

In the present formulation a set of 37 design variables is applied, cf. Tab. 5 and Fig. 17. Introduction of the design variable representing the number of transverse frames in a considered section:  $x_4$ , and numbers of longitudinal stiffeners in the regions:  $x_5, x_9, x_{13}, x_{17}, x_{21}, x_{25}, x_{29}, x_{33}, x_{37}$ , enables to perform simultaneous optimization of both topology and scantlings within the topology-scantling optimization model.

Tab. 5. Simplified specification of bit representation of design variables

No. i	Symbol $x_i$	Item	Substring length (no of bits)	Value	
				Lower limit $x_{i,min}$	Upper limit $x_{i,max}$
1	$x_1$	serial No. of mezzanine deck plate	4	1	10
2	$x_2$	serial No. of mezzanine deck bulb	3	1	7
3	$x_3$	serial No. of mezzanine deck T-bulb	4	42	52
4	$x_4$	number of web frames	3	10	16
5	$x_5$	number of mezzanine deck stiffeners	4	25	40
6	$x_6$	serial No. of superstructure I plate	4	1	10
7	$x_7$	serial No. of superstructure I bulb	3	1	7
8	$x_8$	serial No. of superstructure I T-bulb	4	42	52
9	$x_9$	number of superstructure I stiffeners	3	4	11
10	$x_{10}$	serial No. of inner side plate	4	1	10
11	$x_{11}$	serial No. of inner side bulb	3	1	7
12	$x_{12}$	serial No. of inner side T-bulb	4	42	52
13	$x_{13}$	number of inner side stiffeners	3	18	25
14	$x_{14}$	serial No. of bottom plate	4	1	12
15	$x_{15}$	serial No. of bottom bulb	3	1	7
16	$x_{16}$	serial No. of bottom T-bulb	4	42	52
17	$x_{17}$	number of bottom stiffeners	4	15	25
18	$x_{18}$	serial No. of outer side plate	4	1	12
19	$x_{19}$	serial No. of outer side bulb	3	1	7
20	$x_{20}$	serial No. of outer side T-bulb	4	42	52
21	$x_{21}$	number of outer side stiffeners	4	18	33
22	$x_{22}$	serial No. of wet deck plate	4	1	12
23	$x_{23}$	serial No. of wet deck bulb	3	1	7
24	$x_{24}$	serial No. of wet deck T-bulb	4	42	52
25	$x_{25}$	number of wet deck stiffeners	4	25	40
26	$x_{26}$	serial No. of main deck plate	4	2	12
27	$x_{27}$	serial No. of main deck bulb	3	1	7
28	$x_{28}$	serial No. of main deck T-bulb	4	42	52
29	$x_{29}$	number of main deck stiffeners	4	25	40
30	$x_{30}$	serial No. of superstructure II plate	4	1	10
31	$x_{31}$	serial No. of superstructure II bulb	3	1	7
32	$x_{32}$	serial No. of superstructure II T-bulb	4	42	52
33	$x_{33}$	number of superstructure II stiffeners	3	4	11
34	$x_{34}$	serial No. of upper deck plate	4	1	10
35	$x_{35}$	serial No. of upper deck bulb	3	1	7
36	$x_{36}$	serial No. of upper deck T-bulb	4	42	52
37	$x_{37}$	number of upper deck stiffeners	4	25	40
Multivariable string length (chromosome length)			135		

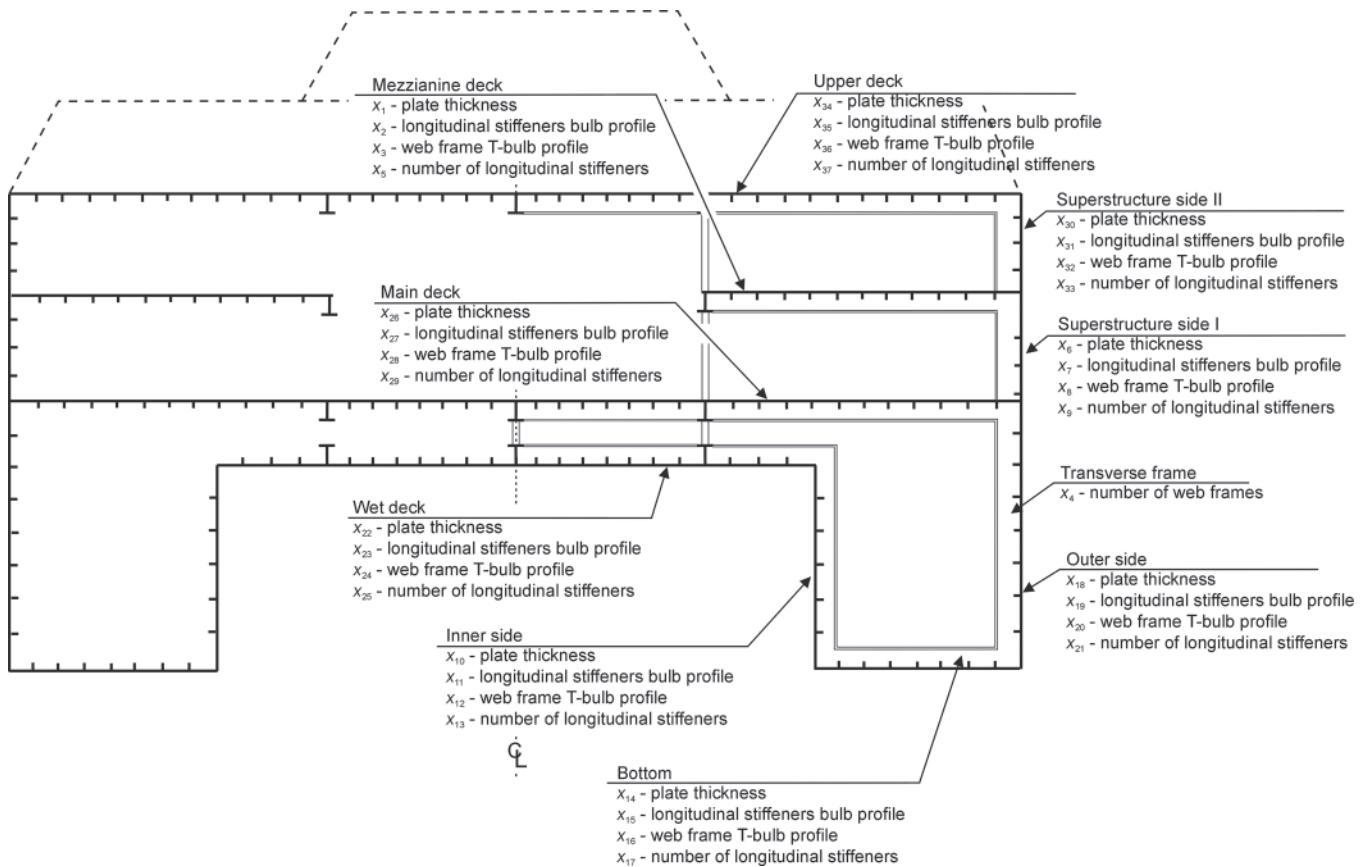


Fig. 17. Assumed model of craft – specification of design variables

Numbers of stiffeners and transverse web frames, varying throughout the processes of optimization, determine corresponding spacings. Scantlings and weights of the structural elements: plating, stiffeners and frames are directly depending on the stiffeners and frames spacings – topological properties of the structure.

When optimizing the structural topology of the ship, a difficult dilemma is to be solved concerning a relation between the number of structural elements in longitudinal and transverse directions, and their dimensions, influencing the structural weight. And, should be also considered constraints related to the manufacturing process and functional requirements of the ship, e.g. transportation corridors, container supporting seats on the container ships (usually realized by longitudinal girders and floors in the double bottom) or positioning supports on the girders in the distance enabling entry of cars on ro-ro vessels.

The behaviour constraints, ensuring that the designed structure is on the safe side, were formulated for each region according to the classification rules [UNITAS (1995)] constituting a part of the set of inequality constraints  $g_j(\mathbf{x})$ :

- the required plate thicknesses  $t_{j,rule}$ , based on the permissible bending stress:

$$t_j - t_{j,rule} \geq 0 \quad (19)$$

where:

$t_j$  – actual value of plate thickness in j-th region,

- the required section moduli of stiffeners  $Z_{s,j,rule}$ :

$$Z_{s,j} - Z_{s,j,rule} \geq 0 \quad (20)$$

where:

$Z_{s,j}$  – actual value of the section modulus of stiffeners in j-th region,

- the required section moduli of web frames  $Z_{f,j,rule}$ :

$$Z_{f,j} - Z_{f,j,rule} \geq 0 \quad (21)$$

where:

$Z_{f,j}$  – actual value of the section modulus of web frames in j-th region,

- the required shear areas of stiffeners  $A_{t,s,j,rule}$ :

$$A_{t,s,j} - A_{t,s,j,rule} \geq 0 \quad (22)$$

where:

$A_{t,s,j}$  – actual value of shear area of stiffeners in j-th region,

- the required shear areas of web frames  $A_{t,f,j,rule}$ :

$$A_{t,f,j} - A_{t,f,j,rule} \geq 0 \quad (23)$$

where:

$A_{t,f,j}$  – actual value of the shear area of web frames in j-th region.

The side constraints  $h_k(\mathbf{x})$ , mathematically defined as equilibrium constraints, for design variables are given in Tab. 5. They correspond to the limitations of the range of the profile set. Some of them are formulated according to the author's experience in improving the calculation convergence.

The additional geometrical constraints were introduced due to the “good practice” rules:

- the assumed relation between the plate thickness and web frame thickness:

$$t_j - t_{f,wj} \geq 0 \quad (24)$$

where:

$t_j$  – actual value of the plate thickness in j-th region,  
 $t_{f,wj}$  – actual value of web frame thickness in j-th region,



- the assumed relation between the plate thickness and stiffener web thickness:

$$t_j - t_{s,w,j} \geq 0 \quad (25)$$

where:

- $t_j$  – actual value of the plate thickness in j-th region,
- $t_{s,w,j}$  – actual value of stiffener web thickness in j-th region,

- the assumed minimum distance between the edges of frame flanges:

$$l(x_{4+1}) - b_{f,j} \geq 0.3 \text{ m} \quad (26)$$

where:

- $b_{f,j}$  – actual value of frame flange breadth in j-th region.

The relationships supplement the set of inequality constraints  $g_j(\mathbf{x})$ .

After formulating constraints it is necessary to formulate mathematical form of the penalty function  $P_{ii}$ . The choice of mathematical form of penalty function is actually free, however certain basic requirements must be met:

- promoting (preferring, awarding) the solutions which do not violate constraints, increasing in this manner the value of fitness function (selection probability) of the solutions,
- penalizing the solutions which do not fulfil (violate) the constraints, decreasing, in this manner, the value of fitness function and consequently selection probability,
- normalizing the value of fitness function to one.

After conducting series of test computations, the identical mathematical exponential form of penalty function was assumed for all constraints, Eq. 9. Weight coefficients  $w_k$  allow for implementing comparative, in relation to the others, meaning of a given constraint identified by coefficient  $k$ .

Finally by taking into consideration all the specified assumptions, the evolutionary multi-objective optimization model can be written as follows:

- find the vector of design variables  $\mathbf{x} = [x_1 \dots x_i \dots x_n]^T$ ,  $x_i$ ,  $i = 1, \dots, 37$  as shown in Tab. 5,
- optimize the combined objective function  $f(\mathbf{x}) \rightarrow \min!$  given by Eq. 17,
- subject to behaviour constraints given by Eq. 19÷23, side constraints given in Ta. 5 and geometrical constraints given by Eq. 24÷26, build a set of equality  $h_j(\mathbf{x})$  and inequality  $g_j(\mathbf{x})$  constraints,
- exponential forms of penalty functions for representing of constraints violation, Eq. 9.

## Genetic model of the ship hull structure

### General

The ship structural multi-objective optimization problem described earlier contains a large number of discrete design variables and also a large number of constraints. In such a case the GA seems to be especially useful. Solving of the optimization problem by using GA requires to formulate an appropriate optimization model. The optimization model specified earlier was reformulated into an optimization model according to requirements of the GA, which was further used to develop suitable procedures and define search parameters to be used in the computer code.

The genetic type model should cover:

- specification of chromosome structure,
- specification of fitness function:  $\text{fitness} \rightarrow \max!$ ,

- specification of genetic operators suitable for the defined chromosome structures and optimization task,
- specification of the searching control parameters.

### Chromosome structure

In this work, the space of possible solutions is the space of possible structural variants of the assumed model. The ship hull structural model is described (identified) as a collection of 37 design variables,  $x_i$ , described above. Each of them can be represented by a string of bits. For example the deck structural model is described (identified) as a collection of five design variables,  $x_i$ , presented on Fig. 18. As we mentioned above the bit string is used as chromosome in GAs. Defining the chromosome structure consists in assuming:

- a sequence in which variables in chromosome will be coded,
- a number of genes for recording every variable,
- resolution capability of coding actual variable values,
- the lowest and the highest values of the variables.

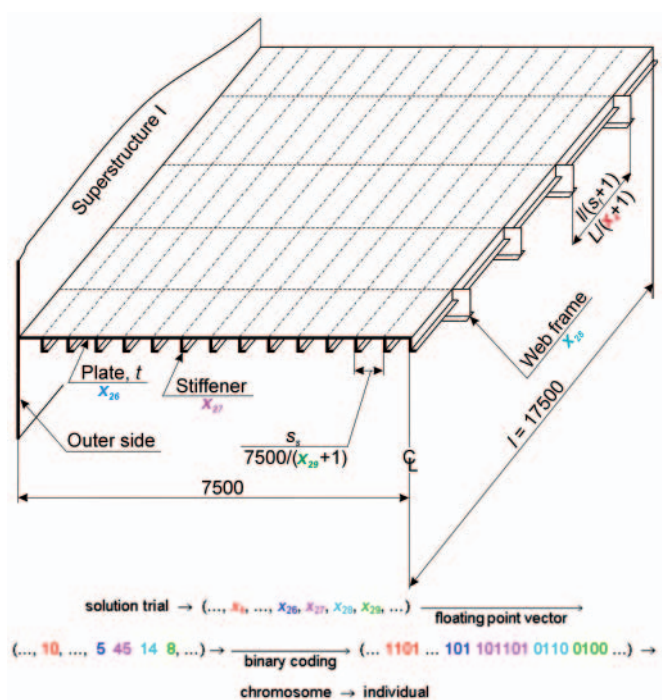


Fig. 18. Design variables and chromosome structure: main deck

Coding sequence is free to choose and it does not affect algorithm computational characteristics, but this knowledge is essential for proper genotype decoding to decisive variables values - phenotypes.

Number of genes in chromosome requires more attention. Generally, the higher gene number the greater demand for memory and increased computing time. Therefore number of genes cannot be too high. On the other hand, greater chromosome length allows for examination of objective space in greater detail. It cannot be too small otherwise mutation and crossover operators would not be able to function effectively on extremely short chromosomes and the resolution will be lower. The compromise is set by the user according to his own experience aiming at required resolution and acceptable time of computing. In this case memory size is of secondary significance. Bibliography review and the author's own experience suggest that usually one variable is coded in a chromosome section containing 5 to 20 genes.

Resolution capability determines sampling density of objective space. Greater resolution capability enables to

examine more points in objective space which increases probability of detecting interesting extremes. On the other hand, increased resolution capability results in increasing a number of computations and extends simulation time. The author's opinion is that resolution capability should be set on the lowest acceptable level. In case the algorithm does not detect any interesting solutions the increasing of resolution capability should be considered.

The user sets the lowest and highest values of variables on the basis of his own experience, according to the task being solved and providing appropriate convergence of algorithm while leaving discretion in exploration of objective space.

A simplified specification for bit representation of all design variables is given in Tab. 5. The solution variant can be represented simply by a string of bits.

The space of possible solutions is a space of structural variants of the assumed model. The hull structural model is identified by the vector  $\mathbf{x}$  of 37 design variables,  $x_i$ . Each variable is represented by a string of bits used as chromosome substring in GA. The simple binary code was applied. Such coding implies that each variant of solution is represented by a bit string named chromosome. Length of chromosome which represents of structural variant is equal to the sum of all substrings. Number of possible solutions is equal the product of values of all variables. In the present work the chromosome length is equal to 135 bits making the number of possible solutions equal approximately to  $10^{38}$ .

### Fitness function

A fitness function is used to determine how much the ship structure is suitable for a given condition in the optimum design with a GA. Because the combined objective function  $f(\mathbf{x})$  expressed by the relation Eq. 13 is: (1) well defined, (2) single-valued, (3) ascending, having real values and positive in the search space, it has been adopted directly to serve as the combined fitness function:

$$\begin{aligned} f(\mathbf{x}) = & w_1 u_1(\mathbf{x}) + w_2 u_2(\mathbf{x}) + \\ & w_{\text{rank}} R_{\text{fi}}(\mathbf{x}) + w_{\text{count}} C_{\text{fi}}(\mathbf{x}) + \\ & + w_{\text{distance}} [1 - d_{\text{fi}}(\mathbf{x})] + \sum_{k=1}^{n_c} w_k P_k(\mathbf{x}) \end{aligned} \quad (27)$$

combined fitness = criteria + rank + count +  
+ distance + constraints

All symbols used in the above given equation were already described. The expression (27) representing inclusion into selection process of test solutions, in addition to the degree with which they adjust to the established optimization criteria and formulated constraints, domination attributes as well as distance to the asymptotic solution, is the key point of the proposed Combined Fitness Multi-Objective Genetic Algorithm (CFMOGA).

### Genetic operators

The basic genetic algorithm (Simple Genetic Algorithm - SGA) produces variants of the new population by using the three main operators which constitute the GA search mechanism: selection, mutation and crossover. In the present work the algorithm was extended by introduction of elitism and updating.

The basic genetic algorithm (Simple Genetic Algorithm -SGA) produces variants of the new population by using

the three main operators which constitute the GA search mechanism: selection, mutation and crossover. In the present work the algorithm was extended by introduction of elitism and updating. Many authors described the selection operators responsible for chromosome selection due to their fitness function value [Goldberg and Deb (1991)], [De Jong (1995)], [Back (1996)], [Michalewicz (1996)]. After the analysis of the selection operators a roulette concept was applied for proportional selection. The roulette wheel selection is a process in which individual chromosomes (strings) are chosen according to their fitness function values; it means that strings with higher fitness value have higher probability of reproducing new strings in the next generation. In this selection strategy the greater fitness function value makes the individuals more important in a process of population growth and causes transmission of their genes to the next generations.

The mutation operator which introduces random changes of the chromosome, was also described [Back (1996)], [Michalewicz (1996)]. Mutation is a random modification of the chromosome. It gives new information to the population and adds diversity to the mate pool (pool of parents selected for reproduction). Without the mutation it is hard to reach solution point which is located far from the current direction of search, while due to introduction of the random mutation operator the probability of reaching any point in the search space never equals zero. This operator also prevents against the premature convergence of GA to one of the local optimum solutions, thus supporting exploration of the global search space.

The crossover operator combines the features of two parent chromosomes to create new solutions. The crossover allows to explore a local area in the solution space. Analysis of the features of the described operators [Goldberg and Deb (1991)], [Back (1996)], [Michalewicz (1996)] led to developing a new, n-point, random crossover operator. The crossover parameters in this case are: the lowest  $n\_x\_site\_min$  and the greatest  $n\_x\_site\_max$  number of the crossover points and the crossover probability  $p_c$ . The operator works automatically and independently for each pair being intersected (with probability  $p_c$ ), and it sets the number of crossover points  $n\_x\_site$ . The number of points is a random variable inside the set range [ $n\_x\_site\_min$ ,  $n\_x\_site\_max$ ]. The test calculations proved high effectiveness and quicker convergence of the algorithm in comparison with algorithm realizing single-point crossover. It was also found that the number of crossover points  $n\_x\_site\_max$  greater than 7 did not improve convergence of the algorithm. Therefore, the lowest and greatest values of the crossover points were set as follows:  $n\_x\_site\_min = 1$ ,  $n\_x\_site\_max = 7$ .

The effectiveness of the algorithm was improved with application of an additional updating operator as well as introduction of elitist strategy.

Random character of selection, mutation and crossing operators can have the effect that these are not the best fitting variants of the parental population which will be selected for crossing. Even in the case they will be selected, the result will be that progeny may have a lower adaptation level. Thus the efficient genome can be lost. Elitist strategy mitigates the potential effects of loss of genetic material copying certain number of best adapted parental individuals to progeny generation. In the most cases the elitist strategy increases the rate of dominating population by well-adapted individuals, accelerating the convergence of the algorithm. The algorithm selects fixed number of parental individuals  $n_p$  having the greatest values of the fitness function and the same number of descendant individuals having the least values of the fitness. Selected descendants are substituted by selected parents. In this way the operator increases exploitation of searching

space. Update operator with fixed probability of updating  $p_u$  introduces an individual, randomly selected from the parental population, to the progeny population, replacing a descendant less adapted individual. This operator enhances exploration of searching space at the expense of decreasing the search convergence. It also prevents the algorithm from converging to a local minimum. Both operators acts in opposite directions, and they should be well balanced; exploitation of attractive areas found in the searching spaces as well as exploration of searching space to find another attractive areas in the searching space depend on the user's experience.

### Control parameters

Single program run with the defined genetic model is characterized by values of eighteen control parameters. In this case the set of genetic model parameters set for each simulation run signed as symi includes 18 elements:

$$\text{symi} = (n_{dv}, l_{ch}, n_g, n_i, n_p, p_m, p_c, c\_strategy, n\_x\_site\_min, n\_x\_site\_max, p_u, elitist, w\_strategy, w_1, w_2, w_{rank}, w_{count}, w_{distance})$$

where:

$n_{dv}$	– number of design variables (number of genes),
$l_{ch}$	– chromosome length (number of bits),
$n_g$	– number of generations, $n_i$ - size of population,
$n_p$	– number of pretenders,
$p_m$	– mutation probability,
$p_c$	– crossover probability,
$c\_strategy$	– denotation of crossover strategy (0 for fixed, 1 for random number of crossover points),
$n\_x\_site\_min$	– the lowest number of crossover points,
$n\_x\_site\_max$	– the greatest number of crossover points,
$p_u$	– update probability,
$elitist$	– logical variable to switch on (elitism = yes) and off (elitism = no) the pretender selection strategy,
$w\_strategy$	– denotation of strategy for aggregation of objective function,
$w_1$	– weight coefficient of weight of structure,
$w_2$	– weight coefficient of surface area of structural element intended for cleaning and painting,
$w_{rank}$	– weight coefficient of solution dominance rank,
$w_{count}$	– weight coefficient of individual dominance count,
$w_{distance}$	– weight coefficient of distance of individual from asymptotical solution.

These 18 parameters control the successive simulation runs and identify them unambiguously for the adopted structure model.

For selection of more control parameters it is not possible to formulate quantitative premises because of the lack of an appropriate mathematical model for analysis of GA convergence in relation to control parameters. The control parameters were set due to test calculations results to achieve a required algorithm convergence.

All genetic parameters are specified by the user in advance of the calculations. This option is very important; the control of the parameter permits to perform search in the direction expected by the designer and in some cases it allows to find solution faster. The population size, number of variables and number of bits per variable, the total genome length, number

of individuals in the population are limited by the available computer memory.

### Conclusion

Finally, with taking into consideration all specified assumptions, the genetic model can be determined by the following:

- chromosome structure specified in Tab. 5,
- fitness function given by Eq. 28,
- genetic operators,
- control parameters.

## COMPUTATIONAL INVESTIGATIONS – THE SEARCH FOR SET OF NON-DOMINATED SOLUTIONS

### Computational investigations program

In order to verify the suitability of the proposed method and the computer code developed for the seeking of Pareto-optimal solutions of the formulated multi-objective seagoing ship structure optimization problem, a number of calculation experiments have been performed, Tab. 7, by using the ship structure models earlier formulated and discussed in Section 6.

From the multi-objective optimization point of view, the aim of the simulation was searching for non-dominated variants with respect to two optimization criteria with varying strategies for setting the values of weight coefficients for various criteria as well as dominance attributes:

**(1) Series 1.:** the simulations marked with symbols sym1-1, sym1-2 and sym1-3 having the following values of control parameters:

sym1-1: (37, 135, 10.000, 5.000, 10, 0.086, 0.800, 1, 1, 7, 0.33, yes, 2, 0.5, 0.5, 0.0, 0.0, 0.0),

sym1-2: (37, 135, 10.000, 5.000, 10, 0.086, 0.800, 1, 1, 7, 0.33, yes, 3, random in [0,1], random in [0,1], 0.0, 0.0, 0.0),

sym1-3: (37, 135, 10.000, 5.000, 10, 0.086, 0.800, 1, 1, 7, 0.33, yes, 4, random 0 or 1, random 0 or 1, 0.0, 0.0, 0.0).

In the simulation marked as **sym1-1** the fixed values of weight coefficients are used for whole simulation:  $w_1 = 0.5$  and  $w_2 = 0.5$ ; which refers to a classical method of weighted criteria. In the simulation marked as **sym1-2** the values of weight coefficients  $w_1$  and  $w_2$  were generated by the computer code as **random variables in the range [0, 1]**, which was done independently for each variant whenever the value of fitness function is calculated. In the simulation marked as **sym1-3** the values of weight coefficients  $w_1$  and  $w_2$  were generated by the computer code as **random variables equal to either 0 or 1**, which was done independently for each variant whenever the value of fitness function is calculated; the value of 1 was used only for one, randomly selected criterion, with the remaining ones equal to 0.

**(2) Series 2.:** the simulations marked with symbols sym2-1, sym2-2 and sym2-3 having the following values of control parameters:

sym2-1: (37, 135, 10.000, 5.000, 10, 0.086, 0.800, 1, 1, 7, 0.33, yes, 1, 0.0, 0.0, 3.0, 0.0, 0.0),

sym2-2: (37, 135, 10.000, 5.000, 10, 0.086, 0.800, 1, 1, 7, 0.33, yes, 1, 0.0, 0.0, 0.0, 3.0, 0.0),

sym2-3: (37, 135, 10.000, 5.000, 10, 0.086, 0.800, 1, 1, 7, 0.33, yes, 1, 0.0, 0.0, 0.0, 0.0, 3.0).

Search for non-dominated variants while excluding the optimization criteria from the process of variant selection

Tab. 7. Control parameters of computational investigations

No.	Designation symi	Specification
		( $n_d, l_{ch}, n_g, n_i, n_p, p_m, p_c, c\_strategy, n\_x\_site\_min, n\_x\_site\_max, p_u, elitist, w\_strategy, w_1, w_2, w_{rank}, w_{count}, w_{distance}$ )
<b>Series 1.</b>		
1.	sym1-1	(37, 135, 10,000, 5,000, 10, 0.086, 0.800, 1, 1, 7, 0.33, yes, 2, 0.5, 0.5, 0.0, 0.0, 0.0)
2.	sym1-2	(37, 135, 10,000, 5,000, 10, 0.086, 0.800, 1, 1, 7, 0.33, yes, 4, random in [0,1], random in [0,1], 0.0, 0.0, 0.0)
3.	sym1-3	(37, 135, 10,000, 5,000, 10, 0.086, 0.800, 1, 1, 7, 0.33, yes, 3, random 0 or 1, random 0 or 1, 0.0, 0.0, 0.0)
<b>Series 2.</b>		
4.	sym2-1	(37, 135, 10,000, 5,000, 10, 0.086, 0.800, 1, 1, 7, 0.33, yes, 1, 0.0, 0.0, 3.0, 0.0, 0.0)
5.	sym2-2	(37, 135, 10,000, 5,000, 10, 0.086, 0.800, 1, 1, 7, 0.33, yes, 1, 0.0, 0.0, 0.0, 3.0, 0.0)
6.	sym2-3	(37, 135, 10,000, 5,000, 10, 0.086, 0.800, 1, 1, 7, 0.33, yes, 1, 0.0, 0.0, 0.0, 0.0, 3.0)

$w_1 = w_2 = 0.0$  ( $w\_strategy = 1$ ) which was governed in particular simulations only by: (i) the value of the dominance rank of feasible solution,  $w_{rank} = 3.0$ ,  $w_{count} = 0.0$ ,  $w_{distance} = 0.0$ , in the simulation marked as **sym2-1**, (ii) the value of feasible variant dominance count,  $w_{count} = 3.0$ ,  $w_{rank} = 0.0$ ,  $w_{distance} = 0.0$ , in the simulation marked as **sym2-2**, (iii) the distance between the feasible variant and the asymptotic solution,  $w_{distance} = 3.0$ ,  $w_{rank} = 0.0$ ,  $w_{count} = 0.0$ , in the simulation marked as **sym2-3**. The purpose of the simulation series was to find out whether the developed tool is effective in case of evolution being governed only by (i) dominance rank, (ii) dominance count, or (iii) distance from a asymptotic solution. This refers to modern algorithms of evolutionary multi-objective optimization, where the evolution is governed only by dominance attributes.

In all the simulations the functions of penalties imposed in the violations of constraints were active,  $w_k \neq 0, k = 1, 2, \dots, n_c$ .

The computational investigations were carried out first of all for two-objective problems, as in this case it is possible to present obtained results graphically in a multitude of ways, which facilitate their interpretation and analysis.

### Results of computational investigations

#### Results of computational investigations – Series1: the simulation marked with symbols sym1-1, sym1-2 and sym1-3

The results of simulation sym1-1 are going to be discussed in the most detailed way by presenting the results characteristic

for the developed method. For other simulations only the most important results will be presented.

The Fig. 19 presents the evolution of macroscopic values characterizing the evolution of generated and evaluated population of ship structure solutions in the simulation **sym1-1**: (1) the greatest fitness function value  $f_{max}$ , (2) the lowest distance of the feasible solution from the asymptotic solution. Multi-objective optimization of ship structure was performed with regard to the structure weight  $f_1$  and the surface area for maintenance  $f_2$  in case of fixed values of weight coefficients  $w_1 = w_2 = 0.5$  used for optimization criteria. Dominance attributes: dominance rank, dominance count and distance from asymptotic solution, being excluded from selection. The figure shows a desired continuous rise of the greatest value of fitness function  $f_{max}$  indicating rising quality of the best generated test solutions. The highest values of fitness function saturate already in 1668 generation, which means that in the following generations no solutions were generated being better adapted in the sense of the fitness function used, and the computation resources were squandered replicating the non-dominated solutions set. The lowest distance between a non-dominated solution and the asymptotic solution changes during the evolution, but above the threshold of 87.38% of the highest value found during the simulation this takes place to a very small extent. For example, in the 857th generation the distance of the closest solution  $f_{857}^*(x)$  from the asymptotic solution is 1.114<sup>1)</sup>, see Fig. 20a, while in the successive 858th generation the distance of the closest solution  $f_{858}^*(x)$  to the asymptotic solution increased to 1.177, Fig. 20b. For the same

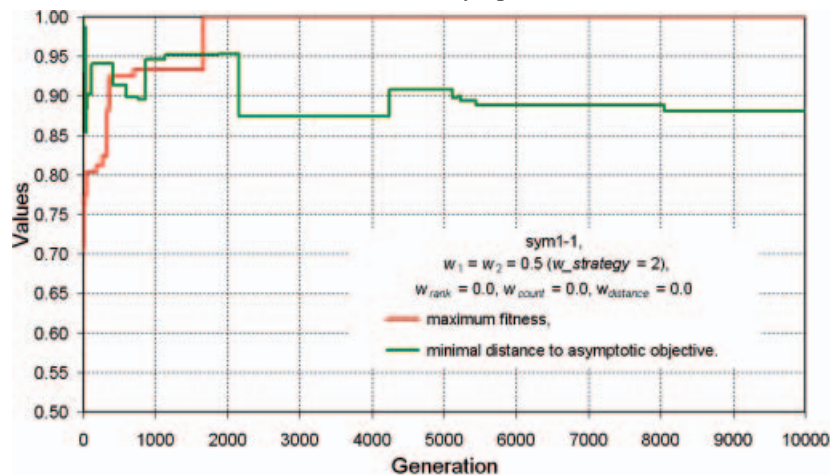
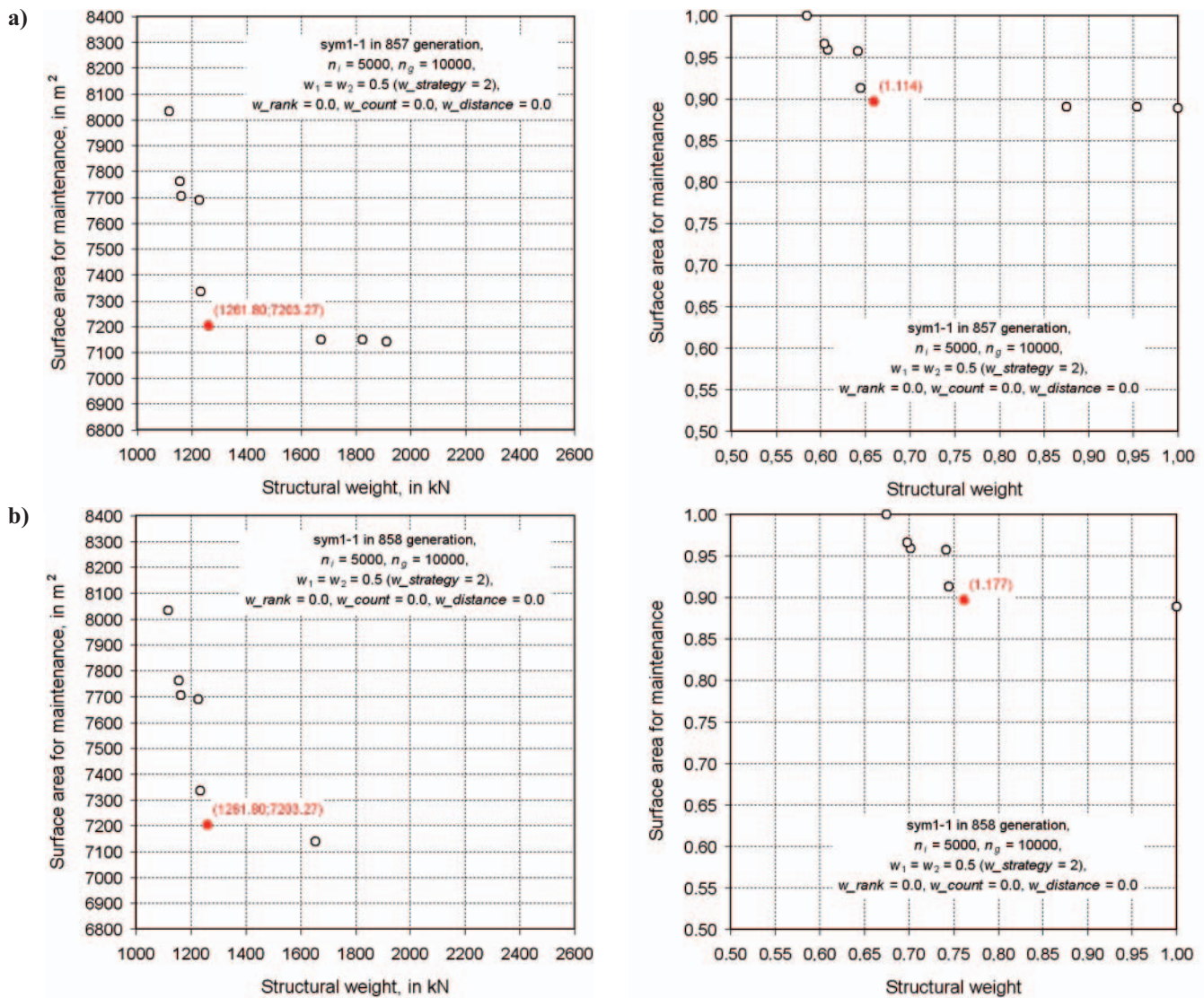


Fig. 19. The results of multi-objective genetic optimization of ship structure with respect to structure weight  $f_1$  and the area of element surface  $f_2$  in case of fixed values of optimization criteria weight coefficients  $w_1 = w_2 = 0.5$  with dominance attributes being excluded from selection (**sym1-1**); the curves present the evolution of a highest value of fitness function  $f_{max}$ , the lowest value of non-dominated solution distance from a asymptotic one; the values are dimensionless and standardized in  $[0,1]$  range in relation to the highest values found during the simulation

<sup>1)</sup> All values of distance from the asymptotic solution are calculated in normalized space because it is impossible to calculate the Euclidean distance in physical objective space when different objectives are measured in different units.



**Fig. 20.** Change of a structure of non-dominated solutions set when moving from generation 857 (a) to generation 858 (b); during the genetic multi-objective optimization of ship structure with respect to structure weight  $f_1$  and surface area  $f_2$  in case of the fixed values of optimization criteria weight coefficients  $w_1 = w_2 = 0.5$  with dominance attributes being excluded from selection (sym1-1); circles represent non-dominated solutions, red points represent non-dominated solutions closest from the asymptotic one; dimensionless values are normalized to the interval  $[0,1]$  in relation to the highest values in the set<sup>2)</sup>; change of non-dominated solution set structure and change of non-dimensional (normalized) of distance of the nearest solution from asymptotic solution caused not by change of values of partial optimization criteria but only change of set of non-dominated solutions set structure can be observed

solution the change of the distance to the asymptotic solution occurs only due to the change of the structure of the set of non-dominated solutions. On the other hand, for example, in the 2156th generation the distance of the closest solution  $f_{2156}^{\approx}(\mathbf{x})$  from to the asymptotic solution is 1.187, Fig. 21a, while in the successive 2157th generation the distance of the closest solution  $f_{2157}^{\approx}(\mathbf{x})$  from the asymptotic solution decreased to 1.087, Fig. 21b. In this case the change of the set structure caused another solution, already present in the set, became the solution closest to the asymptotic solution.

In Fig. 22 the evolution of the structure of non-dominated solutions set in simulation sym1-1 is shown by using the selected time-based cross-sections of this set, e.g. for 1, 2000, 4000, 6000, 8000 and 10.000 generations as examples. A systematic growth of the size of non-dominated solutions set is apparent with 6, 6, 9, 12, 11 and 14 non-dominated solutions respectively in the consecutive time-based cross-sections as well as the desired evolution of this set in the direction of more advantageous values of partial optimization criteria.

Fig. 23 presents a detailed structure of the non-dominated solution set of the last generation, presented in the physical space of objectives and normalized space of objectives. It can be seen that the set of non-dominated solutions including 14 variants of ship structure was found during the simulation. For each non-dominated variant the values of optimization criteria were specified as:  $f_1(\mathbf{x})$  – structural weight and  $f_2(\mathbf{x})$  – cleaned/painted surface area. The designer may select for further development one of these variants or a group of them deemed by him to be the best. For the variant closest from the asymptotic solution which was found in 5116 generation,  $f_{5116}^{\approx}(\mathbf{x})$ , the distance equals 1.096 in the normalized objective space, the structural weight is  $f_1(\mathbf{x}) = 1086.28$  kN and the cleaned/painted surface area is  $f_2(\mathbf{x}) = 7422.10$  m<sup>2</sup>. This variant may be recommended if there is a need to select a single solution for the formulated ship structure multi-objective optimization problem:

$$\begin{aligned} \tilde{\mathbf{f}}_{\text{sym1-1}} &= \tilde{f}_{5116}^{\approx}(\mathbf{x}) = [f_{1;5116}^{\approx}(\mathbf{x}) \ f_{2;5116}^{\approx}(\mathbf{x})]^T = \\ &= [1086.28 \ 7422.10]^T \cdot [\text{kN} \ \text{m}^2] \end{aligned}$$

<sup>2)</sup> Normalization of the optimization objective values makes it possible to calculate the distance from asymptotic objective in the Euclidean sense in cases when the axes of the co-ordinate system represent the objectives denoted in various units.

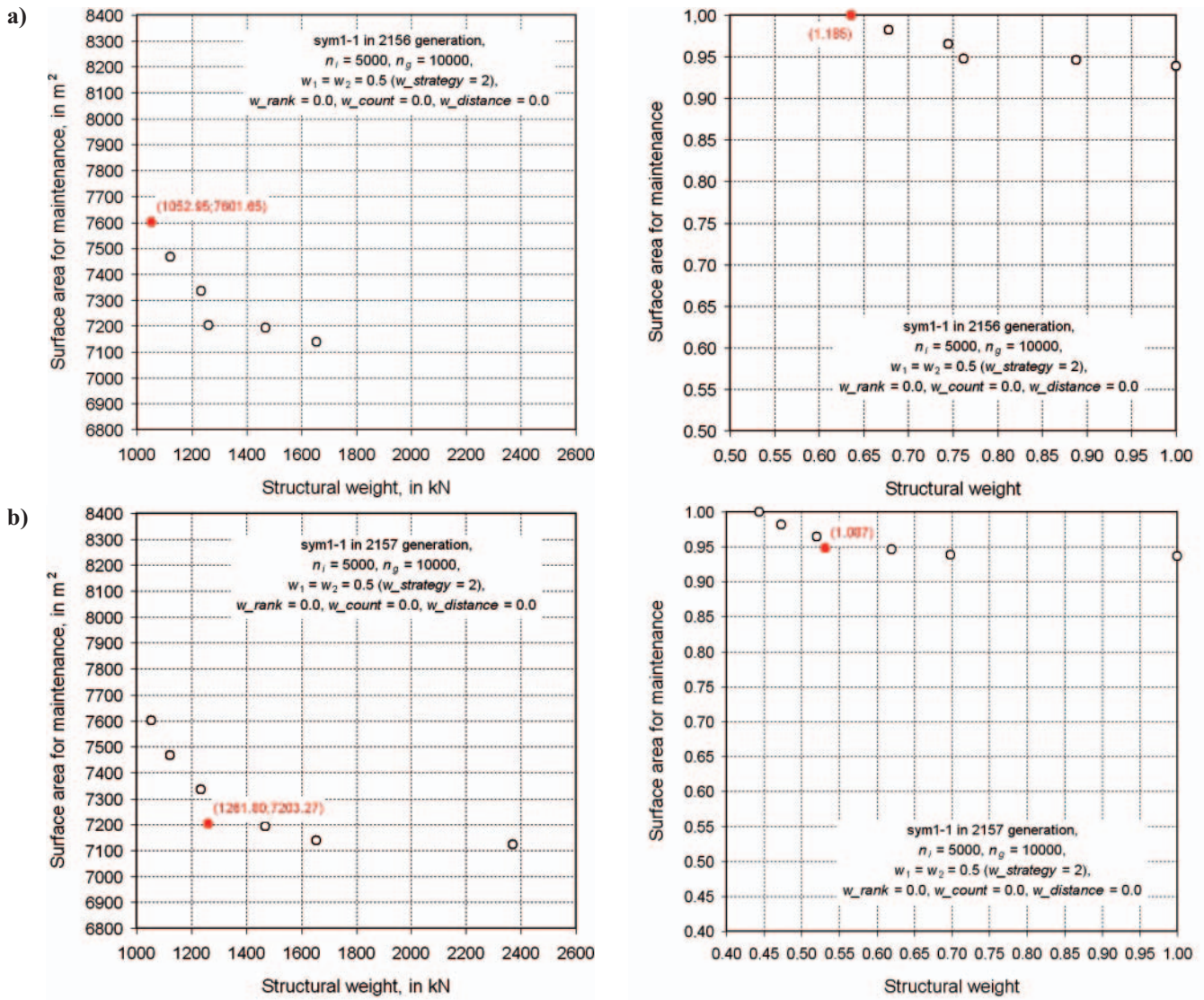


**Fig. 21.** Change of a structure of non-dominated solutions set when moving from generation 2156 (a) to generation 2157 (b); during the genetic multi-objective optimization of ship structure with respect to structure weight  $f_1$  and surface area  $f_2$  in case of the fixed values of optimization criteria weight coefficients  $w_1 = w_2 = 0.5$  with dominance attributes being excluded from selection (sym1-1); circles represent non-dominated solutions, red points represent non-dominated solutions closest to the asymptotic one; dimensionless values are normalized to the interval  $[0,1]$  in relation to the highest values in the set; change of non-dominated solution set structure and change of non-dimensional (normalized) of distance of the nearest solution from asymptotic solution caused not by change of values of partial optimization criteria but only change of set of non-dominated solutions set structure can be observed

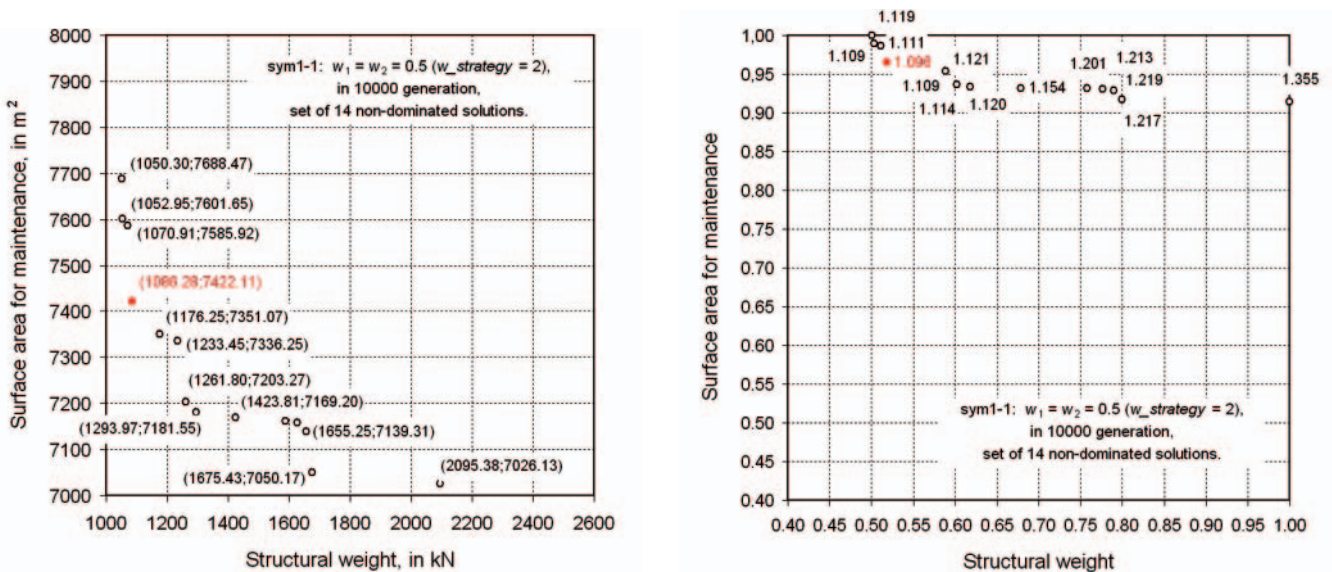


**Fig. 23.** Detailed specification of non-dominated solutions set obtained during the genetic multi-objective optimization of ship structure with respect to structure weight  $f_1$  and surface area  $f_2$  in case of fixed values of optimization criteria weight coefficients  $w_1 = w_2 = 0.5$  with dominance attributes being excluded from selection (sym1-1); black circles represent non-dominated solutions, red dots represent non-dominated solutions closest from the asymptotic one; dimensionless values are normalized to the interval  $[0,1]$  in relation to the highest values in the set

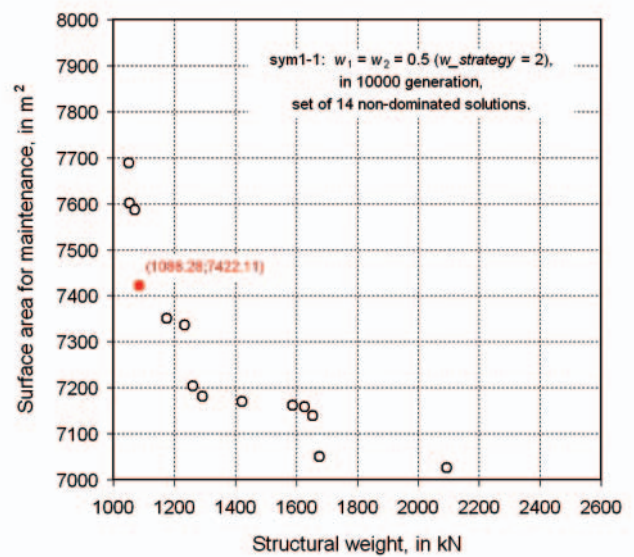
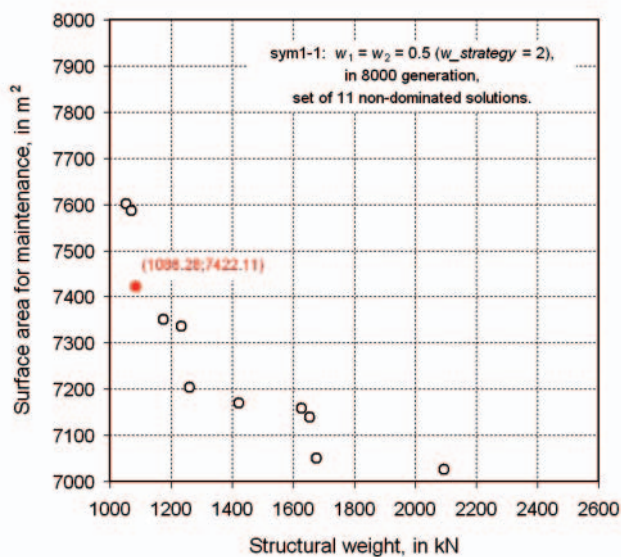
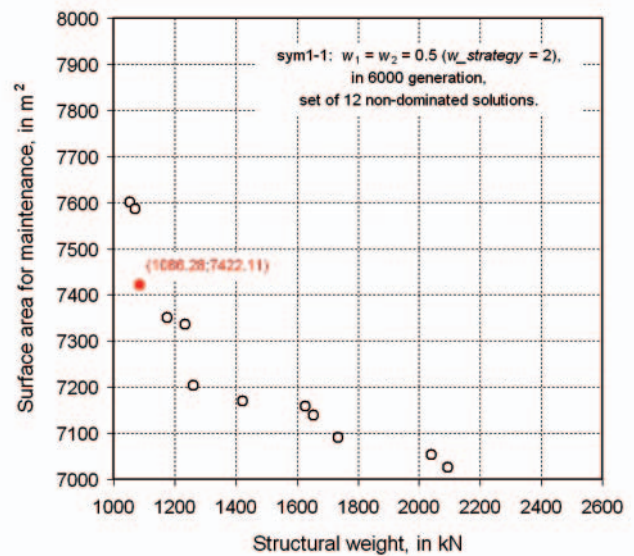
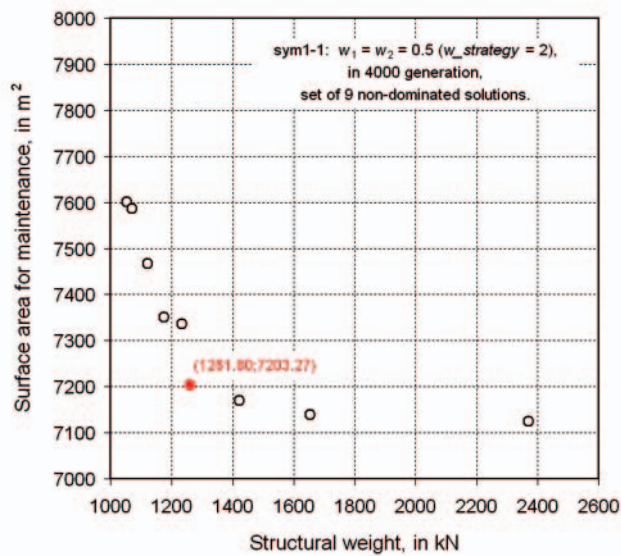
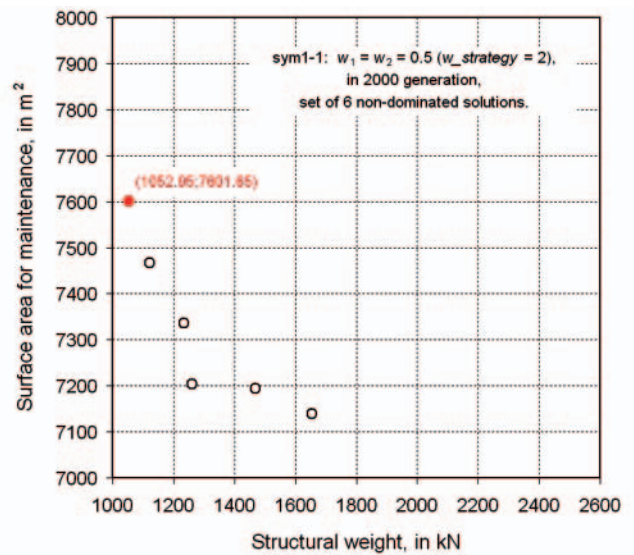
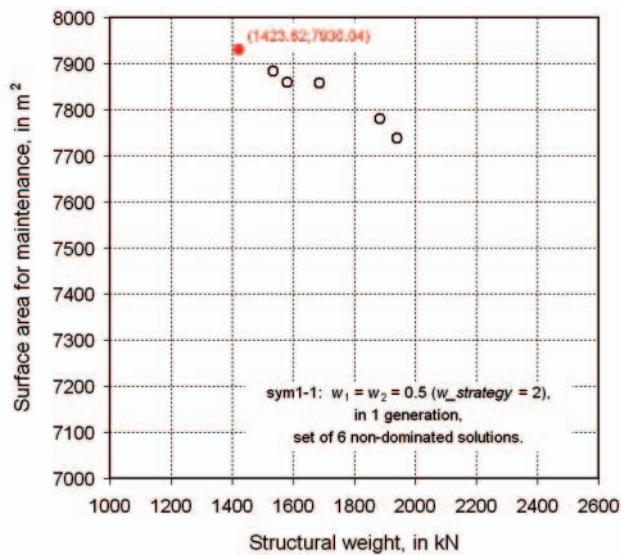


Fig. 22. History of the evolution of non-dominated solutions set during the genetic multi-objective optimization of ship structure with respect to structure weight  $f_1$  and surface area  $f_2$  in case of the fixed values of optimization criteria weight coefficients  $w_1 = w_2 = 0.5$  with dominance attributes being excluded from selection (sym1-1); black circles represent non-dominated solutions, red dots represent non-dominated solutions closest from the asymptotic one

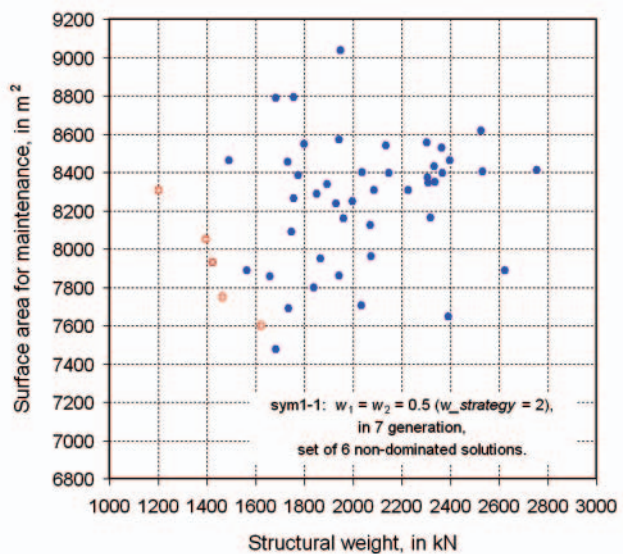
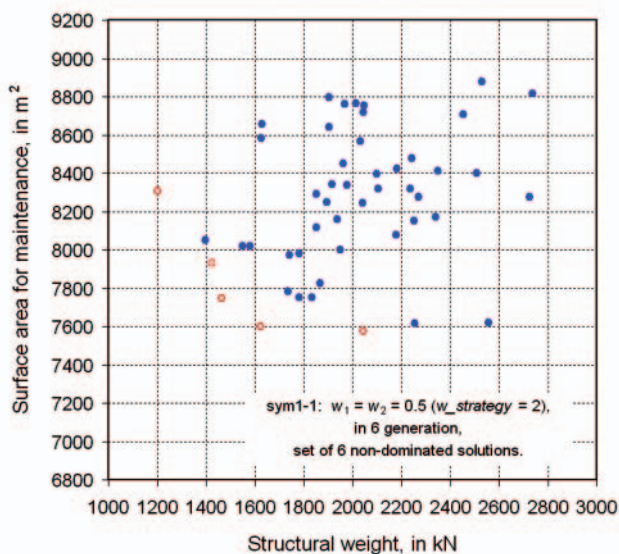
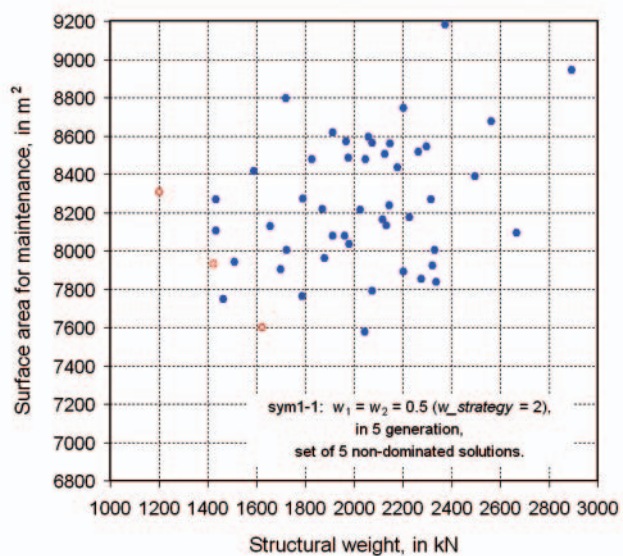
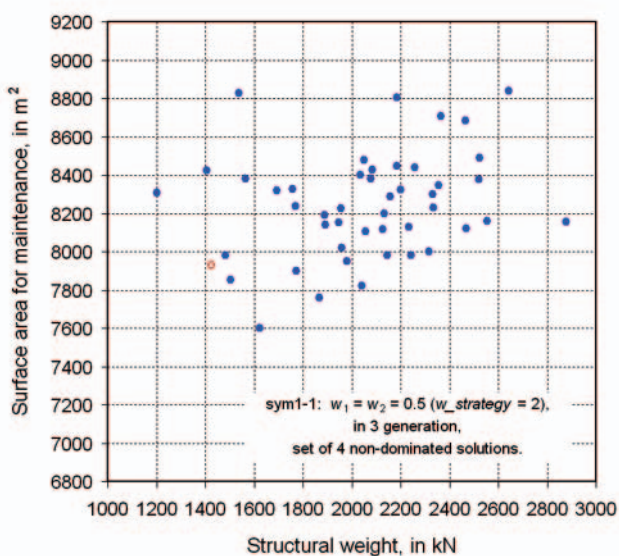
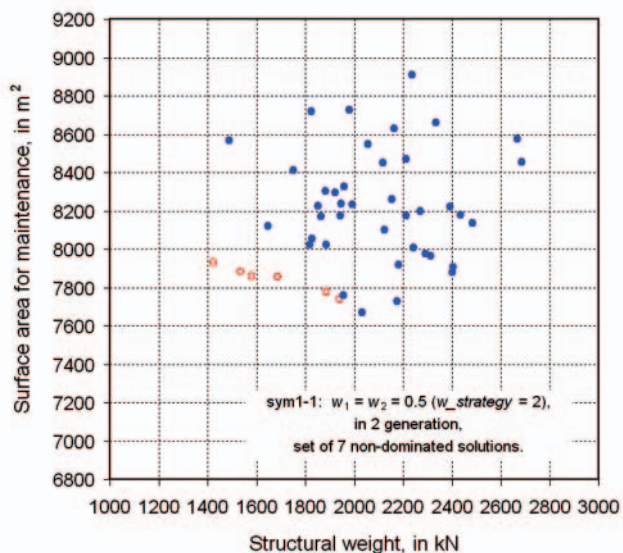
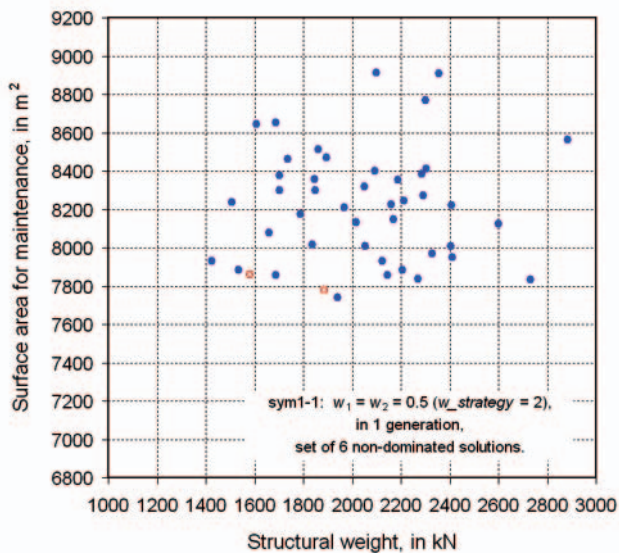


Fig. 24. History of creating a set of non-dominated solutions in the first six timeframes in which a change in structure of the set of non-dominated solutions has occurred during the genetic multi-objective optimization of ship structure with respect to structure weight  $f_1$  and surface area  $f_2$  in case of the fixed values of optimization criteria weight coefficients  $w_1 = w_2 = 0.5$  with dominance attributes being excluded from selection (sym1-1); red circles represent non-dominated solutions, blue dots represent feasible solutions in present generations; in case of the first generation two existed already non-dominated solutions are coming from initial generation



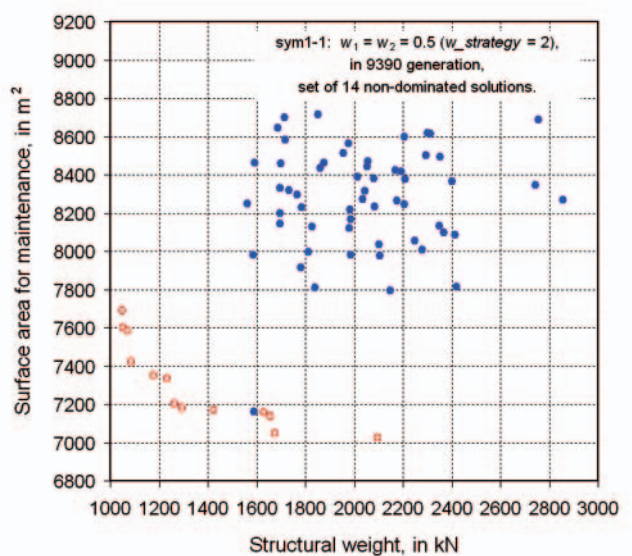
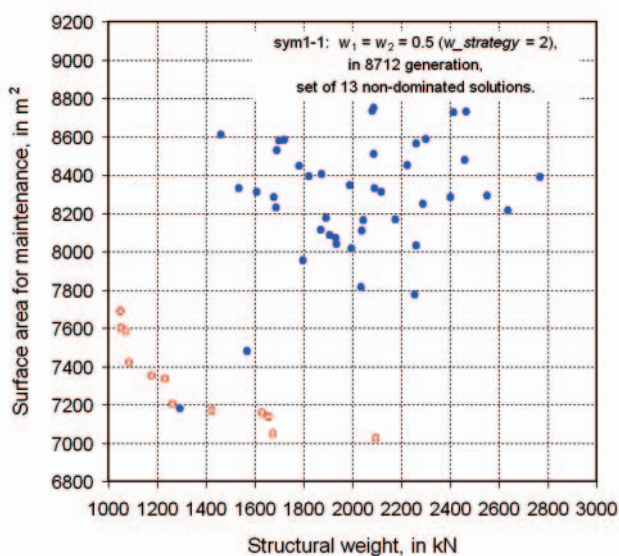
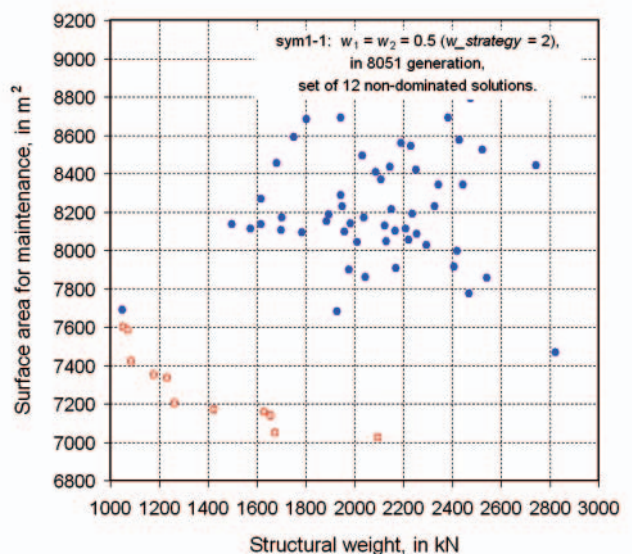
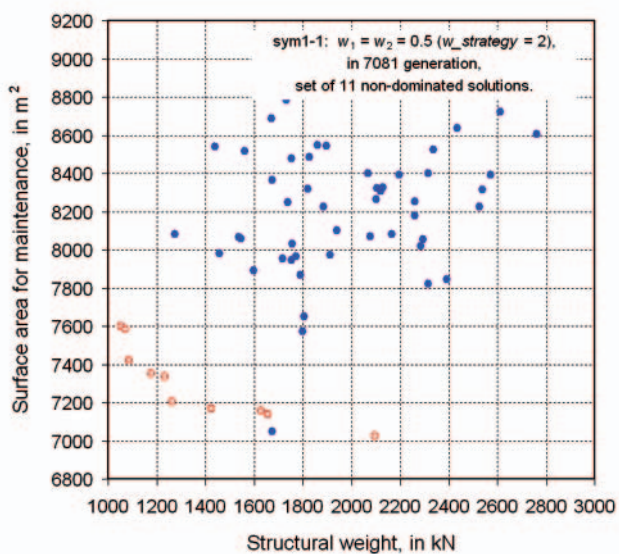
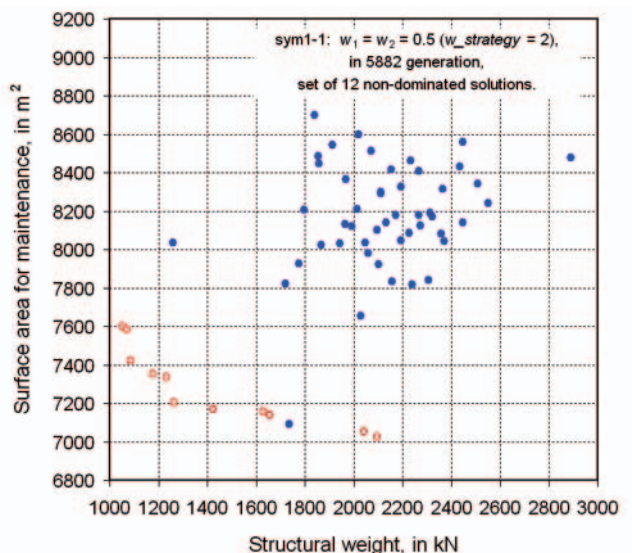
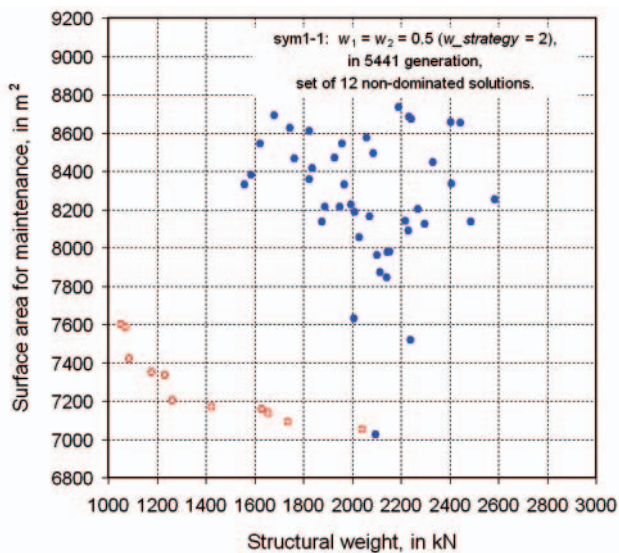


Fig. 25. History of creating a set of non-dominated solutions in the last six timeframes in which a change in structure of the set of non-dominated solutions has occurred during the genetic multi-objective optimization of ship structure with respect to structure weight  $f_1$  and surface area  $f_2$  in case of the fixed values of optimization criteria weight coefficients  $w_1 = w_2 = 0.5$  with dominance attributes being excluded from selection (sym1-1); red circles represent non-dominated solutions, blue dots represent feasible solutions in present generations

The author found it an interesting task to examine in which way the evolutionary optimization algorithm is builds a set of non-dominated solutions (approximation of Pareto set). Is the hypothesis correct, which states that during the evolution the set of feasible solutions as a whole shifts in direction of asymptotic solution, and is the set of non-dominated solutions approximating Pareto front is an edge of the set of feasible solutions? To verify the hypothesis, in Fig. 24 are presented feasible sets and approximation sets for time intersections corresponding to six first modifications of approximation set, i.e. 1, 2, 3, 5, 6 and 7 generations. In Fig. 25 are also presented approximation sets for time intersections corresponding six last modifications of approximation set, i.e. 5441, 5882, 7081, 8051, 8712 and 9390 generations. Modification of the approximation set took place by including, to the successive approximation set, selected solutions, non-dominated in the ongoing feasible set and non-dominated by existing approximation set simultaneously.

Figure 24 confirms, according to Fig. 18 that the algorithm builds the approximation set very intensively in early generations; in practice, in every following generation a new solution is being incorporated to the approximation set. The slow receding of the approximation set from the set of non-dominated solutions in the direction of the origin of the coordinate system

is visible. Set of feasible solutions maintains steady position in the objective space, preserving also similar range in this space. Fig. 25 confirms very slowly progressing building of the approximation set in final phases of the simulation; sequentially generated non-dominated variants are separated in spaces about 1000 generations of evolution simulated by the algorithm. The approximation set is already separated from the set of feasible solutions and sequentially incorporated to its non-dominated solutions already overcoming significant distance from the feasible set and approximation set in the objective space. To overcome so the large distance in the objective space is possible in the way of very high attractive mutations in the chromosomes of individuals. Location of the set of feasible solutions and its range in the objective space do not undergo significant changes in course of evolution. Slightly larger concentration of set of feasible solutions in the later generations is visible presented in the Fig. 25, however confirmation if it is an actual or apparent effect requires further research.

The presented results of the evolution of non-dominated solutions set indicate that non-dominated solutions set evolution can proceed also in such a way that the set of dominated feasible solutions preserves more less stable position in evaluation space, in turn discovered in sequence of non-dominated solutions are discovered sparse very good solutions found in course of

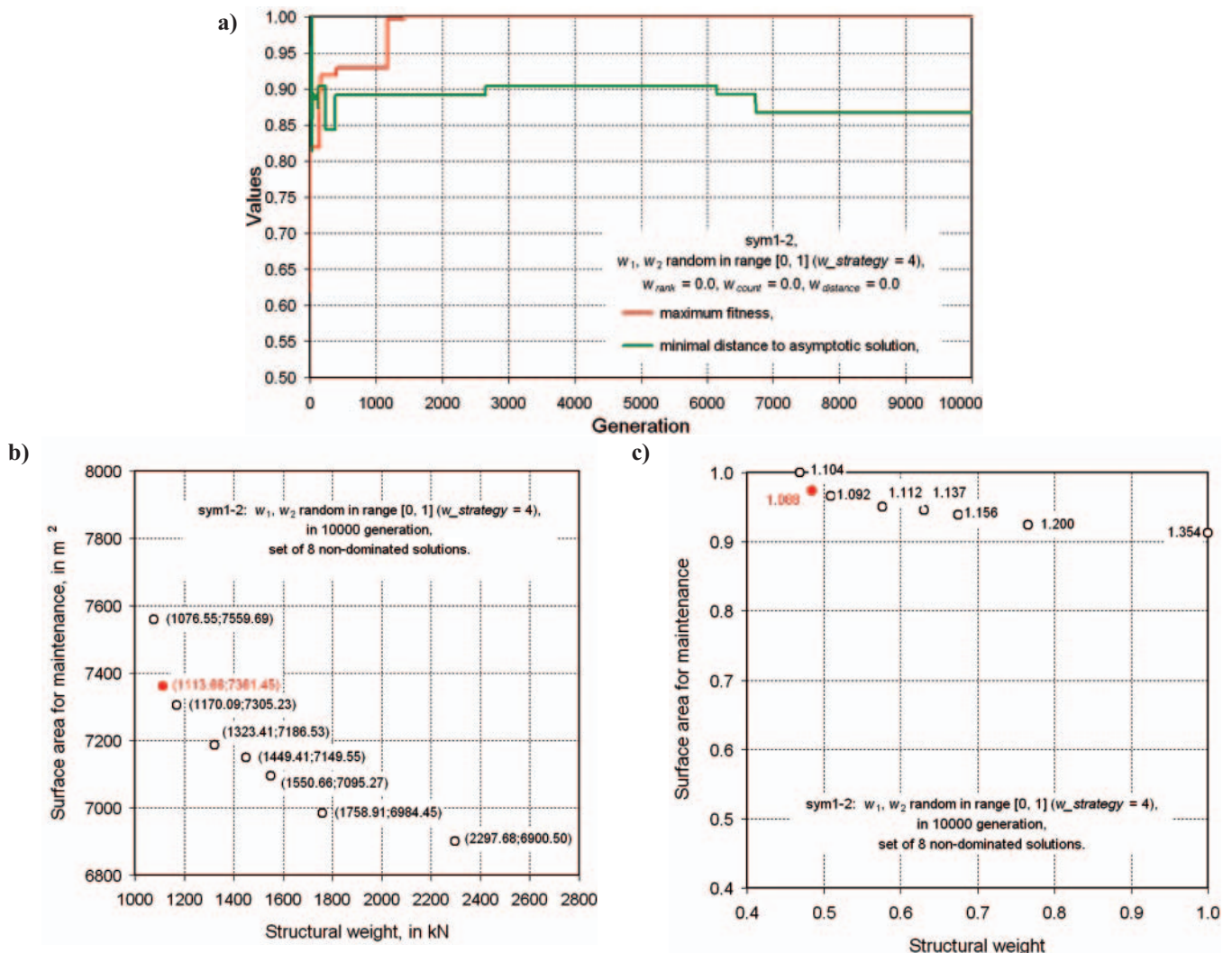


Fig. 26. Results of genetic multi-objective optimization of ship structure with respect to structure weight  $f_1$  and surface area  $f_2$  in case of random values of optimization criteria weight coefficients  $w_1$  and  $w_2$  in range of  $[0, 1]$  with dominance attributes being excluded from selection (sym1-2); a) the curves present the evolution of the highest value of fitness function  $f_{max}$ , the lowest value of non-dominated solution distance from a asymptotic one, b) detailed specification of final non-dominated solutions set in objective space, c) detailed specification of final non-dominated solutions set in normalized objective space; black circles represent non-dominated solutions, red circles represent non-dominated solution closest from the asymptotic one; dimensionless values are normalized to the interval  $[0,1]$  in relation to the highest values in the set

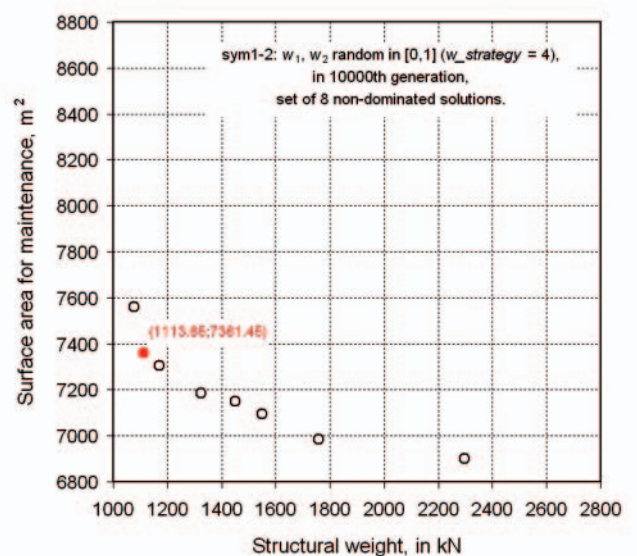
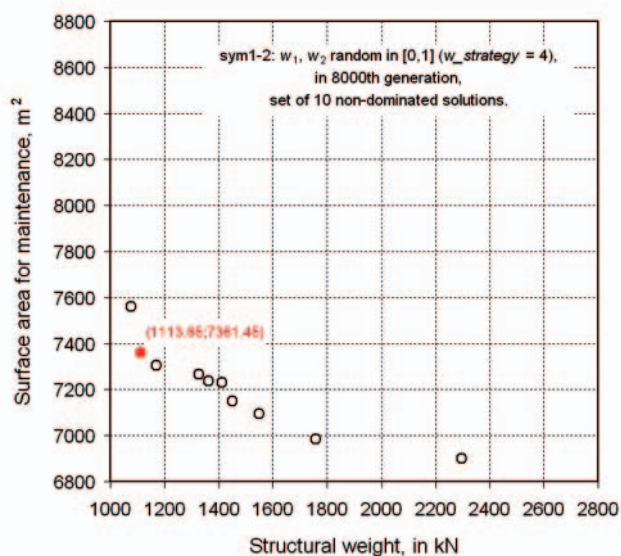
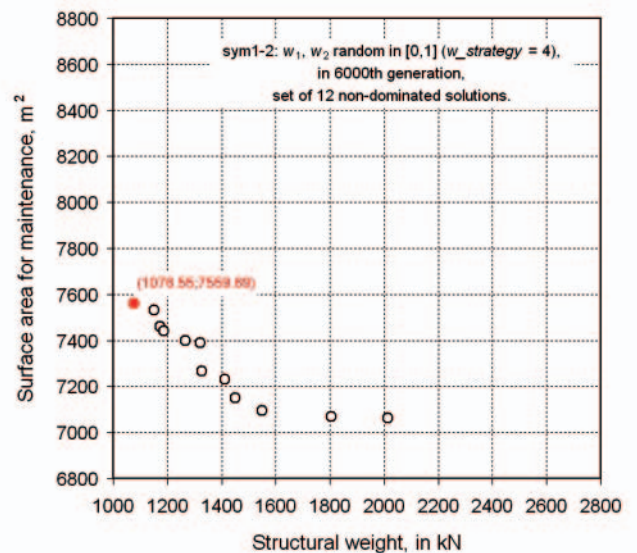
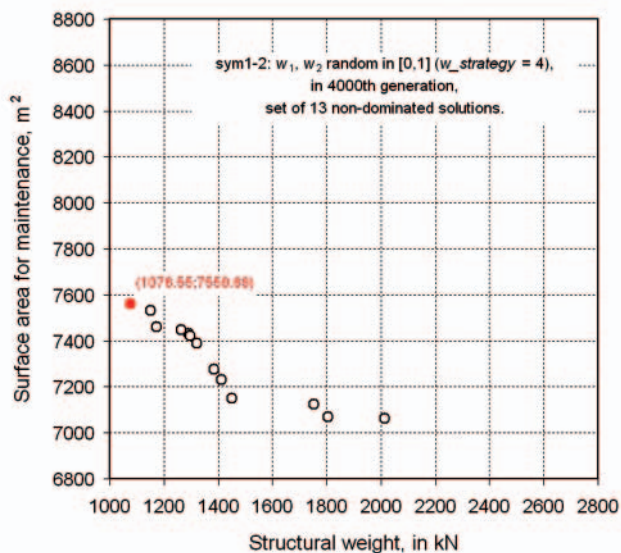
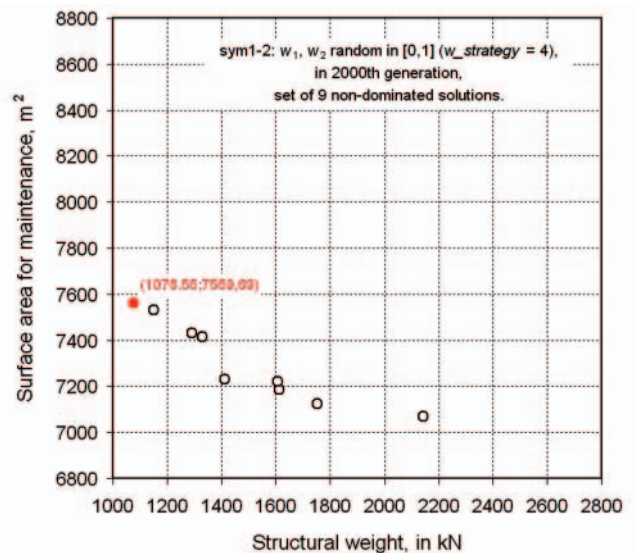
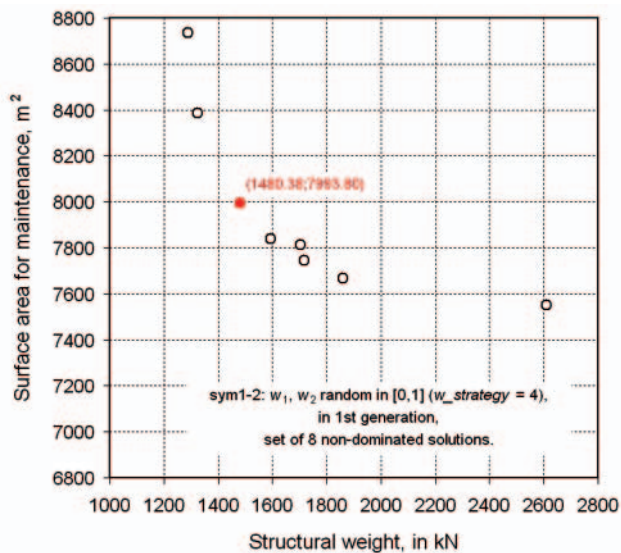


Fig. 27. History of the evolution of the non-dominated solutions set during the genetic multi-objective optimization of ship structure with respect to structure weight  $f_1$  and surface area  $f_2$  in case of random values of optimization criteria weight coefficients  $w_1$  and  $w_2$  in range of  $[0, 1]$  with dominance attributes being excluded from selection (sym1-2); black circles represent non-dominated solutions, red dots represent non-dominated solutions closest from the asymptotic one

an algorithm simulated evolution; they create a set of non-dominated solutions receding in the act of the simulation from the set of feasible solutions to asymptotic ideal evaluations. This way of evolution the author suggests to call “drop by drop”, because it resembles rain drops falling on the ground; in this case the set of dominated feasible solutions represents a rain cloud while the set of non-dominated solutions, approximation set, represents drops that have fallen onto the ground.

Figure 26a presents the evolution of macroscopic values characterizing the evolution of generated and evaluated ship structure variants population in simulation **sym1-2** in case of **random values of weight coefficients  $w_1$  and  $w_2$  in range of  $[0, 1]$**  with dominance attributes being excluded from selection. The figure shows a desired continuous rise of the greatest value of fitness function  $f_{max}$  indicating rising quality of the best generated test variants. The highest values of fitness function saturate already in 1416 generation. The lowest distance between a non-dominated solution and the asymptotic solution changes during the evolution but above the threshold of 86,69% of the highest value found during the simulation is results in insignificant changes.

In Fig. 27 the evolution of the structure of the non-dominated solutions set in simulation **sym1-2** is shown by

using, as examples, the selected time-based cross-sections of this set, e.g. for 1, 2000, 4000, 6000, 8000 and 10,000 generations. The size of non-dominated solutions set in the selected generations is apparent with 8, 9, 13, 12, 10 and 8 non-dominated solutions and it does not change significantly in the course of simulation.

Figures 26b and 26c presents the detailed structure of the non-dominated solutions set of the last generation produced in simulation **sym1-2**. It can be seen that a set of non-dominated solutions including 8 variants of ship structure has been found during the simulation. For the solution closest from the asymptotic solution, which was found in 6145 generation,  $f_{6145}^{\approx}(\mathbf{x})$ , the distance equals 1.088 in the normalized objective space, the structure weight is  $f_1(\mathbf{x}) = 1113.66$  kN and the surface area for maintenance is  $f_2(\mathbf{x}) = 7361.45$  m<sup>2</sup>:

$$\begin{aligned} \mathbf{f}_{\text{sym1-2}}^{\approx} &= f_{6145}^{\approx}(\mathbf{x}) = [f_{1;6145}^{\approx}(\mathbf{x}) \ f_{2;6145}^{\approx}(\mathbf{x})]^T = \\ &= [1113.66 \ 7361.45]^T \cdot [\text{kN} \ \text{m}^2] \end{aligned}$$

Figure 28a presents the evolution of macroscopic values characterizing the evolution of generated and evaluated ship structure variants population in simulation **sym1-3** in case of **random values of weight coefficients  $w_1$  and  $w_2$  equal to 0 or 1**, used for optimization criteria with dominance attributes

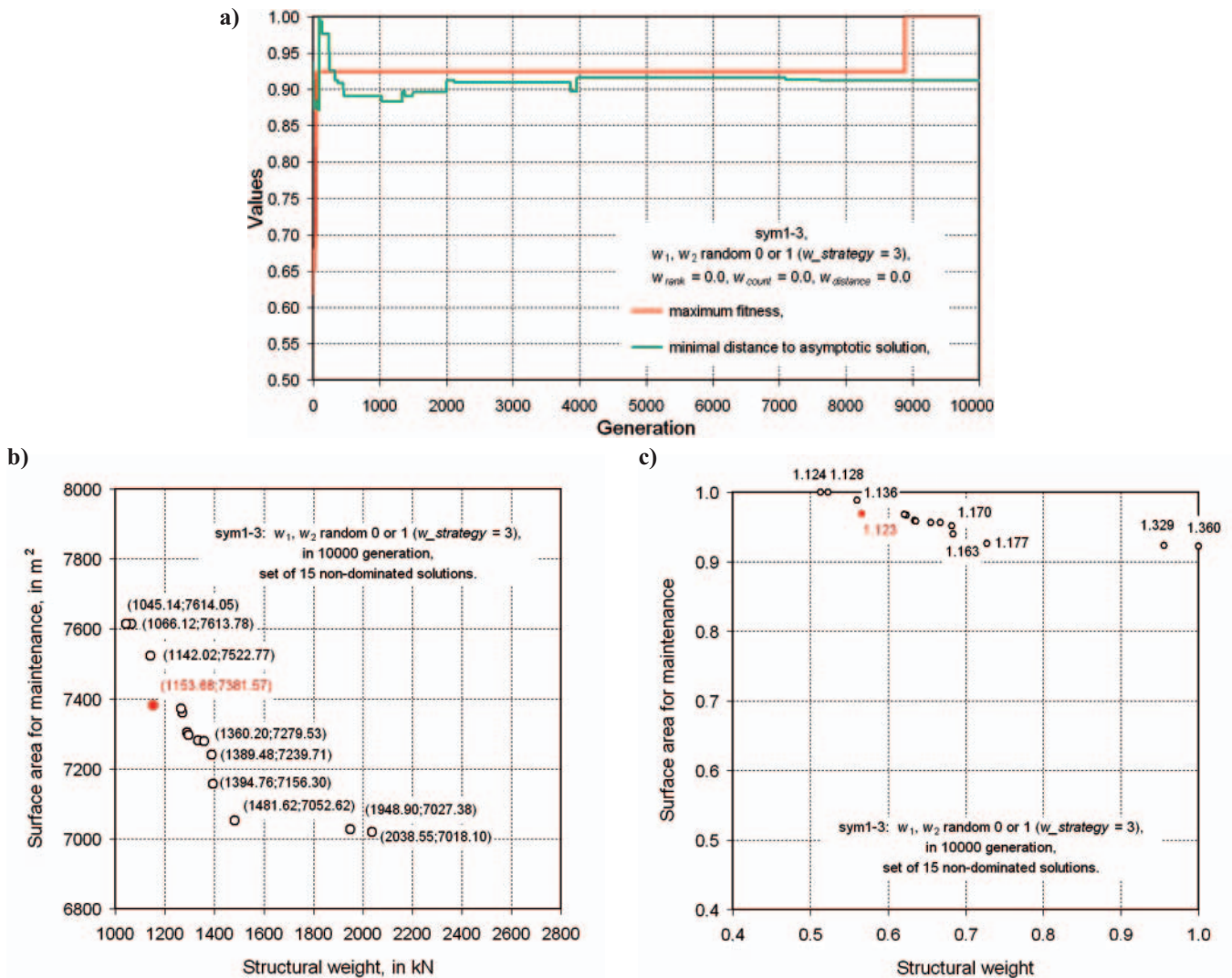


Fig. 28. Results of genetic multi-objective optimization of ship structure with respect to structural weight  $f_1$  and surface area  $f_2$  in case of **random values of weight coefficients  $w_1$  and  $w_2$  equal to 0 or 1** with dominance attributes being excluded from selection (**sym1-3**); **a)** the curves present the evolution of a highest value of fitness function  $f_{max}$ , the lowest value of non-dominated solution distance from a asymptotic one, **b)** detailed specification of final non-dominated solutions set in objective space, **c)** detailed specification of final non-dominated solutions set in normalized objective space; black circles represent non-dominated solutions, red dots represent non-dominated solution closest to the asymptotic one; dimensionless values are normalized to the interval  $[0,1]$  in relation to the highest values in the set

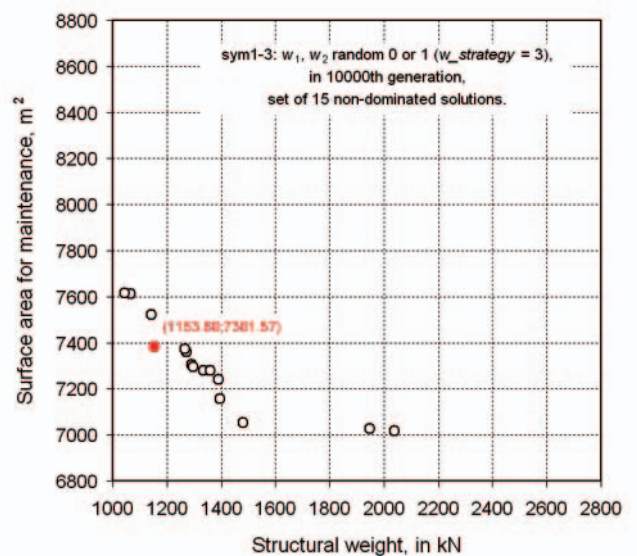
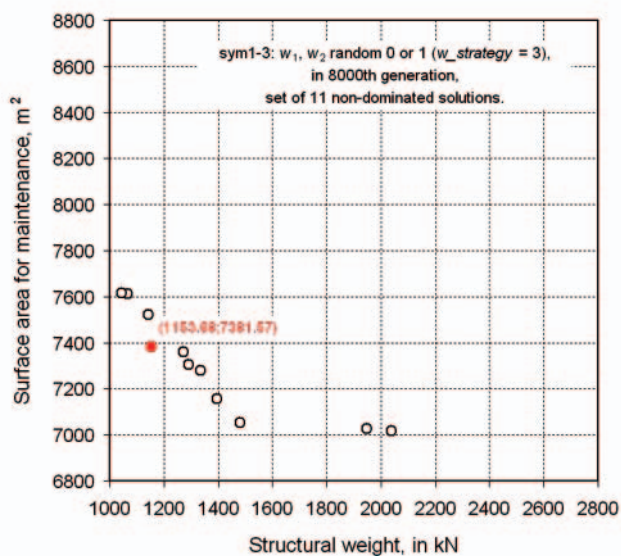
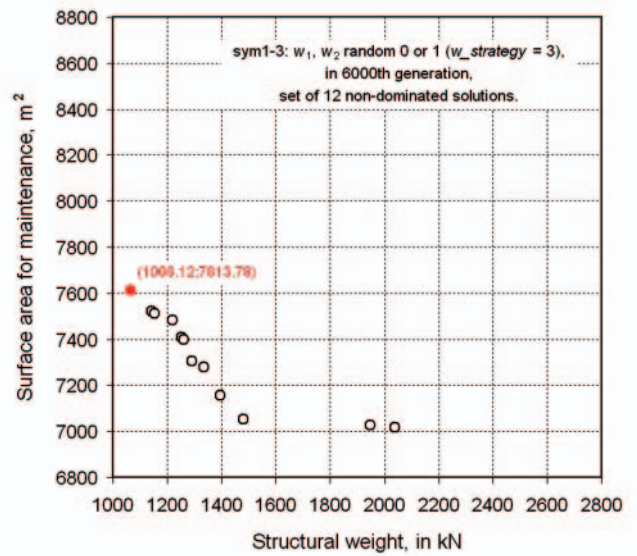
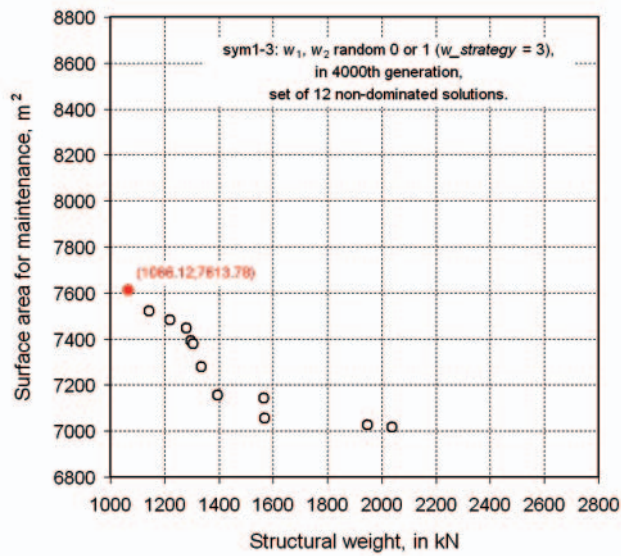
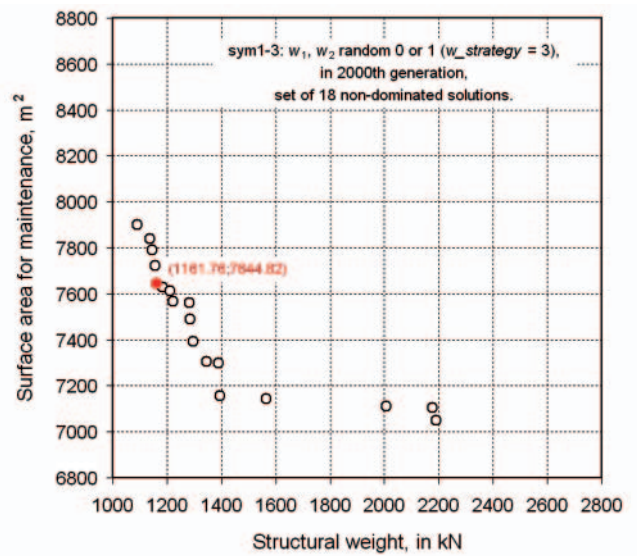
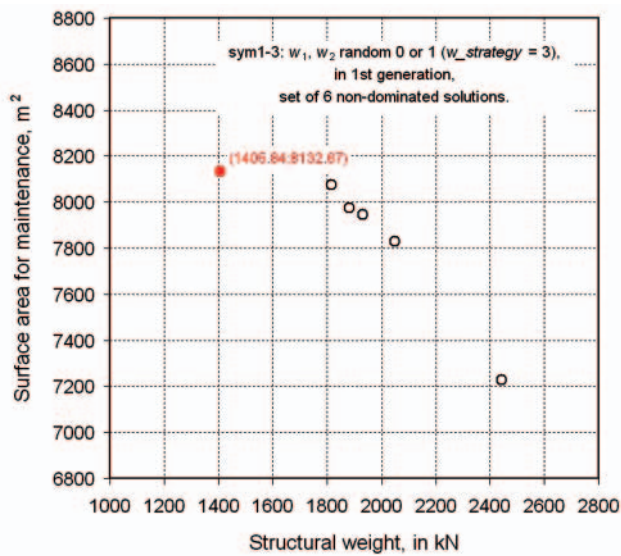


Fig. 29. History of the evolution of non-dominated solutions set during the genetic multi-objective optimization of ship structure with respect to structure weight  $f_1$  and surface area  $f_2$  in case of random values of weight coefficients  $w_1$  and  $w_2$  equal to 0 or 1 with dominance attributes being excluded from selection (sym1-3); black circles represent non-dominated solutions, red dots represent non-dominated solutions closest from the asymptotic one

being excluded from selection. The figure shows a desired continuous rise of the greatest value of fitness function  $f_{\max}$  indicating rising quality of the best generated test solutions. The highest values of fitness function do not saturate before 8888 generation. i.e. very close to the end of simulation. The lowest distance between a non-dominated solution and the asymptotic solution changes during the evolution, but above the threshold of 88.30% of the highest value found during the simulation it takes place only to a very small extent.

In Fig. 29 the evolution of the structure of the non-dominated solutions set in simulation sym1-3 is shown by using, as examples, the selected time-based cross-sections of this set, e.g. for 1, 2000, 4000, 6000, 8000 and 10.000 generations. Cardinality of non-dominated solutions set in the selected generations amounts to 6, 18, 12, 12, 11 and 15, respectively, and it does not change significantly in the course of simulation.

Figures 28b and 28c present a detailed structure of a non-dominated solutions set of the last generation produced in simulation sym3. In can be seen that the set of non-dominated solutions including 15 ship structural variants has been found during the simulation. For the solution closest to the asymptotic solution which was found in 7611 generation,  $f_{7611}^{\approx}(\mathbf{x})$ , the distance of 1.123 in the normalized objective space, the structural weight is  $f_1(\mathbf{x}) = 1153.68$  kN and the surface area for maintenance is  $f_2(\mathbf{x}) = 7381.57$  m<sup>2</sup>:

$$\begin{aligned} \tilde{\mathbf{f}}_{\text{sym1-3}} &= \tilde{\mathbf{f}}_{7611}^{\approx}(\mathbf{x}) = [f_{1,7611}^{\approx}(\mathbf{x}) \ f_{2,7611}^{\approx}(\mathbf{x})]^T = \\ &= [1153.68 \ 7381.57]^T \cdot [\text{kN} \ \text{m}^2] \end{aligned}$$

### Results of computational investigations – Series2: the simulation marked with symbols sym2-1, sym2-2 and sym2-3

Figure 30 presents the evolution of macroscopic values characterizing the evolution of generated and evaluated ship structure variants population in simulation **sym2-1**: (1) the greatest fitness value  $f_{\max}$ , and (2) the lowest distance between the feasible variant and the asymptotic solution. Multi-objective optimization of ship structure with respect to structural weight  $f_1$  as well surface area for cleaning and painting,  $f_2$ , in the case of the values of optimization criteria weight coefficients,  $w_1 = w_2 = 0.0$ , dominance count,  $w_{\text{count}} = 0.0$  and the distance from asymptotic solution,  $w_{\text{distance}} = 0.0$ ; evolution of generations is governed by dominance rank,  $w_{\text{rank}} = 3.0$ , and constraints components,  $w_k \neq 0, k = 1, 2, \dots, n_c$ . The figure

shows a desired continuous rise of the greatest value of fitness function  $f_{\max}$  indicating rising quality of the best generated test variants. There can also be seen a very early, reached already in 585 generation, saturation of the fitness function maximum value  $f_{\max}$ . The smallest distance of the non-dominated solution from the asymptotic solution varies in course of evolution, but only in a small range over 79.42% of the greatest value found during the simulation.

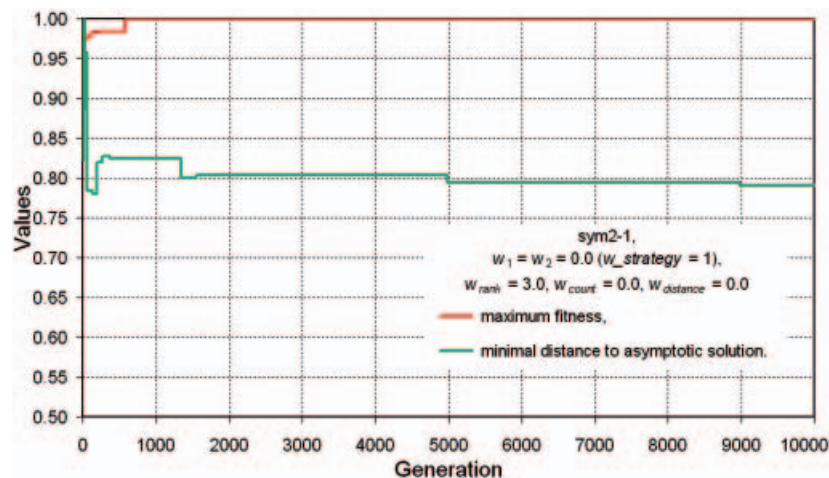
In Fig. 31 the evolution of the structure of the non-dominated solutions set in simulation sym2-1 is shown by using as examples the selected time-based cross-sections of this set, e.g. for 1, 2000, 4000, 6000, 8000 and 10.000 generations. Cardinality of non-dominated solutions set in the selected generations amounts to 4, 8, 6, 8, 8 and 10, respectively, and it does not change significantly in the course of simulation.

Figure 32 presents the detailed structure of the non-dominated solutions set of the last generation, presented in a physical space of objectives and the normalized space of objectives. In can be seen that a set of non-dominated solutions including 10 variants of ship structure has been found during the simulation. For each non-dominated variant the values of optimization criteria have been specified as:  $f_1(\mathbf{x})$  – structural weight and  $f_2(\mathbf{x})$  – cleaned/painted surface area. The designer may select, for further development, one of the variants or a group of them deemed by him to be the best. For the variant closest from the asymptotic solution, which was found already in 196 generation, the distance equals 1.064 in the normalized objective space, the structural weight is  $f_1(\mathbf{x}) = 1105.95$  kN and the cleaned/painted surface area is  $f_2(\mathbf{x}) = 7345.11$  m<sup>2</sup>:

$$\begin{aligned} \tilde{\mathbf{f}}_{\text{sym2-1}} &= \tilde{\mathbf{f}}_{196}^{\approx}(\mathbf{x}) = [f_{1,196}^{\approx}(\mathbf{x}) \ f_{2,196}^{\approx}(\mathbf{x})]^T = \\ &= [1105.95 \ 7345.11]^T \cdot [\text{kN} \ \text{m}^2] \end{aligned}$$

This variant may be recommended if there is a need to select a single solution for the formulated ship structure multi-objective optimization problem.

Figure 33 presents the evolution of macroscopic values characterizing the evolution of generated and evaluated ship structure variants population in simulation **sym2-2**. Multi-objective optimization of ship structure with respect to the structural weight  $f_1$  as well as surface for cleaning and painting  $f_2$  in case of the values of optimization criteria weight coefficients,  $w_1 = w_2 = 0$ , dominance rank,  $w_{\text{rank}} = 0.0$  as well as the distance from asymptotic solution,  $w_{\text{distance}} = 0.0$ ; evolution of generations is governed by dominance count,  $w_{\text{count}} = 3.0$ , and constraints components,  $w_k \neq 0, k = 1, 2, \dots, n_c$ . The figure



**Fig. 30.** The results of multi-objective genetic optimization of ship structure with respect to the structure weight  $f_1$  and the area of element surface  $f_2$ , in case of the fixed values of weight coefficients  $w_1 = w_2 = 0.0$ , with dominance count and the distance from a asymptotic solution being excluded from selection:  $w_{\text{count}} = 0.0$ ,  $w_{\text{distance}} = 0.0$ , the evolution is governed by dominance rank,  $w_{\text{rank}} = 3.0$ , and constraints components, (**sym2-1**); the curves present the evolution of the highest value of fitness function  $f_{\max}$  and the lowest value of the non-dominated solution distance from a asymptotic one; the values are dimensionless and standardized in  $[0,1]$  range in relation to the highest values found during the simulation

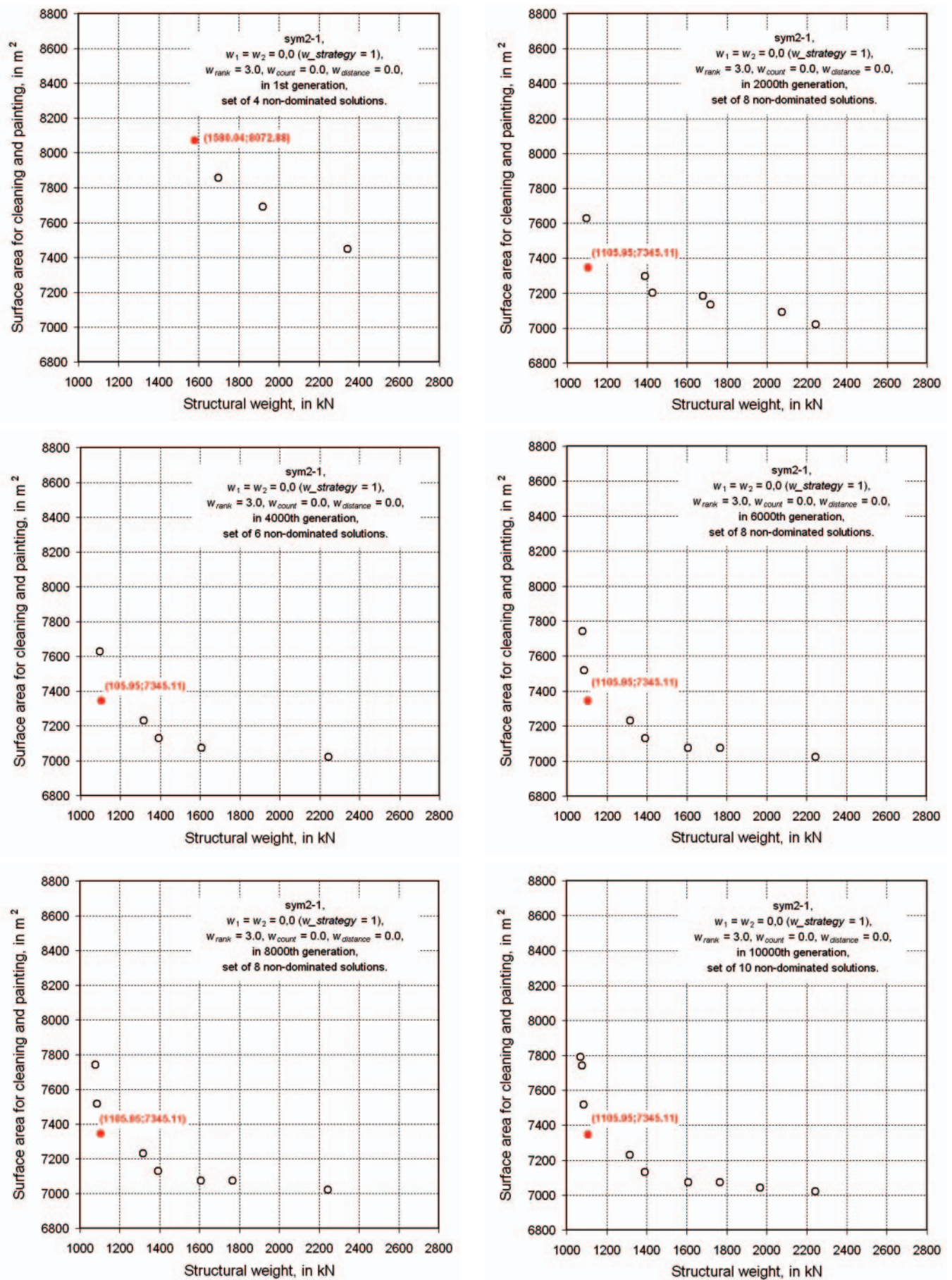


Fig. 31. History of the evolution of the non-dominated solutions set during the genetic multi-objective optimization of ship structure with respect to the structure weight  $f_1$  and surface area  $f_2$  in case of the fixed values of weight coefficients  $w_1 = w_2 = 0.0$ , with dominance count and the distance from a asymptotic solution being excluded from selection:  $w_{count} = 0.0$ ,  $w_{distance} = 0.0$ , the evolution is governed by dominance rank,  $w_{rank} = 3.0$ , and constraints components, (sym2-1); black circles represent non-dominated solutions, red dots represent non-dominated solutions closest to the asymptotic one

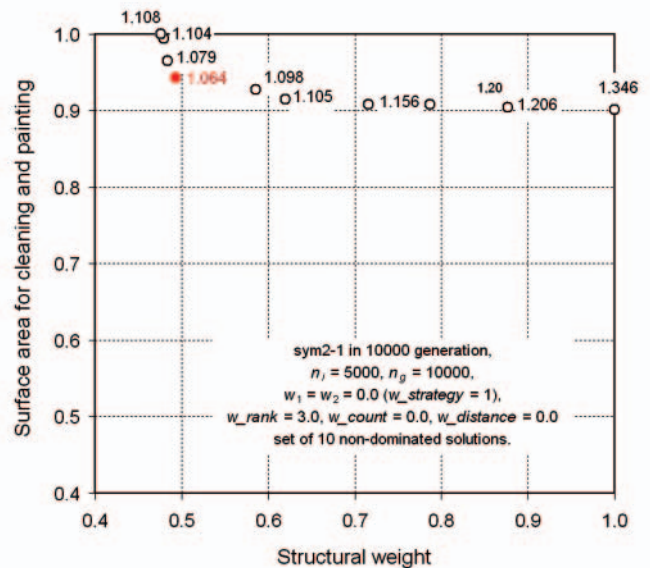
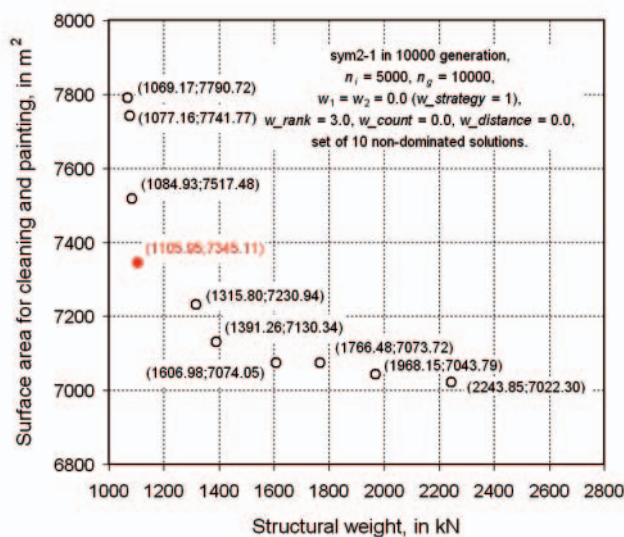


Fig. 32. Detailed specification of the non-dominated solutions set obtained during the genetic multi-objective optimization of ship structure with respect to the structure weight  $f_1$  and surface area  $f_2$ , in case of exclusion from selection: optimization criteria,  $w_1 = w_2 = 0.0$ , dominance count,  $w_{count} = 0.0$  and distance from asymptotic solution,  $w_{distance} = 0.0$ ; the evolution is governed by dominance rank,  $w_{rank} = 3.0$ , and constraints components, (sym2-1); black circles represent non-dominated solutions, red dots represent non-dominated solutions closest from the asymptotic one; dimensionless values are normalized to the interval  $[0,1]$  in relation to the highest values in the set

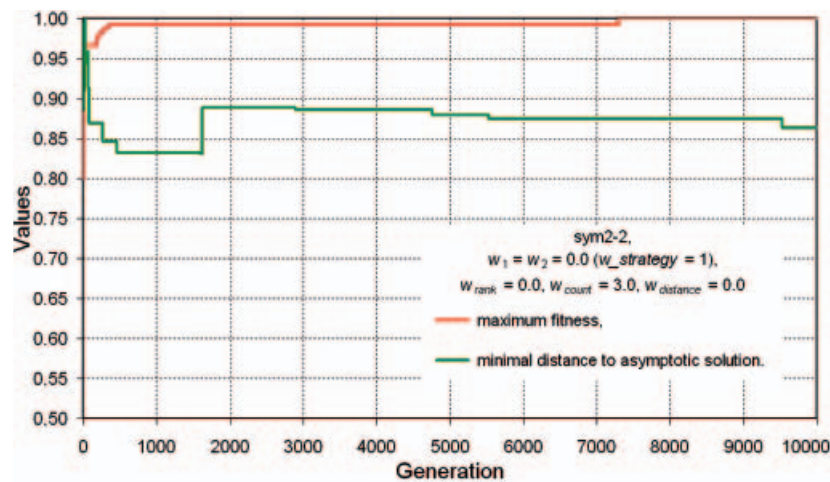


Fig. 33. The results of multi-objective genetic optimization of ship structure with respect to the structure weight  $f_1$  and the area of element surface  $f_2$  in case of the fixed values of weight coefficients  $w_1 = w_2 = 0.0$ , with dominance rank and the distance from a asymptotic solution being excluded from selection:  $w_{rank} = 0.0$ ,  $w_{distance} = 0.0$ , the evolution is governed by dominance count,  $w_{count} = 3.0$ , and constraints components, (sym2-2); the curves present the evolution of the highest value of fitness function  $f_{max}$  and the lowest value of non-dominated solution distance from a asymptotic one; the values are dimensionless and standardized in  $[0,1]$  range in relation to the highest values found during the simulation

shows a desired continuous rise of the greatest value of fitness function  $f_{max}$  indicating rising quality of the best generated test variants. The figure also shows fairly late, reached in 7301 generation, saturation of the maximum value of fitness function  $f_{max}$ . Minimum distance of the non-dominated solution from the asymptotic solution varies during the simulation but only in a small range over 83.18% of the greatest value found during the simulation.

In Fig. 34 the evolution of the structure of the non-dominated solutions set in simulation sym2-2 is shown by using as examples the selected time-based cross-sections of this set, e.g. for 1, 2000, 4000, 6000, 8000 and 10.000 generations. Cardinality of non-dominated solutions set in the selected generations amounts respectively to 4, 12, 12, 12, 13 and 13, and it does not change significantly in the course of simulation.

Figure 35 presents a detailed structure of the non-dominated solutions set of the last generation, presented in a physical space of objectives and the normalized space of objectives. In can be seen that a set of non-dominated solutions including 13

variants of ship structure has been found during the simulation. For each non-dominated variant the values of optimization criteria have been specified as:  $f_1(\mathbf{x})$  – structural weight and  $f_2(\mathbf{x})$  – cleaned/painted surface area. The designer may select, for further development, one of these variants or a group of them deemed by him to be the best. For the variant closest from the asymptotic solution, which was found in 5533 generation, the distance equals 1.047 in the normalized objective space, the structural weight is  $f_1(\mathbf{x}) = 1192.04$  kN and the cleaned/painted surface area is  $f_2(\mathbf{x}) = 7327.41$  m<sup>2</sup>:

$$\begin{aligned} \tilde{\mathbf{f}}_{\text{sym2-2}} &= \tilde{\mathbf{f}}_{5533}(\mathbf{x}) = [f_{1,5533}(\mathbf{x}) \ f_{2,5533}(\mathbf{x})]^T = \\ &= [1192.04 \ 7327.41]^T \cdot [\text{kN} \ \text{m}^2] \end{aligned}$$

This variant may be recommended if there is a need to select a single solution for the formulated ship structure multi-objective optimization problem.

Figure 36 presents the evolution of macroscopic values characterizing the evolution of generated and evaluated ship structure variants population in simulation sym2-3. Multi-objective optimization of ship structure with respect to the



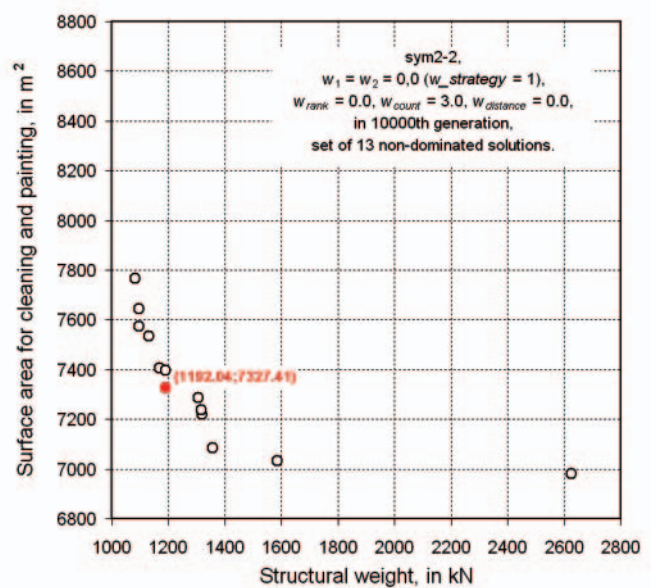
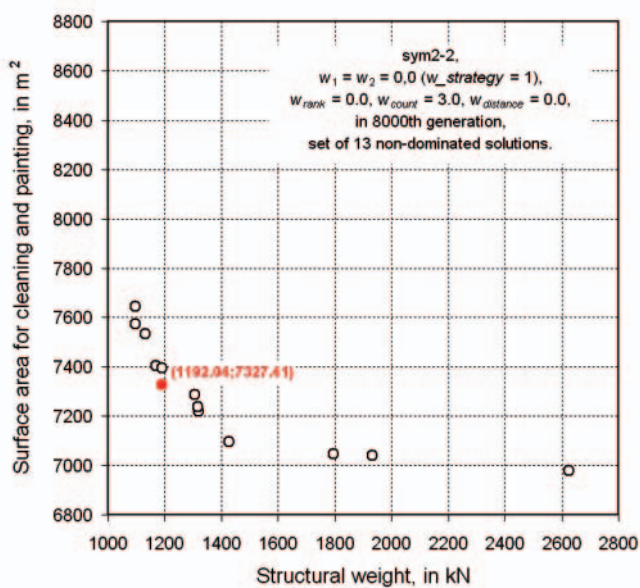
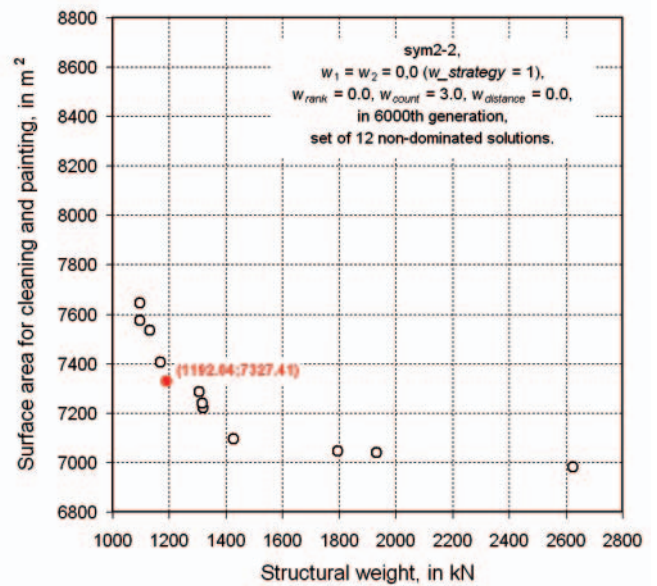
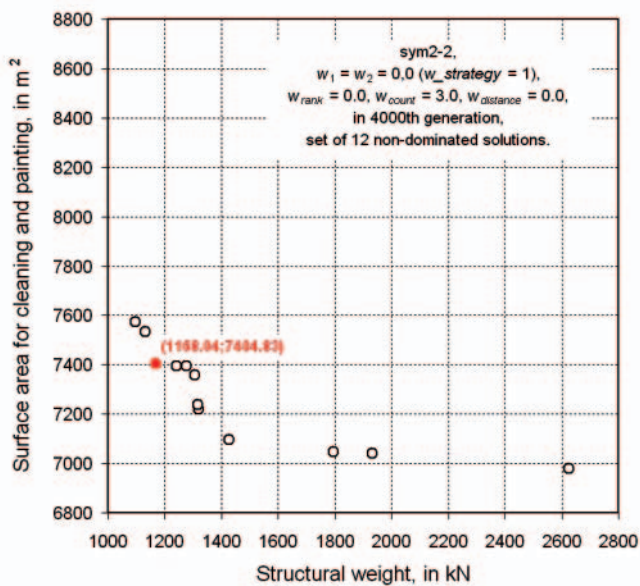
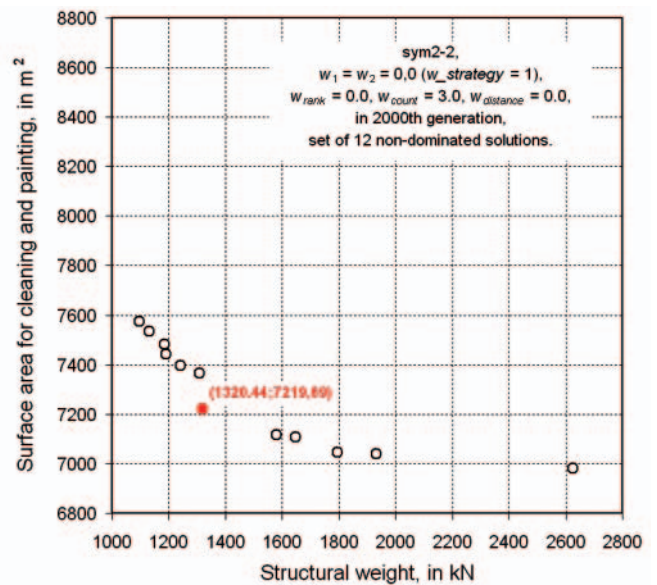
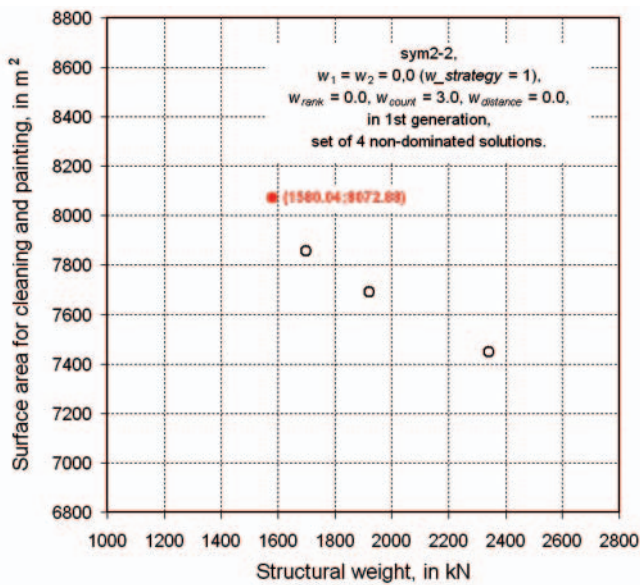


Fig. 34. History of the evolution of the non-dominated solutions set during the genetic multi-objective optimization of ship structure with respect to the structure weight  $f_1$  and surface area  $f_2$  in case of the fixed values of weight coefficients  $w_1 = w_2 = 0.0$ , with dominance rank and the distance from a asymptotic solution being excluded from selection:  $w_{rank} = 0.0$ ,  $w_{distance} = 0.0$ , the evolution is governed by dominance count,  $w_{count} = 3.0$ , and constraints components, (sym2-2); black circles represent non-dominated solutions, red dots represent non-dominated solutions closest from the asymptotic one

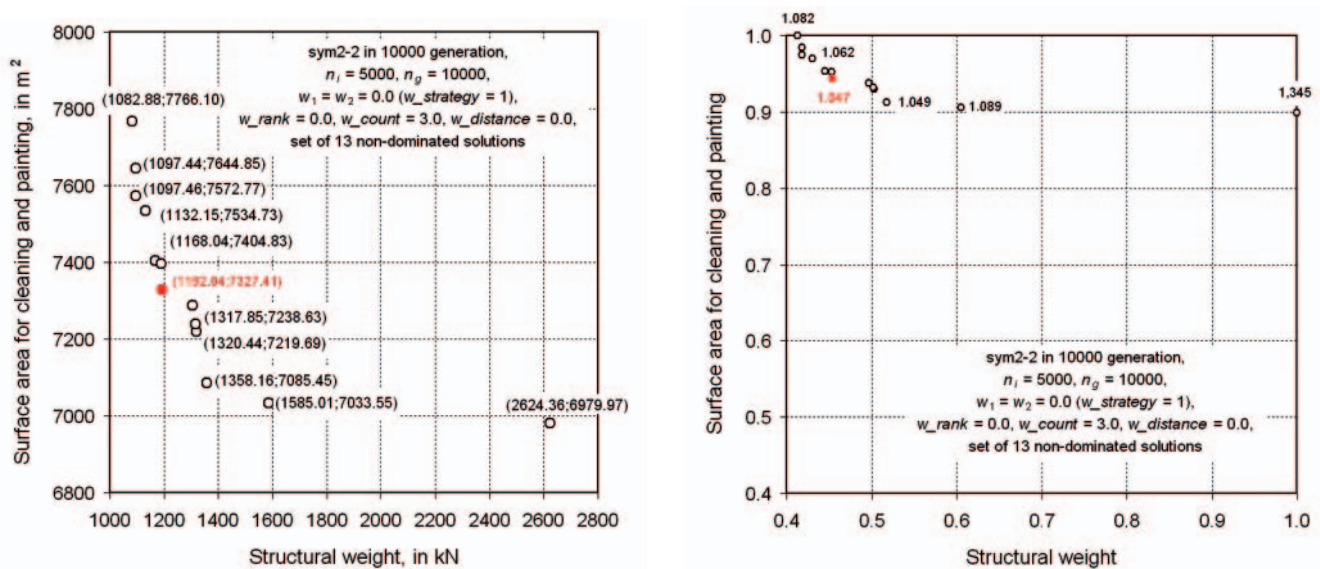


Fig. 35. Detailed specification of the non-dominated solutions set obtained during the genetic multi-objective optimization of ship structure with respect to the structure weight  $f_1$  and surface area  $f_2$  in case of exclusion from selection: optimization criteria,  $w_1 = w_2 = 0.0$ , dominance rank,  $w_{rank} = 0.0$  and distance from asymptotic solution,  $w_{distance} = 0.0$ ; evolution is governed by dominance count,  $w_{count} = 3.0$ , and penalty components, (sym2-2); black circles represent non-dominated solutions, red dots represent non-dominated solutions closest from the asymptotic one; dimensionless values are normalized to the interval  $[0,1]$  in relation to the highest values in the set

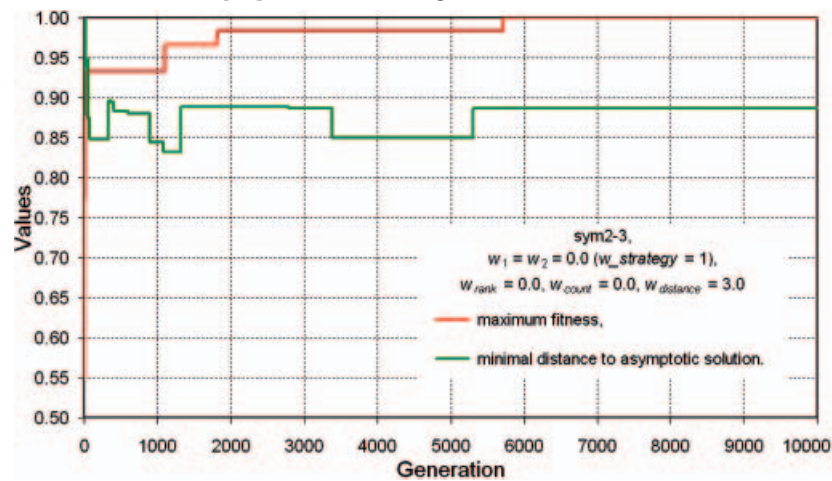


Fig. 36. The results of multi-objective genetic optimization of ship structure with respect to the structure weight  $f_1$  and the area of element surface  $f_2$  in case of the fixed values of weight coefficients:  $w_1 = w_2 = 0.0$ , with dominance rank and the dominance count being excluded from selection:  $w_{rank} = 0.0$ ,  $w_{count} = 0.0$ , the evolution is governed by the distance from asymptotic solution,  $w_{distance} = 3.0$ , and constraints components, (sym2-3); the curves present the evolution of the highest value of fitness function  $f_{max}$  and the lowest value of non-dominated solution distance from an asymptotic one; the values are dimensionless and standardized in  $[0,1]$  range in relation to the highest values found during the simulation

structural weight  $f_1$  as well as surface area for cleaning and painting,  $f_2$ , in the weight coefficients values of optimization criteria  $w_1 = w_2 = 0$ , dominance rank,  $w_{rank} = 0.0$  and the dominance count,  $w_{count} = 0.0$ ; evolution of generations is governed by the distance from asymptotic solution,  $w_{distance} = 3.0$ , and constraints components,  $w_k \neq 0$ ,  $k = 1, 2, \dots, n_c$ . The figure shows a desired continuous rise of the greatest value of fitness function  $f_{max}$  indicating rising quality of the best generated test variants. The figure also shows fairly late, reached in 5714 generation, saturation of the maximum value of fitness function  $f_{max}$ . Minimum distance of the non-dominated solution from the asymptotic solution varies during the simulation but only in a small range over 83.25% of the greatest value found during the simulation.

In Figure 37 the evolution of the structure of the non-dominated solutions set in simulation sym2-3 is shown by using, as examples, the selected time-based cross-sections of this set, e.g. for 1, 2000, 4000, 6000, 8000 and 10.000 generations. Cardinality of non-dominated solutions set in these selected generations amounts to 4, 10, 12, 11, 14 and 13, respectively, and it does not change significantly in the course of simulation.

Figure 38 presents the detailed structure of a non-dominated solutions set of the last generation, presented in a physical space of objectives and the normalized space of objectives. In can be seen that a set of non-dominated solutions including 13 variants of ship structure has been found during the simulation. For each non-dominated variant the values of optimization criteria have been specified as:  $f_1(\mathbf{x})$  – structural weight and  $f_2(\mathbf{x})$  – cleaned/painted surface area. The designer may select, for further development, one of these variants or a group of them deemed by him to be the best. For the variant closest to the asymptotic solution, which was found in 5305 generation, the distance equals 1.085 in the normalized objective space, the structural weight is  $f_1(\mathbf{x}) = 1060.03$  kN and the cleaned/painted surface area is  $f_2(\mathbf{x}) = 7485.93$  m<sup>2</sup>:

$$\begin{aligned} \mathbf{f}_{\text{sym2-3}}^* &= \mathbf{f}_{5305}^*(\mathbf{x}) = [f_{1,5305}^*(\mathbf{x}) \ f_{2,5305}^*(\mathbf{x})]^T = \\ &= [1060.03 \ 7485.93]^T \cdot [\text{kN} \ \text{m}^2] \end{aligned}$$

This variant may be recommended if there is a need to select a single solution for the formulated ship structure multi-objective optimization problem.

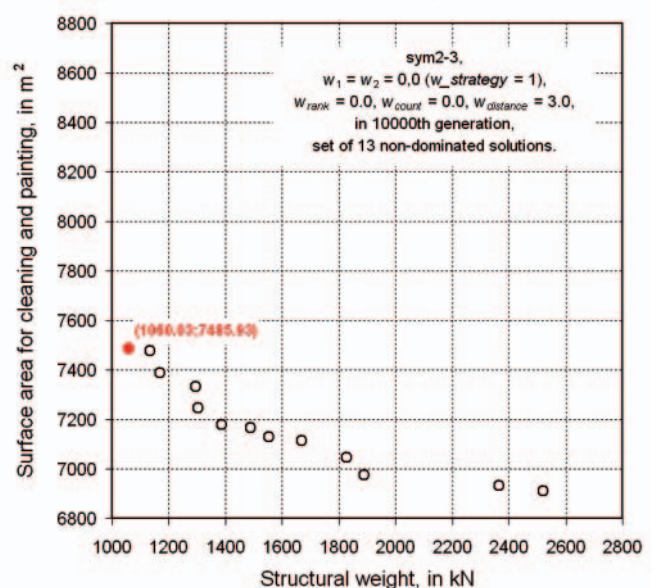
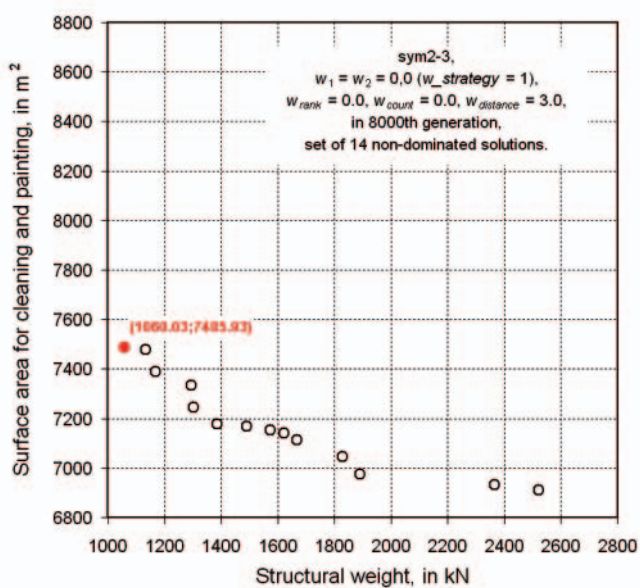
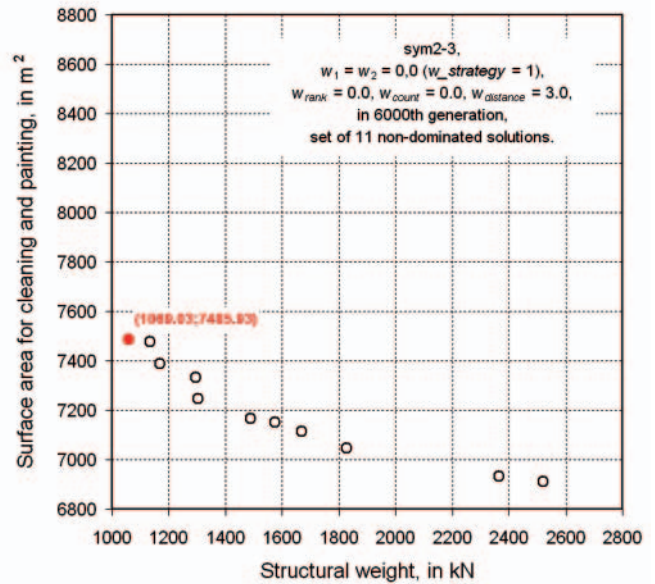
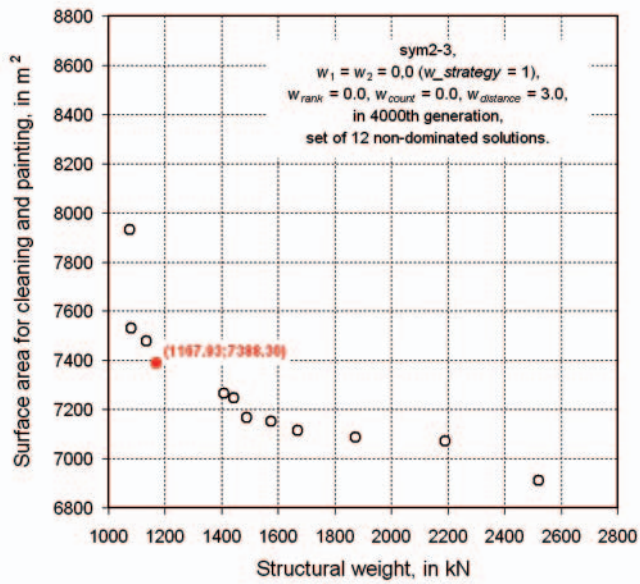
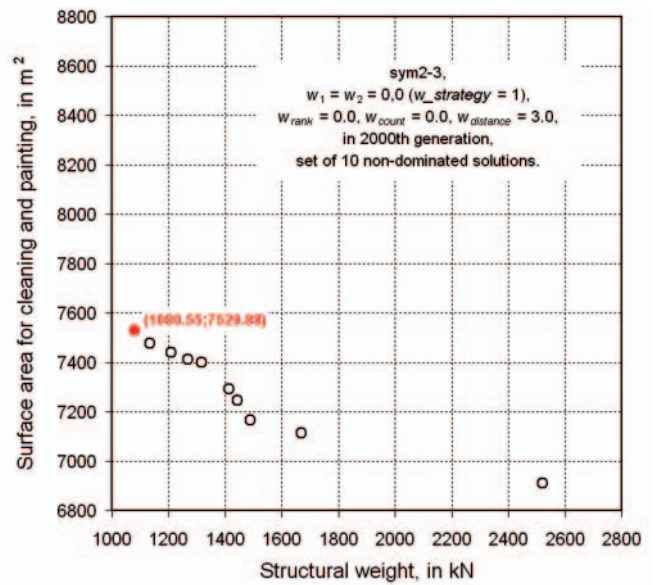
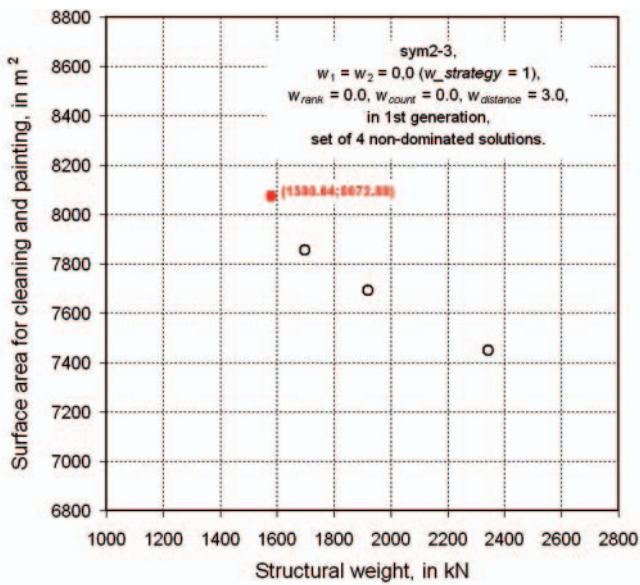


Fig. 37. History of the evolution of the non-dominated solutions set during the genetic multi-objective optimization of ship structure with respect to the structure weight  $f_1$  and surface area  $f_2$  in case of the fixed values of weight coefficients  $w_1 = w_2 = 0.0$ , with dominance rank and the dominance count being excluded from selection:  $w_{rank} = 0.0, w_{count} = 0.0$ , the evolution is governed by distance from asymptotic solution,  $w_{distance} = 3.0$ , and constraints components, (sym2-3); black circles represent non-dominated solutions, red dots represent non-dominated solutions closest from the asymptotic one

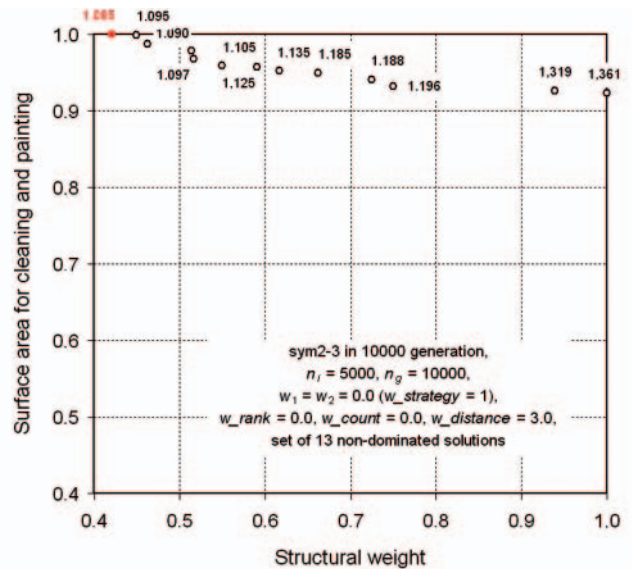
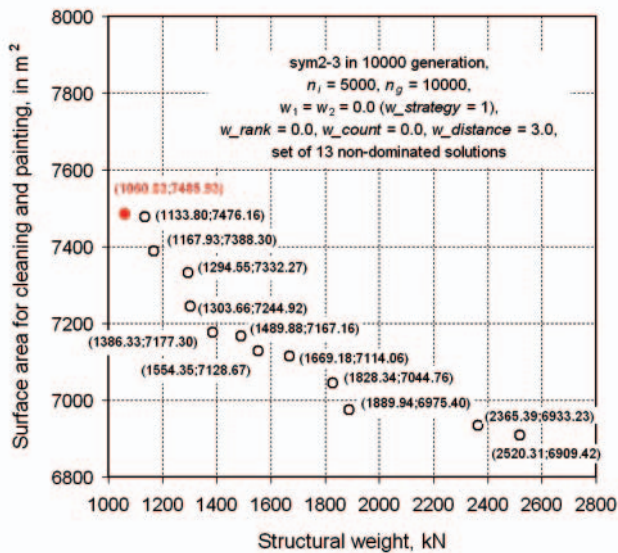


Fig. 38. Detailed specification of the non-dominated solutions set obtained during the genetic multi-objective optimization of ship structure with respect to the structure weight  $f_1$  and surface area  $f_2$  in case of exclusion from selection: optimization criteria,  $w_1 = w_2 = 0.0$ , dominance rank,  $w\_rank = 0.0$  and dominance count,  $w\_count = 0.0$ ; evolution is governed by distance from the asymptotic solution,  $w\_distance = 3.0$ , and constraints components, (sym2-3); black circles represent non-dominated solutions, red dots represent non-dominated solutions closest from the asymptotic one; dimensionless values are normalized to the interval  $[0,1]$  in relation to the highest values in the set

## REFERENCES

1. Abraham, A., Jain, L. and Goldberg, R., 2005. *Evolutionary Multiobjective Optimization*. Springer.
2. Back, T., 1996. *Evolutionary Algorithms in Theory and Practice*. Oxford University Press, New York.
3. Binh, T.T. and Korn, U., 1997. MOBES: A Multiobjective Evolution Strategy for Constrained Optimization Problems. In: *The Third International Conference on Genetic Algorithms (Mendel 97)*, 25-27 June 1997, Brno, Czech Republic, 176-182.
4. Darwin, Ch., 1859. *Origin of Species*. John Murray, London.
5. Coello Coello, C.A., Lamont, G.B. and Veldhuizen, D.A., 2007. *Evolutionary Algorithms for Solving Multi-objective Problems*. Springer.
6. Cohon, J.L., 1978. *Multiobjective Programming and Planning*. New York, Academic Press.
7. Coley, D.A., 1999. *An Introduction to Genetic Algorithms for Scientists and Engineers*. World Scientific, Singapore.
8. Das, P.K., 1993. Reliability – Based Design Procedure of Stiffened Cylinder Using Multiple Criteria Optimisation Techniques. In: *Proceedings of Offshore Technology Conference, OTC 1993*, Vol. 3, No. 7236, 297-313.
9. Das, P.K., Tolikas, C., Morandi, A.C., Zanic, V. and Warren, N.F., 1993. Multiple Criteria Synthesis Technique Applied to the Reliability Based Structural Design of Hull Components of A Fast Swath Ship. In: *Proceedings of Second International Conference on Fast Sea Transportation, FAST '93*, Japan, Tokyo, Vol. 1, 473-487.
10. Davis, L. 1991. *Handbook of Genetic Algorithms*. New York: Van Nostrand.
11. De Jong, K., 1995. On Decentralizing Selection Algorithms. In: *Proceedings of the Sixth International Conference on Genetic Algorithms*, 15-19 July 1995, Pittsburgh, PA, USA, Morgan Kaufmann Publishers, San Francisco, 17-23.
12. Deb, K., 2001. *Multi-Objective Optimization using Evolutionary Algorithms*. John Wiley & Sons.
13. Deb, K., Agrawal, S., Pratap, A. and Meyarivan, T., 2000. *A Fast Elitist Non-Dominated Sorting Genetic Algorithm for Multi-Objective Optimization: NSGA-II*. KanGAL Report 200001, Indian Institute of Technology, Kanpur, India.
14. Edgeworth, F.Y., 1881. *Mathematical Physics: An Essay on the Application of Mathematics to the Moral Sciences*. Paul Keagan, London, England.
15. Eschenauer, H., Koski, J. and Osyczka, A., 1990. *Multicriteria Design Optimisation*. Berlin: Springer-Verlag, Berlin.
16. Fonseca, C.M. and Fleming, P.J., 1993. Genetic Algorithms for Multiobjective Optimization: Formulation, Discussion and Generalization. In: *5th International Conference on Genetic Algorithms, Proceedings*, 416-423.
17. Fonseca, C.M. and Fleming, P.J., 1996. On the Performance Assessment and Comparison of Stochastic Multiobjective Optimizers. In: *Parallel Problem Solving from Nature – PPSN IV*, September 1996, Berlin, Germany, Lecture Notes in Computer Science, Springer-Verlag, Berlin, Germany, 585-593.
18. Fonseca, C.M., Knowles, J.D., Thiele, L. and Zitzler, E., 2005. A Tutorial on the Performance Assessment of Stochastic Multiobjective Optimizers. Invited talk. In: *Evolutionary Multi-Criterion Optimization Conference (EMO 2005)*, 9-11 March 2005, Guanajuato, Mexico, Lecture Notes in Computer Science 3410, Springer 2005,
19. Fox, R.L., 1971. *Optimization Methods for Engineering Design*. Addison-Wesley Publishing Company, Inc., Reading.
20. Goldberg, D.E., 1989. *Genetic Algorithms in Search, Optimization and Machine Learning*. Addison-Wesley Longman Publishing Co., Inc. Boston, MA, USA.
21. Goldberg, D.E. and Deb K., 1991. A Comparative Analysis of Selection Schemes Used in Genetic Algorithms. In: *Foundations of Genetic Algorithms*. Morgan Kaufmann Publishers, San Mateo, 69-93.
22. Hajela, P. and Lin, C.Y., 1992. Genetic Search Strategies in Multicriterion Optimal Design. *Structural Optimization*, 4: 99-107.
23. HANSA, 1997. *Polish fast ferry "Boomerang"*. 6:26-29.
24. Hansen, M.P. and Jaszkiewicz, A., 1998. *Evaluating the quality of approximations of the non-dominated set*. Technical report, Institute of Mathematical Modeling, Technical University of Denmark, IMM Technical Report IMM-REP-1998-7.
25. Horn, J., Nafpliotis, N. and Goldberg, D.E., 1994. A Niche Pareto Genetic Algorithm for Multiobjective Optimization. In: *First IEEE Conference on Evolutionary Computation*, IEEE World Congress on Computational Intelligence, 1: 82-87.
26. Hughes, E.J., 2003. Multiple Single Objective Sampling. In: *Proceedings of 2003 Congress on Evolutionary Computation, CEC 2003*, 8 - 12 December 2003, Canberra, Australia, 2678-2684.
27. Hughes, E.J., 2005. Evolutionary Many-objective Optimization: Many Once or One Many? In: *Proceedings of 2005 Congress of Evolutionary Computation, CEC 2005*, 2-4 September 2005, Edinburgh, Scotland, UK, IEEE Press, 222-227.

28. Hutchinson, K., Todd, D. and Sen, P., 1998. An evolutionary multiple objective strategy for the optimisation of made-to-order products with special reference to the conceptual design of high speed mono hull roll-on/roll-off passenger ferries. *In: Proceedings of International Conference of Royal Institution of Naval Architects*.
29. Ishibuchi, H. and Murata, T., 1996. Multi-objective genetic local search algorithm. *In: Proceedings of IEEE International Conference on Evolutionary Computation (ICEC '96)*, Piscataway, NJ, IEEE Press, 119-124.
30. Jang, C.D. and Shin, S.H., 1997. A Study on the Optimal Structural Design for Oil Tankers Using Multi Objective Optimization. *In: Proceedings of 6th International Marine Design Conference, IMDC '97*, Newcastle, 23-25 June 1997, University of Newcastle, United Kingdom, Vol. 1, Penshaw Press, 217-231.
31. Jaskiewicz, A., 2004. On the Computational Efficiency of Multiple Objective Metaheuristics: The Knapsack Problem Case Study. *European Journal of Operational Research*, 158:418-433.
32. Jianguo, W. and Zuoshui, X., 1996. Symmetric Solution of Fuzzy Multi-Objective Optimization for Ship Structure. *Journal East China Shipbuilding Institute*, 10(1): 1-7.
33. Kitamura, M., Nobukawa, H. and Yang, F., 2000. Application of a genetic algorithm to the optimal structural design of a ship's engine room taking dynamic constraints into consideration. *Journal of Marine Science and Technology*, Vol. 5, 131-146.
34. Klanac, A., Ehlers, S. and Jelovica, J., 2009. Optimization of crashworthy marine structures. *Marine Structures*, Vol. 22, 670-690.
35. Knowles, J. and Corne, D., 1999. The Pareto Archived Evolution Strategy: a New Baseline Algorithm for Multiobjective Optimisation. *In: 1999 Congress on Evolutionary Computation, CEC99*, Washington, D.C., 6-9 July 1999, IEEE Service Center, 98-105.
36. Knowles, J.D., Thiele, L. and Zitzler, E., 2006. *A tutorial on the Performance Assessment of Stochastic Multiobjective Optimizers*. Computer Engineering and Networks Laboratory, ETH Zurich, Switzerland, TIK-Report No. 214.
37. Kursawe, F., 1991. A variant of evolution strategies for vector optimization. *In: Proceedings of the 1st Workshop on Parallel Problem Solving from Nature (PPSN I)*, 1-3 October 1990, Dortmund, Berlin, Springer-Verlag, 193-197.
38. Leyland, G., 2002. *Multi-objective Optimization Applied to Industrial Energy Problems*. PhD Thesis, École Polytechnique Fédérale de Lausanne.
39. Man, K.F., Tang, K.S. and Kwong, S., 1999. *Genetic Algorithms*. Springer-Verlag, London.
40. Michalewicz, Z., 1996. *Genetic Algorithms + Data Structures = Evolutionary Programs*. Berlin-Heidelberg: Springer-Verlag.
41. Murata, T. and Ishibuchi, H., 1995. MOGA: Multi-objective genetic algorithms. *In: Proceedings of the Second IEEE International Conference on Evolutionary Computation*, 289-294. *In Proceedings of the Second IEEE International Conference on Evolutionary Computation*, IEEE Press, 289-294.
42. Okada, T. and Neki, I., 1992. Utilization of Genetic Algorithm for Optimizing the Design of Ship Hull Structure. *Journal of the Society of Naval Architect of Japan*, 171: 71-83.
43. Osyczka, A., 2002. *Evolutionary Algorithms for Single and Multicriteria Design Optimization*. Heidelberg: Physica-Verlag.
44. Pareto, V., 1896. *Cours D'Economie Politique, Volume 1*. Lausanne: F. Rouge.
45. Parsons, M.G. and Singer, D., 2000. A Fuzzy Logic Agent for Design Team Communications and Negotiations. *In: Conference on Computer Applications and Information Technology in the Maritime Industries, COMPIT 2000*, March 2000, Potsdam/ Berlin.
46. Purshouse, R.C. and Fleming, P.J., 2003. Evolutionary Many-Objective Optimization: An Exploratory Analysis. *In: Proceedings of 2003 Congress on Evolutionary Computation, CEC2003*, 8-12 Dec 2003, Canberra, Australia, IEEE, Piscataway, N.J., USA, 2066-2073.
47. Ray, T. and Sha, O.P., 1994. Multicriteria Optimisation Model for a Containership Design. *Marine Technology*, 31(4): 258-268.
48. Reklaitis, G.V., Ravindran, A. and Ragsdell, K.M., 1983. *Engineering Optimization. Methods and Applications*. New York: John Wiley and Sons, New York.
49. Ryan, D.M., 1974. Penalty and Barrier Functions. *In: P.E. Gill and W. Murray (Eds.) Numerical Methods for Constrained Optimization*, Academy Press, London.
50. Sarker, R. and Coello Coello, C.A., 2002. Evolutionary Optimization, Chapter 7, Assessment methodologies for multiobjective evolutionary algorithms. *In: R. Sarker, M. Mohammadian, X. Yao (Editors) Evolutionary Optimization*, Academic Publishers, Boston, 177-195.
51. Sarker, R., Mohammadian, M. and Yao, X., (Eds.), 2002. *Evolutionary Optimization, Part III, Multi-objective Optimization*. Boston: Kluwer Academic Publishers.
52. Schaffer, J.D., 1985. Multiple Objective Optimization with Vector Evaluated Genetic Algorithms. *In: Proceedings of an International Conference on Genetic Algorithms and Their Applications*, 24-26 July 1985, Carnegie-Mellon University, Pittsburgh, Pa, 93-100.
53. Sekulski, Z., 2010. Multi-objective topology and size optimization of high-speed vehicle-passenger catamaran structure by genetic algorithm. *Marine Structures*, Vol. 23, 405-433.
54. Sen, P. and Yang, J.B., 1995. An Investigation Into the Influence of Preference Modelling in Ship Design with Multiple Objectives. *In: Proceedings, PRADS '95*, Vol. 2, Society of Naval Architecture of Korea, 1252-1263.
55. Sen, P. and Yang, J.B., 1998. *Multiple Criteria Decision Support in Engineering*. London: Springer-Verlag.
56. Shi, W.B., 1992. In-Service Assessment of Ship Structures: Effect of General Corrosion on Ultimate Strength. *In: Spring Meeting, RINA*.
57. Significant Ships, 1997. *Boomerang: catamaran ferry for Baltic Service*, 21-21.
58. Srinivas, N. and Deb, K., 1995. Multiobjective Optimization Using Nondominated Sorting in Genetic Algorithms. *Evolutionary Computation*, 2(3): 221-248.
59. Stadler, W., 1988. *Multiobjective Optimization in Engineering and in the Sciences*. New York: Plenum Press.
60. Statnikov, R.B. and Matosov, J.B., 1995. *Multicriteria Optimization and Engineering*. New York: Chapman & Hall.
61. Trincas, G., Zanic, V. and Grubisic, I., 1994. Comprehensive Concept Design of Fast RO-RO Ships by Multi-Attribute Decision-Making. *In: Proceedings, IMDC '94*, Delft, 403-417.
62. UNITAS, 1995. Rules for the Construction and Classification of High Speed Craft.
63. Vanderplaats, G.N., 1984. *Numerical Optimization Techniques for Engineering Designs*. New York: McGraw-Hill.
64. Veldhuizen Van, D.A., 1999. *Multiobjective Evolutionary Algorithms: Classifications, Analyses, and New Innovations*. Ph. D. thesis, Air Force Institute of Technology, Wright-Patterson AFB, Ohio.
65. Veldhuizen Van, D.A. and Lamont, G.B., 2000. On measuring multiobjective evolutionary algorithm performance. *In: A. Zazala, R. Eberhart (Eds.) Congress on Evolutionary Computation (CEC 2000)*, vol. 1, Piscataway, NY, IEEE Press, 204-211.
66. Zitzler, E., 1999. *Evolutionary Algorithms for Multiobjective Optimization: Methods and Applications*. Dissertation for degree of Doctor of Technical Sciences, Swiss Federal Institute of Technology Zurich.
67. Zitzler, E., Deb, K. and Thiele, L., 1999. *Comparison of Multiobjective Evolutionary Algorithms: Empirical Results*. TIK-Report, No. 70, Computer Engineering and Communication Networks Lab, Swiss Federal Institute of Technology, Zurich, Switzerland.
68. Zitzler, E., Deb, K. and Thiele, L., 2000. Comparison of multiobjective evolutionary algorithms: Empirical results. *Evolutionary Computation*, 8(2): 173-195.
69. Zitzler, E., Laumanns, M. and Bleuler, S., 2002. A tutorial on evolutionary multiobjective optimization. *In Workshop on multiple objective metaheuristics (MOMH 2002)*, Springer-Verlag, Berlin.

70. Zitzler, E., Laumanns, M. and Thiele, L., 2001. SPEA-2: Improving the Strength Pareto Evolutionary Algorithm. Evolutionary Methods for Design. In: *Proceedings of the EUROGEN'2001 Conference on Optimization and Control with Applications to Industrial Problems*, 19-21 September 2001, International Center for Numerical Methods in Engineering, Greece, p. 95-100.
71. Zitzler, E. and Thiele, L., 1998. Multiobjective Optimization Using Evolutionary Algorithms – A Comparative Case Study. In: *Parallel Problem Solving from Nature – PPSN*, Amsterdam, 292-301.
72. Zitzler, E. and Thiele, L., 1998. Multiobjective Optimization Using Evolutionary Algorithms – A Comparative Case Study. In: *Proceedings of the PPSN V - Fifth International Conference on Parallel Problem Solving from Nature*, Amsterdam, The Netherlands, 27-30 September 1998, Springer, Berlin, Germany, 292-301.
73. Zitzler, E. and Thiele, L., 1999. Multiobjective Evolutionary Algorithms: A Comparative Case Study and Strength Pareto Approach. *IEEE Transactions on Evolutionary Computation*, 3(4): 257-271.
74. Zitzler, E. and Thiele, L., Laumanns, M., Fonseca, C.M., Grunert da Fonseca V., 2002. *Performance Assessment of Multiobjective Optimizers: An Analysis and Review*. TIK-Report No. 139, Swiss Federal Institute of Technology (ETH) Zurich, Switzerland.
75. Zitzler, E., Thiele, L., Laumanns, M., Fonseca, C.M. and Grunert da Fonseca V., 2003. Performance Assessment of Multiobjective Optimizers: An Analysis and Review. *IEEE Transactions on Evolutionary Computation*, 7(2):117-132.

---

**CONTACT WITH THE AUTHOR**

Zbigniew Sekulski, Ph. D.  
 West Pomeranian University of Technology, Szczecin  
 Faculty of Marine Technology  
 Al. Piastów 41  
 71-065 Szczecin, POLAND  
 e-mail: zbigniew.sekulski@zut.edu.pl

# A method for evaluating theoretical and real operation of diesel engines in energy conversion formulation taking into account their operating indices

Jerzy Girtler, Prof.  
Gdansk University of Technology

## ABSTRACT

*The article proposes valuating the operation of an arbitrary diesel engine, based on the sample case of a ship's main engine in which energy conversion processes take place in a given time. The above operation is understood as the energy transfer to the screw propeller in the given time in which the energy conversion into work and/or heat and its further transmission take place. The here proposed method for evaluating the operation of the main engines installed in marine power plants consists in comparing the operation of these engines to a physical quantity the measuring unit of which is the joule-second (joule×second). A new term is introduced which bears the name of the theoretical engine operation and is the standard (ideal) operation which can be compared to the operation of real engines revealing different levels of wear. It was shown that the calculations of the theoretical operation defined in the above way cannot make direct use of commonly known theoretical Diesel and Sabathe cycles. Instead they should use the cycles modified by heat abstraction taking place in accordance with the isobaric, or isothermal process. Other new terms introduced in the article are: the degree of excellence of energy conversion to work, considered as the measure of excellence of engine operation, and the degree of engine operation dissipation, being the measure of its real operation. It is shown that if in time  $t$  of engine operation the case takes place that:  $L_i = idem$  and  $L_e = idem$ , then the engine operation dissipation is equal to its mechanical efficiency.*

**Key words:** operation, energy, diesel engine, ship's main engine

## INTRODUCTION

The engine operation can be interpreted (in a descriptive formulation) as the result of the existence of the engine energy state which enables the engine to convert the energy  $E$  into heat and work in a given time  $t$  [2, 6, 9, 10, 13]. That means that when analysing the operation of these engines we have to take simultaneously into account the energy generated by the engines and the time of its conversion [6, 7]. In this interpretation the engine operation (in valuating formulation) can be compared to a physical quantity which is described by a numerical value and the measure unit bearing the name of the joule-second [joule×second]. The engine operation understood in the above way becomes worse when the engine wear increases. This means that the value of the operation of each engine will decrease with time, compared to the operation of the (ideal) reference engine.

Obviously, the energy conversion into heat and work, which is observed in the working spaces of each internal combustion engine, may take place in different times. In practice, it is essential that the work done in a given time is possibly the largest, or the given work is done in the shortest possible time. In is also important in practice that the maximum heat is released during the combustion, while the lost heat is possibly the smallest. If the most favourable energy conversion cannot be

achieved, we conclude that the engine is in the partial capability state [3, 4, 10, 12]. Consequently, of high importance is the analysis of the engine operation and its comparison with the theoretical operation represented by the (ideal) reference engine operating in accordance with the theoretical cycle. Therefore there is a need for determining the theoretical operation of the ideal engine. An attempt to determine such theoretical operation will be presented using the marine engine as the sample case [6, 7], but it will also refer to other piston internal combustion engines.

## MAIN ENGINE OPERATION IN DETERMINISTIC FORMULATION

In the deterministic formulation, the operation of the main engine can be analysed in two cases. In the first case we assume that the energy  $E$  transmitted by the engine to the screw propeller does not change in the time interval  $[0, t]$ . In that case we can assume that the engine operation ( $D$ ) can be given by the formula:

$$D = Et \quad (1)$$

In the second case, when the energy ( $E$ ) transmitted by the engine to the screw propeller depends on time ( $t$ ), the operation  $D(t)$  is to be calculated using the formula:

$$D(t) = D = \int_0^t E(\tau) d\tau \quad (2)$$

$E$  – energy converted and transmitted during engine operation,  
 $[0, t]$  – time interval of engine operation.

The energy is released in the form of work or heat. Therefore, according to formula (2) the engine operation can be interpreted as [4]:

$$D_L = \int_0^t L(\tau) d\tau ; D_Q = \int_0^t Q(\tau) d\tau \quad (3)$$

where:

$D_L$  – operation connected with the performed work ( $L$ ),  
 $D_Q$  – operation connected with the heat transfer ( $Q$ ),  
 $[t_1, t_2]$  – time interval of engine operation,  
 $t$  – time, independent variable.

The conditions of main engine operation are mainly determined by the external conditions in which the sea-going ship sails and tasks done by the ship users (the crew) [8]. These conditions and tasks are the reason why in different time intervals different amounts of energy are converted inside the working spaces of these engines. However, in each case the main engine operation is determined by their performance areas [6, 9, 15]. These areas are limited by their velocity characteristics, such as the external and control characteristics. If these characteristics are mapped against the main engine propeller characteristics, which also belong to the velocity characteristics, then the ranges of operation of these engines are defined, which can be illustrated in the form of areas (Fig. 1).

The real characteristics differ from their theoretical equivalents (Fig. 1) as the average torque ( $M_o$ ) of the piston internal combustion engine is the function of the average effective pressure ( $p_e$ ), i.e.

$$M_o = c_s p_e \quad (4)$$

and the effective pressure ( $p_e$ ) depends remarkably not only on the fuel charge, but also on the engine rotational speed ( $n$ ) [2, 9, 13]:

$$p_e = f(\Delta G_p, W_d, p_d, R_\mu, T_d, L_o, \lambda, \eta_v, \eta_i, \eta_m) \quad (5)$$

where:

$c_s$  – coefficient determining constructional properties of the engine,  
 $\Delta G_p$  – fuel charge,  
 $W_d$  – (net) calorific value of the fuel,  
 $p_d$  – pressure of the air supplied to engine working spaces,  
 $R_\mu$  – universal (absolute) gas constant ( $R_\mu \equiv R \cdot M$ ),  
 $T_d$  – temperature of the air supplied to the engine working spaces,  
 $L_o$  – theoretical amount of air needed for combustion of 1 kg of fuel,  
 $\lambda$  – excess air number,  
 $\eta_v$  – efficiency of filling of the engine working space (cylinder),  
 $\eta_i$  – indicated efficiency,  
 $\eta_m$  – mechanical efficiency of the engine.

The main engine operation is time-limited in the overload area, especially in the torque overload area, the area  $9^*-3^*-4-9-9^*$  in the real characteristic (Fig. 1). The engine cannot also operate long in the area of pure speed overload, the area  $6-7^*-10^*-9-6$ . Obviously, the engine operation is even more time-limited in

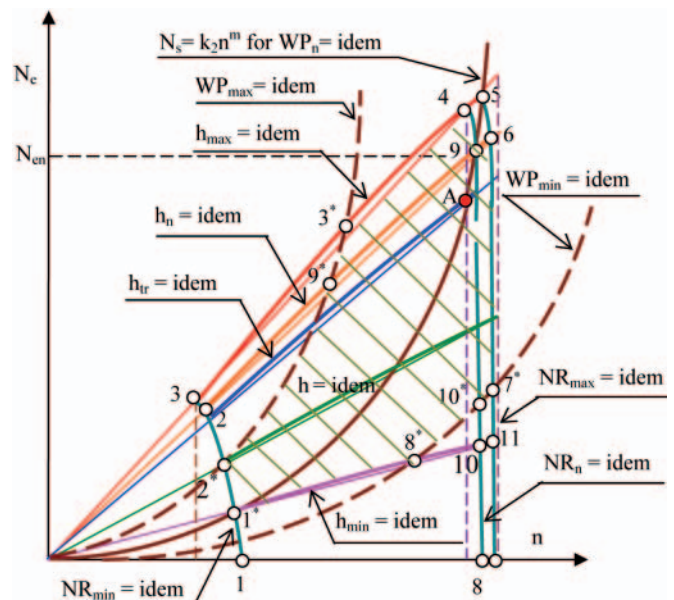


Fig. 1. Speed characteristics of the real piston engine (main engine) installed on a sea-going ship [6]:

- engine performance area (the area of permissible engine loads, the area of so-called stable engine operation):  $1^*-2^*-9^*-9-10^*-10-8^*-1^*$ ,
- engine overload area:  $2-3-3^*-4-5-6-7^*-10^*-9-2$ ,
- area illustrating the range of engine operation:  $1^*-2^*-9^*-3^*-4-5-6-7^*-10^*-8^*-1^*$ ,

$N_e$  – effective power,  $N_{en}$  – nominal (rated) effective power,  $n$  – rotational speed,  $h_{max}$  – maximal setting of the injection pump,  $h_n$  – nominal (rated) setting of the injection pump,  $h_{tr}$  – continuous setting of the injection pump,  $h_{min}$  – minimal setting of the injection pump,  $NR_{max}$  – maximal setting of the controller,  $NR_n$  – nominal (rated) setting of the controller,  $NR_{min}$  – minimal setting of the controller,  $WP_{max}$  – most difficult sailing conditions (largest resistance of ship motion),  $WP_n$  – nominal sailing conditions,  $WP_{min}$  – easiest sailing conditions (smallest resistance of ship motion),  $N_s = k_2 n^m$  – real propeller characteristic illustrating the dependence of the power needed by the propeller on the rotational speed ( $n$ ),  $k_2$  – real power factor,  $m$  – coefficient depending on the ship's hull shape (for displacement hulls  $m \approx 3.0$ )

the area of both torque and speed overload, the area  $4-5-6-9-4$  in Fig. 1.

The real performance area (working area) of the engine is limited by the curves:  $h_{max} = idem$ ,  $NR_{max} = idem$ ,  $h_{min} = idem$  and  $NR_{min} = idem$ . But the range of the main engine operation is smaller than the performance area, as the main engine can only operate in such a way that it secures delivering the energy needed by the screw propeller for executing a given task. The amount of the energy needed by the propeller in given operating conditions depends on the real propeller characteristic  $N_s = f(k_2, n)$ , which is different for different sailing conditions  $WP_n = idem$ .

The WP conditions can change between the easiest ( $WP_{min} = idem$ ) and the most difficult ( $WP_{max} = idem$ ). These conditions determine the range of main engine operation [5], the area:  $1^*-2^*-9^*-3^*-4-5-6-7^*-10^*-8^*-1^*$  in Fig. 1.

The effective power  $N_e$  generated by the main engine (Fig. 1) includes the information how fast the effective work  $L_e$  will be done in the given time  $t$  [3, 9]. That means that the power characterises the engine operation in the aspect of the rate of energy conversion to work, taking into account various losses, in particular thermal loss. But the engine operation consisting in the energy conversion into work is not possible if earlier the energy has not been converted to heat in the engine working spaces [3, 4, 9, 14]. Therefore when analysing the main engine operation we should take into account the energy delivered to the engine in the fuel-air mixture, which is initially converted to heat ( $Q$ ) and then to work ( $L$ ), rather than pure engine power output.



These considerations show that in case of the main engines installed on ships, as well as all other piston internal combustion engines, converting the chemical energy contained in the fuel-air mixture generated in the combustion chambers into heat, and then into the mechanical energy of the crankshaft-piston assembly makes it possible to generate the effective power  $N_e$ . This power is to be generated in time  $t$  needed for executing a given task by the ship. That means that in order to execute this task in the given time, the effective work  $L_e \cdot t$  is to be done by an arbitrary main engine. The realisation of this work is the effect of the torque ( $M_o$ ) generated on the crankshaft at a given rotational speed ( $n$ ) of each piston internal combustion engine, including the main engine [2, 10, 15]. Therefore according to formula (2), the engine operation interpreted as the energy conversion into effective work  $L_e$  in time  $t$  can be given as:

$$D_{L_e} = \int_0^t L_e(\tau) d\tau = 2\pi \int_0^t n(\tau) M_o(\tau) \tau d\tau \quad (6)$$

The main engines used on container ships, bulk carriers, and tankers are two-stroke, low-speed engines, most frequently with uniflow scavenging, or lateral scavenging with inlet ports higher than outlet ports [1, 10, 14]. A sample indicator diagram recorded on such an engine is shown in Fig. 2a for the case of uniflow scavenging, and in Fig. 2b for the engine with lateral scavenging and inlet ports ( $h_d$ ) higher than outlet ports ( $h_w$ ),  $h_d > h_w$ .

The presented real cycles show that the compression of the fresh charge (the mixture of the air delivered to the cylinder and the remnants of the exhaust gas which remained in the cylinder after the previous cycle) takes place after the cylinder scavenging process, consisting in the inflow of the fresh air with the simultaneous outflow of the exhaust gas, has ended. Until then, starting from the time instant of removing the exhaust gas from the cylinder, the heat is abstracted with the exhaust gas to the environment. Therefore theoretical cycles of diesel engines should take into account not only isochoric heat abstraction (like in the Diesel and Sabathe cycles), but also, depending on engine speed [7]:

- heat abstraction at constant pressure (isobaric), in case of low-speed engines,
- heat abstraction at constant temperature (isothermal), in case of medium- and high-speed engines.

The above approach is possible if the assumptions are adopted that:

- in low-speed engines the flow resistances change insignificantly and we can assume that the heat abstraction process takes place at the same pressure.
- however, during the realisation of this process remarkable temperature change can be observed due to a relatively long time of heat transfer to the environment (compared to high-speed engines), before the abovementioned fresh charge compression is initiated in the cylinder.

On the other hand, in medium-speed and, especially, high-speed engines such analyses are possible if we assume that:

- the flow resistances change remarkably (compared to low-speed engines) and we cannot assume that the heat abstraction process takes place at constant pressure.
- the temperature change observed during the realisation of this process is neglectable due to a relatively short time of heat transfer to the environment (compared to low-speed engines) before the fresh charge compression starts in the cylinder. Therefore we can assume in that case that after the isochoric heat abstraction is ended, the isothermal or quasi-isothermal heat abstraction process takes place in these engines before the fresh charge compression starts in the cylinder.

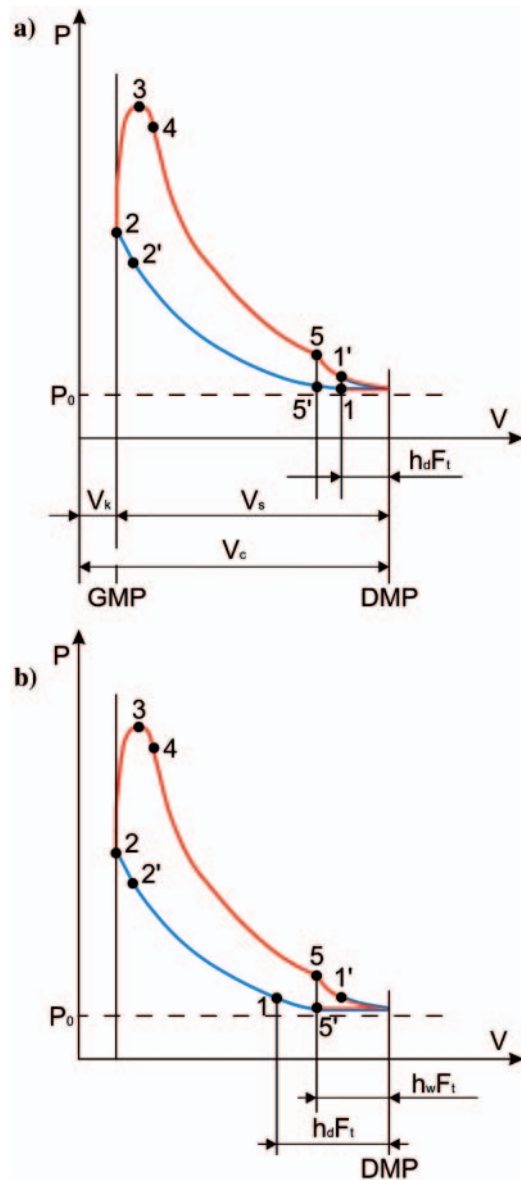


Fig. 2. Working cycles of two-stroke engines with a) uniflow scavenging, b) lateral scavenging for  $h_d > h_w$ , 1 – closing the air inlet ports, 5' – closing the exhaust gas exit valve (Fig. a), closing the exhaust gas outlet ports (Fig. b), 5 – opening the exhaust gas exit valve (Fig. a), opening the exhaust gas outlet ports (Fig. b), 1' – opening the air admission non-return valves (Fig. b),  $p_o$  – ambient pressure,  $V_k$  – combustion chamber volume,  $V_s$  – displacement volume,  $V_c$  – total cylinder volume, GMP – upper dead centre of the piston, DMP – lower dead centre of the piston,  $p$  – pressure,  $V$  – volume

To evaluate the operation of a real engine in given conditions, as described in Ref. [2], its operation should be compared with the theoretical operation.

### THEORETICAL OPERATION OF INTERNAL COMBUSTION ENGINES AND ITS PRACTICAL MEANING

In case of diesel engines, of high importance is not only the possible and needed operation, which depends on the effective work  $L_e$  and time (6), but also the theoretical operation, which makes it possible to assess how far the possible engine operation differs from the standard operation. To do this, we need to know the theoretical work ( $L_t$ ) and the time  $\tau$  of the operation. The work  $L_t$  can be easily calculated based on the average theoretical pressure ( $p$ ). The theoretical operation, in other words: the theoretically possible operation ( $D_{L_t}$ ) can be determined using formula (2) and taking into account relation (6) as:

$$D_{L_t} = \int_0^t L_t(\tau) d\tau \quad (7)$$

The theoretical cycles of diesel engines include thermodynamic cycles of this type of engines, such as the Sabathe cycle and the Diesel cycle. They are used for comparing the ideal and real course of processes of thermal energy conversion into mechanical energy in arbitrary diesel engines (and for this reason are frequently referred to as the reference cycles). The theoretical Sabathe cycle is a relatively good description of the real cycles recorded in high-speed diesel engines, while the theoretical Diesel cycle well models the real cycles taking place in low-speed engines of this type [8].

The calculations of the work ( $L_t$ ) need the information of the work ( $L_t$ ) done during one theoretical cycle of engine operation. Unfortunately, the theoretical Sabathe and Diesel cycles cannot be directly used in this case. Instead, we should use their modified versions which take into account the specifics of operation of particular internal combustion engine types. In case of two-stroke engines with uniflow scavenging, this specific results from the delay of the outlet valve closing, which makes the fresh charge compression start not after reaching DMP by the piston, but after the exhaust gas outlet valve has been closed (Fig. 2 a, point 5'). At the same time for engines with lateral scavenging and port heights  $h_d > h_w$ , this specific results from the delay in closing the air inlet ports by the piston with respect to the DMP (Fig. 2b, point 1). The theoretical cycles, (Fig. 3a and Fig. 3b), in which compression of the working medium also does not begin at the DMP, but later at point 1, reflect the specifics of the both types of engines. A separate problem is taking into account the fact that the exhaust gas decompression ends at point 5' of the real diagram, and not at DMP (Fig. 2).

The presented discussion shows that for low-speed engines the theoretical cycle in the form of the modified Diesel cycle additionally taking into account the isobaric heat abstraction can be used (Fig. 3a), while the cycle used for medium-speed engines is the modified theoretical Diesel cycle taking into account additional isothermal heat abstraction (Fig. 3b).

The assumption that the process along the path 5-1 is isothermal ( $T = idem$ ) can raise some doubts, as this process is difficult to execute. Moreover, we cannot determine the internal energy in this process, as for  $T = idem$  the specific thermal capacity  $c_T \rightarrow \infty$ . But there is no logical, nor empirical reason for not using this process as the reference process. Its applicability is justified by the facts that:

- although in time  $t = t_1 - t_5$  (when the cylinder is filled up with the fresh air) the heat is delivered to the fresh charge, which is heated by the elements composing the working space, but this time is short and the temperature does not change sufficiently to make adopting the assumption  $T_5 = T_1 = T = idem$  impossible. In cases when the temperature is subject to small but recordable changes we can assume that the heat supply to the fresh charge is the isothermal process taking place at a constant average temperature  $T_{1,5}$ ,
- since the time  $t$  of this process is short, we can assume that in that time the fresh charge mass ( $m$ ) and consequently its internal energy ( $U$ ) do not change remarkably, i.e.: if  $m = idem$  then  $U = idem$  at  $T = idem$ .

A distinctive advantage of this process is that it is most economical.

For the modified Diesel cycle taking into account first the isochoric and then the isobaric heat abstraction, the theoretical work done in the cylinder during one cycle is given by the formula [7]:

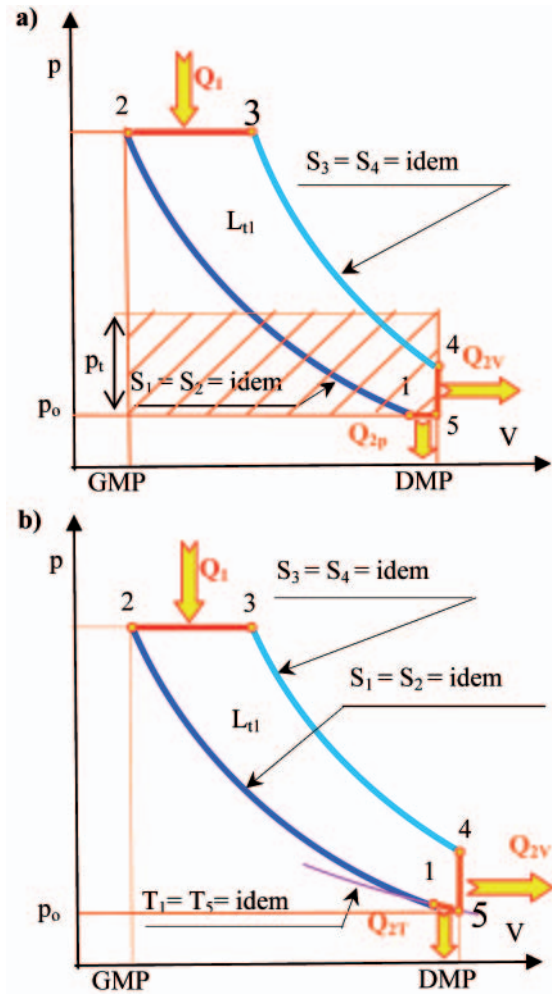


**Fig. 3.** Modified theoretical cycles: **a)** Diesel cycle taking into account isobaric heat abstraction, **b)** Diesel cycle taking into account isothermal heat abstraction:  $L_{t1}$  – theoretical work of the cycle,  $p$  – pressure,  $p_t$  – average theoretical pressure,  $V$  – volume,  $T$  – temperature,  $S$  – entropy,  $Q_1$  – supplied heat,  $Q_{2v}$  – heat abstracted at constant volume (isochoric),  $Q_{2p}$  – heat abstracted at constant pressure (isobaric),  $Q_{2T}$  – heat abstracted at constant temperature (isothermal), **GMP** and **DMP** – upper and lower dead centre of the piston, respectively

$$L_{t1} = Q_1 - (Q_{2v} + Q_{2p}) = mc_v [\kappa(T_3 - T_2) - (T_4 - T_5 + \kappa(T_5 - T_1))] \quad (8)$$

or:

$$L_{t1} = Q_1 - Q_2 = p_3 V_3 + \int_3^4 p dV - \left( p_5 V_5 - p_1 V_1 + \int_1^2 p dV + p_2 V_2 \right) \quad (9)$$

$$p_1 = p_5$$

At the same time for the modified Diesel cycle taking into account first the isochoric and then the isothermal heat abstraction, the abovementioned theoretical work is given by the formula [7]:

$$L_{t1} = Q_1 - (Q_{2v} + Q_{2T}) = mc_v [\kappa(T_3 - T_2) - (T_4 - T_5)] - T_5 (S_5 - S_1) \quad (10)$$

or:

$$L_{t1} = Q_1 - Q_2 = p_3 V_3 + \int_3^4 p dV - \left( \int_5^1 p dV + \int_1^2 p dV + p_2 V_2 \right) \quad (11)$$

Obviously, taking into account the number of realised cycles  $n$  and the number of cylinders  $k$ , the theoretical work ( $L_t$ ) needed for calculating the theoretical engine operation can be given by the formula [7]:

$$L_t = k \cdot n \cdot L_{t1} \quad (12)$$

or, after calculating the average theoretical pressure  $p_t$  (Fig. 4a), by the formula [7]:

$$\begin{aligned} L_t &= k \cdot n \cdot L_{t1} = k \cdot n \cdot p_t \cdot (V_5 - V_2) = \\ &= k \cdot n \cdot p_t \cdot \Delta V_{5,2} \end{aligned} \quad (13)$$

where:

- $V_5 - V_1 = \Delta V_{5,2} = V_s$
- $k$  – number of cylinders in the engine,
- $n$  – number of realised theoretical cycles in the operating time interval  $[0, t]$ ,
- $L_{t1}$  – work of a single theoretical cycle in the cylinder of an ideal engine,
- $p_t$  – average theoretical pressure,
- $V_s$  – cylinder displacement volume,
- $V_5, V_2$  – cylinder working space volumes (having the interpretation resulting from the symbols in Fig. 3).

Comparing the effective work done by the engine in time  $t$  and the theoretical work which can be done by an (ideal) theoretical engine in the same time we can estimate the degree of excellence ( $\varepsilon_{Ln(ob)}$ ) of energy conversion into effective work ( $L_e$ ) by the examined engine, which can be named the degree of excellence of engine operation. This degree can be calculated for two cases. The first case takes place when we cannot assume that during the time  $t$  of engine operation the same effective work is generated in each engine cylinder. Then the degree of excellence ( $\varepsilon_{Ln(ob)}$ ) of energy conversion in the engine can be given by the formula [7]:

$$\varepsilon_{Ln(ob)} = \frac{\sum_{k=1}^m \sum_{j=1}^n L_{e(j)k}}{L_t} \quad (14)$$

where:

- $L_{e(j)k}$  – effective work of the  $j$ -th cycle in the  $k$ -th engine cylinder,
- $L_t$  – theoretical work calculated using formula (13) for the modified Diesel cycle.

The degree of excellence of energy conversion into work, defined by formula (14), describes how far the energy conversion into work in the real engine differs from the theoretical work of an ideal engine, after  $n$  cycles.

The second case takes place when we can assume that in time  $t$  of engine operation the same effective degree of excellence ( $\varepsilon_{Ln(ob)}$ ) can be calculated using formula [7]:

$$\varepsilon_{Ln(ob)} = \frac{L_e}{L_t} = \frac{L_{e1}}{L_{t1}} ; L_e = knL_{e1} \quad (15)$$

where:

- $k$  – number of engine cylinders,
- $n$  – number of realised theoretical cycles in the operating time interval  $[0, t]$ ,
- $L_{e1}$  – effective work of a single real cycle in the engine cylinder.

Of some interest is how far the operation of the real engine as a whole differs from the operation of an ideal engine. Analysing the same cases as for the engine degree of excellence ( $\varepsilon_{Ln(ob)}$ ) of energy conversion into effective work ( $L_e$ ), we can

define the degree of engine operation excellence ( $\varepsilon_{Dn(ob)}$ ). In the first case when we have to assume that different effective work is generated in each cylinder in particular time intervals  $t_{(j)k}$  composing the overall time  $t$  of engine operation, the degree of engine operation excellence ( $\varepsilon_{Dn(ob)}$ ) can be calculated as [7]:

$$\varepsilon_{Dn(ob)} = \frac{\sum_{k=1}^m \sum_{j=1}^n L_{e(j)k} t_{(j)k}}{L_t t} \quad (16)$$

where:

- $L_{e(j)k}$  – effective work of the  $j$ -th cycle in the  $k$ -th engine cylinder,
- $t_{(j)k}$  – time of generation of work  $L_{e(j)k}$ ,
- $L_t$  – theoretical work calculated using formula (13) for the modified Diesel cycle.

In the second case when we can assume that in the time  $t$  of engine operation the same effective work  $L_{e1}$  is generated in each cylinder, the excellence degree ( $\varepsilon_{Dn(ob)}$ ) can be expressed using the same relation as the degree of excellence ( $\varepsilon_{Ln(ob)}$ ) of energy conversion into effective work ( $L_e$ ) by the examined engine (15). Consequently:

$$\sum_{i=1}^n t_{(j)k} = t$$

Therefore we can assume that in the second case the excellence degree ( $\varepsilon_{Dn(ob)}$ ) of operation of an internal combustion engine is equivalent to the excellence degree ( $\varepsilon_{Ln(ob)}$ ) of energy conversion into effective work ( $L_e$ ) in this engine.

If we take into account the indicated work  $L_i$  in these analyses, we can determine the coefficient (degree) of engine operation dissipation, caused by the energy lost for overcoming mechanical resistances. The abovementioned degree of engine operation dissipation could be defined as [7]:

$$\xi_{Dn(ob)} = \frac{\sum_{k=1}^m \sum_{j=1}^n L_{e(j)k} t_{(j)k}}{\sum_{k=1}^m \sum_{j=1}^n L_{i(j)k} t_{(j)k}} \quad (17)$$

If we can assume that in the time  $t$  of engine operation the case takes place that:  $L_i = \text{idem}$  and  $L_e = \text{idem}$ , then the engine operation dissipation degree is equal to its mechanical efficiency.

Formulas (9) and (11) can be only used when the paths of thermodynamic processes of the cycles are known. On the other hand, when we know the functional relations between the pressures and the volumes which are characteristic for these processes, the above formulas take the forms:

$$\begin{aligned} L_{t1} &= Q_1 - Q_2 = p_3 V_3 + \\ &+ \int_{V_3}^{V_4} p(V) dV - \left( p_5 V_5 - p_1 V_1 + \int_{V_1}^{V_2} p(V) dV + p_2 V_2 \right) \end{aligned} \quad (18)$$

$$\begin{aligned} L_{t1} &= Q_1 - Q_2 = p_3 V_3 + \\ &+ \int_{V_3}^{V_4} p(V) dV - \left( \int_{V_5}^{V_1} p(V) dV + \int_{V_1}^{V_2} p(V) dV + p_2 V_2 \right) \end{aligned} \quad (19)$$

The above analysis shows that in the case when the functional relations  $p = f(V)$  for the examined processes are known, formula (18) can be used instead of formula (9) and (19) instead of (11).

## REMARKS AND CONCLUSIONS

- The operation of the internal combustion engine was interpreted as the delivery of the required energy in given time, which can be expressed in the form of a physical quantity having the measure unit called joule-second.
- When discussing energy related advantages of internal combustion engines, we should analyse their operation and not only their work. Beside the work itself, the operation analysis takes into account also time of its realisation.
- The proposed method can be applied for calculating the theoretical standard operation, which enables comparison between different real diesel engines revealing different levels of wear. The theoretical work needed for calculating this operation was calculated based on the modified theoretical Diesel cycles, different for different engine rotational speeds. The modification introduced in those cycles consisted in additional taking into account the heat abstraction according to the isobaric or isothermal processes. For low-speed engines the additional heat abstraction modelled as the isobaric process was proposed, while that in the medium-speed engines was assumed to take place according to the isothermal process.
- The presented analysis reveals that it is not advisable to use traditional and well-known theoretical Diesel cycles for determining the theoretical work making the basis for calculating the engine operation value.
- The article presents the deterministic method applied for evaluating the theoretical operation of the piston internal combustion engine used as the main engine on a ship, but this method can be applied to any piston internal combustion engines.
- A separate problem is developing a method for assessing the operation of internal combustion engines in the stochastic formulation. In this case we should take into account that the energy conversion processes taking place during engine operation have stochastic nature.
- A similar analysis can be performed for four-stroke internal combustion engines, and similar formulas can be derived for determining their theoretical operation.
- The article also illustrates the applicability of the assessment of theoretical internal combustion engine operation, done in the above way, for evaluating real operations of this type of internal combustion engines.

## BIBLIOGRAPHY

1. Aeberli K.: *New high-economy engines for panama containerhips and large tankers*, Wartsila Switzerland Ltd, Winterthur, September 2007

2. Girtler J.: *Work of a compression-ignition engine as the index of its reliability and safety*. II International Scientifically-Technical Conference EXPLO-DIESEL & GAS TURBINE'01. Conference Proceedings. Gdansk-Miedzyzdroje-Copenhagen, 2001, pp.79-86
3. Girtler J.: *Possibility of valuation of operation of marine diesel engines*. Journal of POLISH CIMAC, Vol. 4, No 1, 2009
4. Girtler J.: *Energy-based aspect of operation of diesel engine*. COMBUSTION ENGINES (Silniki Spalinowe) No 2/2009 (137)
5. Girtler J.: *Conception of valuation of combustion engine operation*. Journal of KONES. Powertrain and Transport. Editorial Office Institute of Aeronautics BK, Warsaw 2008
6. Girtler J.: *A method for evaluating the performance of a marine piston internal combustion engine used as the main engine on a ship during its voyage in different sailing conditions*. Polish Maritime Research. Vol. 17, iss. 4(67), 2010
7. Girtler J.: *Possibility of defining theoretical operation for diesel engines in energy terms*. COMBUSTION ENGINES (Silniki Spalinowe) Nr 3/2011(146). Abstract p. 62. Full text CD: PTNSS 2011-SD-005
8. Łosiewicz Z.: *Probabilistic diagnostic model of the marine main engine* (in Polish). Ph.D. thesis, Faculty of Ocean Engineering and Ship Technology, Gdansk University of Technology, Gdansk
9. Piotrowski I., Witkowski K.: *Operation of marine internal combustion engines* (in Polish). AM, Gdynia 2002
10. Piotrowski I., Witkowski K.: *Marine internal combustion engines* (in Polish). Wyd. TRADEMAR, Gdynia 1996
11. Roslanowski J.: *Identification of ships propulsion engine operation by means of dimensional analysis*. Journal of POLISH CIMAC, Vol. 4, No 1, 2009
12. Rudnicki J.: *Loads of ship main diesel engine in the aspect of practical assessment of its operation*. Journal of POLISH CIMAC, Vol. 3, No 1, 2008
13. Rudnicki J.: *On making into account value of operational applied to ship main propulsion engine as an example*. Journal of POLISH CIMAC, Vol. 4, No 1, 2009
14. Wajand J.A., Wajand J. T.: *Medium- and high-speed internal combustion engines* (in Polish). WNT, Warszawa 2005
15. Wojnowski W.: *Marine diesel engine power plants*. (in Polish) Pt. I. Wyd. AMW, Gdynia 1998.

---

## CONTACT WITH THE AUTHOR

Jerzy Girtler, Prof.  
Faculty of Ocean Engineering  
and Ship Technology  
Gdansk University of Technology  
Narutowicza 11/12  
80-233 Gdansk, POLAND  
tel.: (+48 58) 347-24-30; fax: (+48 58) 347-19-81  
e-mail: jgirtl@pg.gda.pl

# Exhaust gas temperature measurements in diagnostic examination of naval gas turbine engines

## Part II Unsteady processes

Zbigniew Korczewski, Assoc. Prof.  
Gdansk University of Technology

### ABSTRACT



*The second part of the article presents the results of operating diagnostic tests of a two- and three-shaft engine with a separate power turbine during the start-up and acceleration of the rotor units. Attention was paid to key importance of the correctness of operation of the automatic engine load control system, the input for which, among other signals, is the rate of increase of the exhaust gas flow temperature. The article presents sample damages of the engine flow section which resulted from disturbed functioning of this system. The unsteady operation of the compressor during engine acceleration was the source of excessive increase of the exhaust gas temperature behind the combustion chamber and partial burning of the turbine blade tips.*

**Key words:** technical diagnostics; naval turbine engines; exhaust gas temperature; unsteady processes; unstable compressor operation; partial blade tip burning

### INTRODUCTION

In unsteady states of turbine engine operation, when it changes from one steady-load state to the other, operating parameters and power indices of the thermal and flow processes taking place inside the engine, as well as the processes themselves change in time. This happens, for instance, when the engine is started up or shut down, during engine acceleration<sup>1)</sup> or deceleration<sup>2)</sup>, as well as during changes of direction of rotation of the driving turbine rotor – in reversal engines.

The behaviour of the naval turbine engines in unsteady states makes their users perform specific actions to secure long-lasting and faultless engine operation. On the one hand, the user should know what course the transient processes take, how the operating parameters change, where and when the overload phenomena take place and what is their nature and time of duration. On the other hand, the opportunities for performing necessary experimental tests of engines in marine conditions are strictly limited by numerous structural and operational restrictions.

The operating practice of naval engines reveals that the realisation of transient processes in extremely unfavourable conditions may result in exceeding the exhaust gas temperature limits and unstable operation of the compressor and the

combustion chamber, which may finally lead to partial burning of turbine blade tips [1, 2, 6, 9]. This refers in particular to the engine start-up and acceleration processes.

### ENGINE START-UP AND ACCELERATION

The start-up of the naval turbine engine is an unsteady process oriented on bringing the rotor units from the state of rest to the idling rotational speed. It is mainly characterised by the fact that the largest changes of energy conversion processes are recorded during its realisation. In as little as a few seconds the structural components of the flow section are subject to strong thermal loads, with the instantaneous temperature of the inflowing exhaust gas increasing by  $\Delta T = 60 - 70$  K/s, Fig. 1. This excessive increase of the exhaust gas temperature may be provoked by the worsened technical state of the flow section, or result from faulty operation of the automatic engine load control system which controls the rates of fuel and supply air [4, 5, 7, 11].

Fig. 2 shows sample time-histories of the exhaust gas temperature behind the low pressure turbine and behind the exhaust gas generator as the functions of the start-up process time duration. These time-histories were recorded during five years of operation of a three-shift engine with a separate

<sup>1)</sup> acceleration - process of increasing the rotational speed of the rotor units.

<sup>2)</sup> deceleration - process of decreasing the rotational speed of the rotor units.

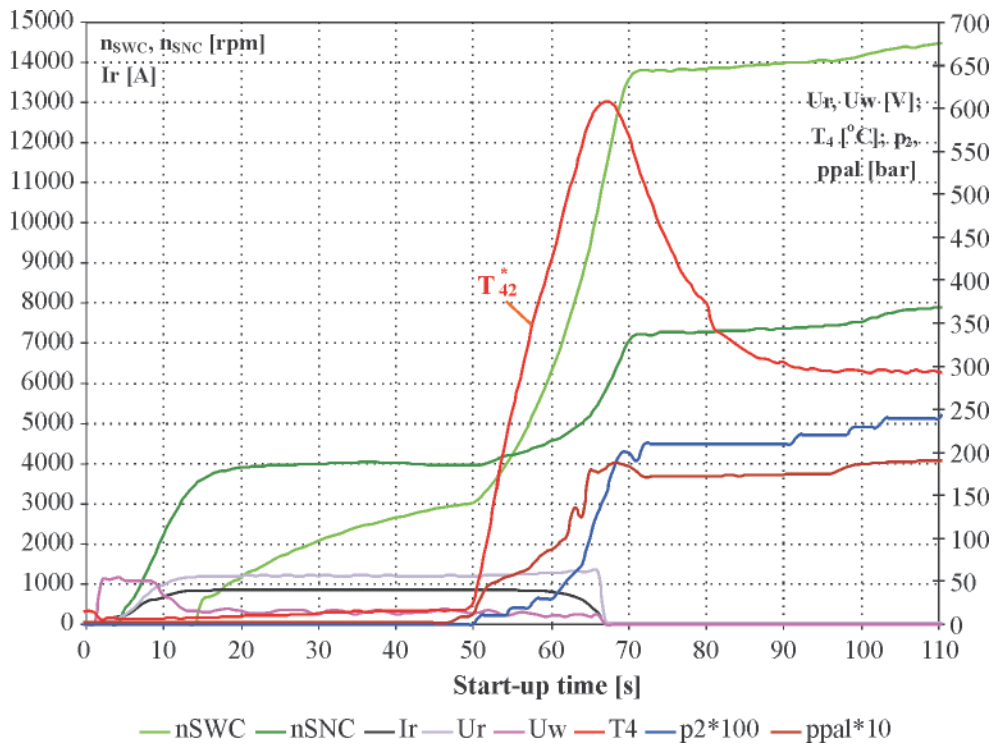


**Fig. 1.** Time-histories of parameters controlling the start-up process of the three-shaft engine with a separate power turbine  $n_{SNC}$ ,  $n_{SWC}$  – rotational speed of, respectively, the low pressure and high pressure compressor;  $I_r$ ,  $U_r$ ,  $U_w$  – current parameters of the electric starter: strength and voltage of the starting current, and the field voltage;  $T_4$  – averaged temperature of the exhaust gas flow behind the exhaust gas generator;  $p_2$  – air pressure behind the high pressure compressor,  $ppal$  – fuel pressure in front of the injectors

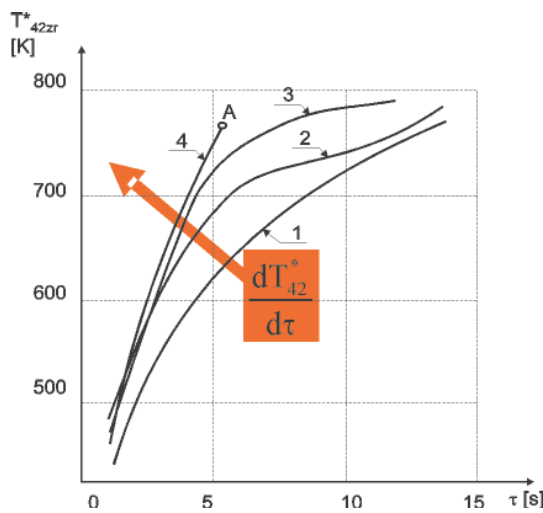


**Fig. 2.** Exhaust gas temperature changes recorded behind TNC of a three-shaft engine with a separate power turbine vs. start-up time: 1 – brand-new engine; 2 – engine in third year of operation; 3 – engine after five years of operation; 4 – unsuccessful engine start-up after five years of operation; A – automatic engine shut-down

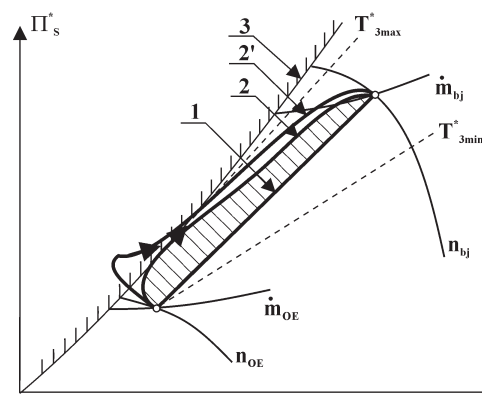


**Fig. 3.** Changes of range of cooperation between compressor, combustion chamber, and turbine during engine start-up: 1 – cooperation line in steady-load states; 2 – change of operating range at  $dT_4^*/d\tau = dop$ ; 2' – change of operating range at  $dT_4^*/d\tau = k\tau$ ; 3 – stable operation limit;  $n_{bj} > n_{OE}$  – isodromes of idling and electric rotation of the compressor-turbine unit,  $\dot{m}_{bj} > \dot{m}_{OE}$  – lines of constant fuel charge for idling and electric rotation (beginning of combustion);  $T_{3max}^*$ ,  $T_{3min}^*$  – isotherms of the exhaust gas flow leaving the combustion chamber

power turbine on a ship. A characteristic trend is observed for continuous increase of the exhaust gas temperature derivative when the engine's operational time increases.

The curves shown in the figure reveal that the increased worsening of the technical state of the engine flow section (confirmed by systematic endoscopic examinations [9]) has finally led to the increase of the exhaust gas temperature to the limit at which the automatic control system stopped the start-up process, thus protecting the engine against the damage (point A on curve 4).

An additional threat for the reliability of the started-up engine is possible excessive deflection of the cooperation line on the compressor characteristic from the optimal line and entering the zone of unstable operation (so-called compressor stall) [3, 8, 12]. The graphical interpretation of the both undesired

phenomena is given in Fig. 3 which shows the combined characteristics of the compressor-combustion chamber-turbine system, with projected hypothetical curves of system cooperation during the engine start-up process.

The fuel ignition and the increasing exhaust gas temperature shift the points of system cooperation from the optimal line for steady-state conditions towards the stable operation limit, which is illustrated by lines 2 and 2' in Fig. 3. The margin of stable operation of the compressor, defined as:

$$\Delta Z_s = (Z_s - 1)100\% \quad (1)$$

where:

$$Z_s = \frac{(\pi_s / \dot{m})_{gr}}{(\pi_s / \dot{m})_p} \quad (2)$$

$Z_s$  – stable compressor operation margin coefficient;

$(\pi_s/\dot{m})_{gr}$  – ratio of the compressor’s compression to the mass flow rate of the working medium at the stable operation limit;

$(\pi_s/\dot{m})_p$  – ratio of the compressor’s compression to the mass flow rate of the working medium when the engine switches from the stable speed of electric rotation to the stable speed of idling, is reduced.

Reducing the stable operation margin of the turbine engine compressor below 5% results in boundary layer separation on convex surfaces of the rotor blades and pulsations of the forced air flow [3, 8, 10].

Similar gasodynamic phenomena take place in the process of acceleration of the engine rotor units when the engine shifts from one stable-load state to the other. It results from the equation of motion of each rotor unit that the acceleration time  $\tau_p$  depends on the mass polar moment of inertia  $J$  of its rotating system and the range of rotational speed changes from  $n_1$  to  $n_2$ , according to formula [3]:

$$\tau_p = \frac{\pi}{30} J \int_{n_1}^{n_2} \frac{dn}{M_p} \quad (3)$$

Increasing the values of the accelerating torque  $M_p$  of the engine shaft, and/or reducing the values of the mass polar moment of inertia of the rotating masses and the rotational speed range shorten the time needed for changing the operating engine parameters to the required higher-load regime. Therefore to increase the engine power, the rate of the fuel supplied to the engine combustion chamber for each intermediate rotational speed of the rotor unit should be larger than in case of engine operation in steady-load conditions at the same rotational speed.

The extremely intensive course of the engine fuel supply process during the acceleration  $\dot{m}_{pal} = f(n)$  is limited by the maximal permissible exhaust gas temperature measured at high-pressure turbine inlet, due to the creep-resistance of constructional materials of the turbine blades, the efficiency of operation of the turbine cooling system, and the limit of stable operation of the compressor. The maximal permissible excess fuel charge determines the minimal time of engine acceleration.

The reserve of stable gasodynamic operation of the compressor  $\Delta Z_{sa}$  which is used in the acceleration process is calculated for each instantaneous engine rotational speed as the product of two coefficients:  $\Delta Z_{su}$  – the reserve of compressor stability determined by the exhaust gas temperature at turbine inlet when the engine operates in steady-load conditions, and  $\Delta Z_{sp}$  – the reserve of compressor stability which characterises permissible exceeding of the exhaust gas temperature at turbine inlet during acceleration:

$$\Delta Z_{sa} = \Delta Z_{sp} \cdot \Delta Z_{su} = \sqrt{\frac{T_{spala}^*}{T_{spalmax}^*} \cdot \frac{T_{spalmax}^*}{T_{spalu}^*}} = \sqrt{\frac{T_{spala}^*}{T_{spalu}^*}} \quad (4)$$

where:

$T_{spalmax}^*$  – exhaust gas temperature at turbine inlet in the maximal steady-load regime,

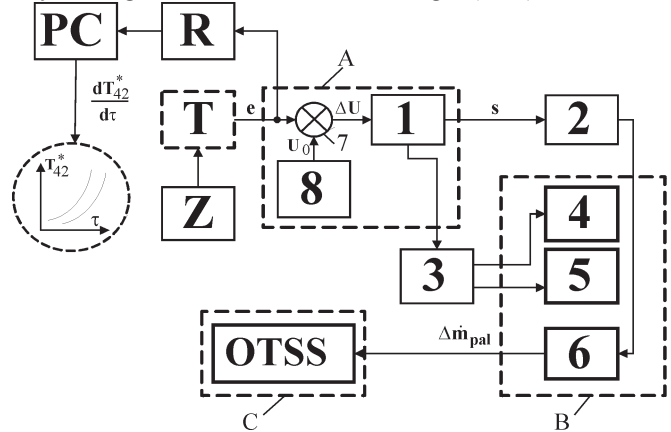
$T_{spala}^*$  – maximal exhaust gas temperature at turbine inlet during the acceleration process,

$T_{spalu}^*$  – exhaust gas temperature at turbine inlet in the steady-load regime.

In order to protect the engine against damages in these situations, the procedure of its use includes numerous limits which are automatically controlled by the start-up and load change process control system. The role of this system is to act on the rate of the energy delivered to the engine (as a result of

burning the fuel supplied from the fuel installation and from the electric starter) and control the flow duct geometry, including the adjustable inlet stator, air bleeding valves behind SWC, supply air valves for the second injector channel, reversal mechanism of the separate power turbine, etc., in order to protect the engine against excessive thermal and mechanical overloads of its constructional components. In Fig 3 this range is represented by the hatched area between lines 1 and 2. The block diagram of the system is shown in Fig. 4.

Fig. 4. Block diagram of the turbine engine exhaust gas temperature limit control system: A – impulse temperature control module, B – module of actuating mechanisms, C – naval turbine engine (OTSS), T – module



of thermo-couples (TXA-1368), Z – temperature setter, R – computer programme for measuring, recording and analysing engine start-up parameters, 1 – signal amplifier and modulator, 2 – electromagnetic control valve (by-pass) control circuit, 3 – main valve and emergency fuel drainage valve control circuit, 4 – main fuel valve (ZGP), 5 – emergency fuel valve (ZAP), 6 – fuel overflow valve (ZPP), 7 – comparing element, 8 – reference voltage generator, e – averaged thermoelectric voltage value, s – pulse control signal

The input signal for the system is the average exhaust gas temperature measured behind the exhaust gas generator. Excessive increase of this temperature can “only” provoke the action of the fuel overflow valve, or, in more severe situations, rapidly shut the engine down by acting simultaneously on the main valve and the emergency fuel drainage valve. It is noteworthy that the measurement of the exhaust gas temperature in the start-up process (and other unsteady processes) is burdened with some relatively large inertia which can be corrected electronically in the engine control system – Fig. 5 [13, 14]. Correction of the measuring inertia

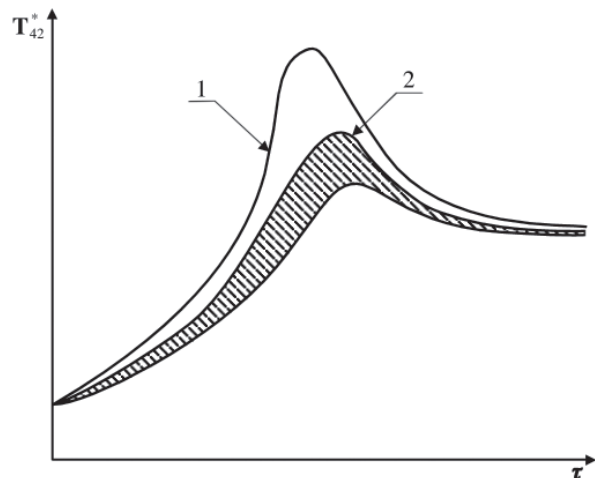


Fig. 5. Hypothetical time-histories of exhaust gas temperature changes during turbine engine start-up (acceleration) – the hatched area represents the range of correction of the measuring thermocouple inertia: 1 – real temperature, 2 – measured temperature

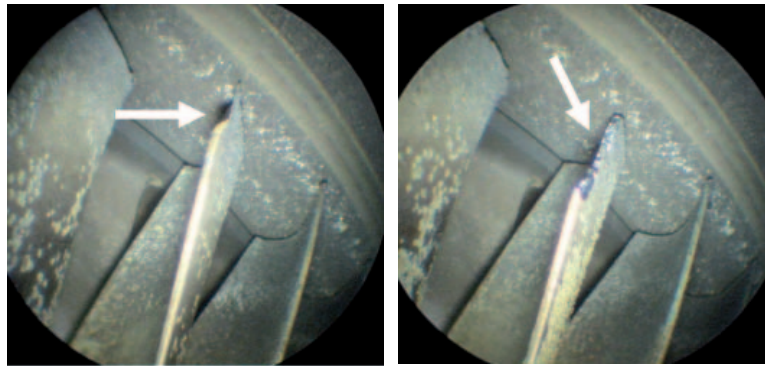


Fig. 6. Partly burned high-pressure turbine rotor blade tips

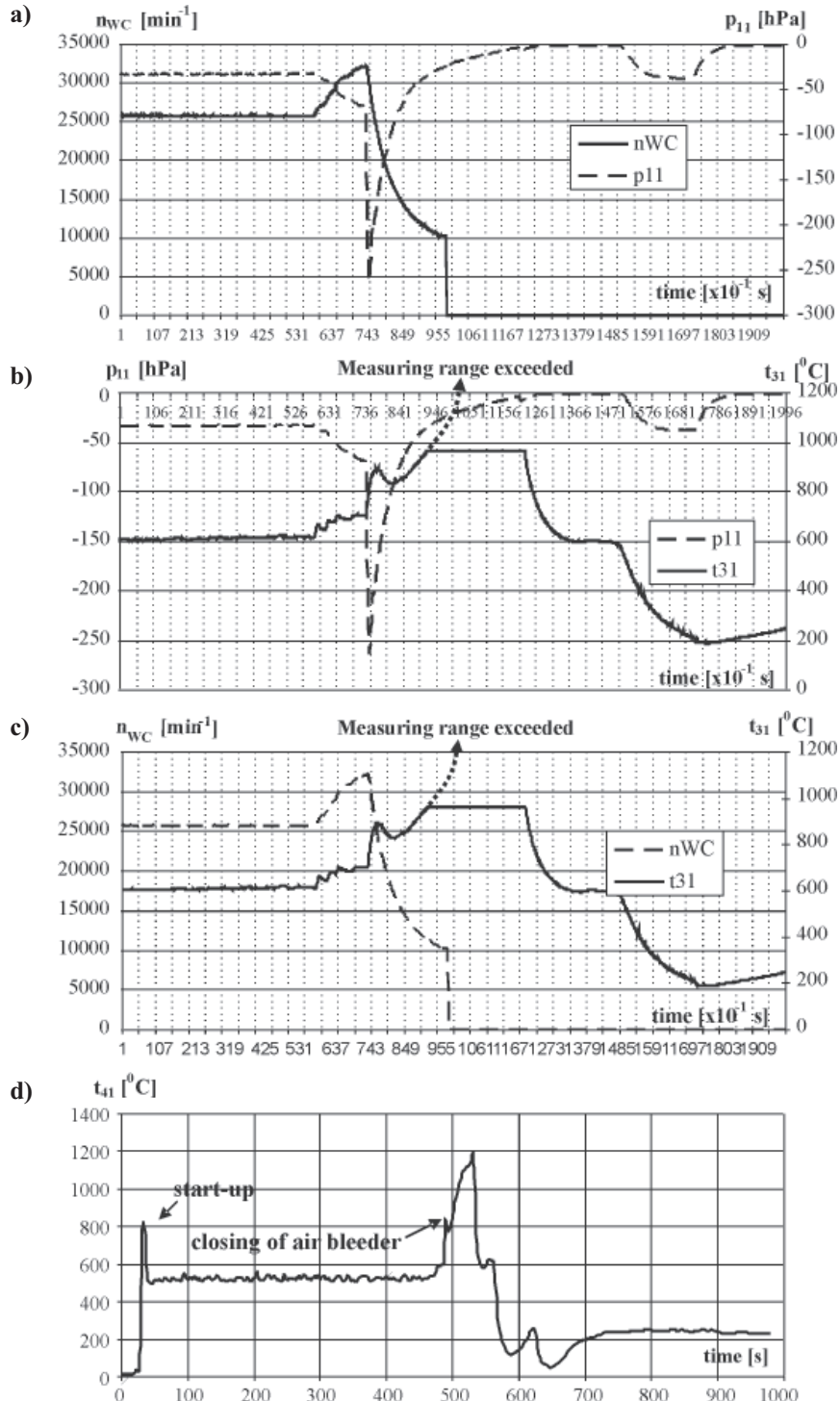


Fig. 7. Time-histories of high-pressure rotor rotational speed, negative pressure at compressor inlet, and exhaust gas temperatures at high-pressure turbine and separate power turbine inlets during the two-shaft engine acceleration process



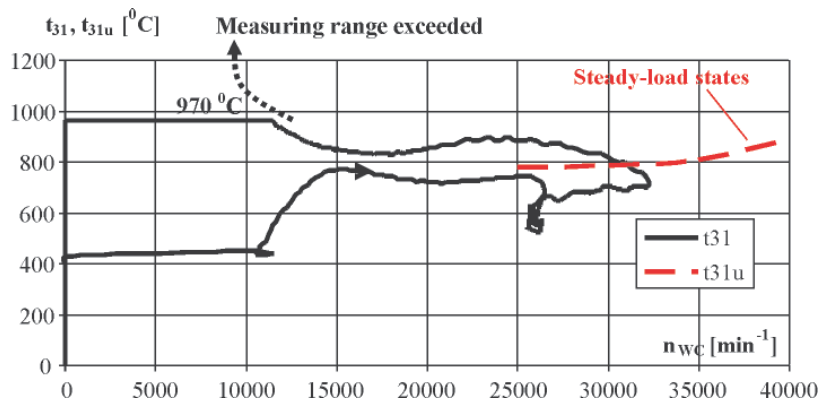


Fig. 8. Changes of exhaust gas temperature at high-pressure turbine inlet during start-up, acceleration, and steady-load engine operation of the two-shaft engine with a separate power turbine vs. high-pressure rotor rotational speed

of the thermocouples, which is done individually for each engine due to unrepeatability of the process of engine manufacturing, may reach as much as a few percent. This correction determines a so-called starting thermal sensitivity of the engine. On the other hand, interfering into producer's settings of the automatic control system during all time of engine operational use is not allowed, in particular in situations when the engine start-up becomes relatively difficult due to the worsened technical state of the flow section or the fuel supply system [13].

The absence or disturbed functioning of the automatic exhaust gas temperature limiter usually leads to huge and irreversible damages of the flow section, after which recovering the technical state of the engine is only possible via emergency repair done by the producer. Fig. 6 shows partly burned blade tips of the high-pressure turbine rotor, being the result of unstable operation of the combustion chamber during the acceleration process of a two-shaft engine with a separate power turbine.

After accidental choking of the air inlet duct and closing of the air bleeder valve, the increased rotational speed of the exhaust gas generator rotor was accompanied by rapid increase of the negative pressure in the compressor's inlet section, the decrease of the compressor output and, as a further consequence, by the increase of the exhaust gas temperature behind the combustion chamber – Fig. 7. The maximal permissible value of the exhaust gas temperature in steady-load states, limited to 970°C, was considerably exceeded, as shown in Figs. 7b,c and 8 (exceeding of the upper limit of the measuring range). Another parameter which was considerably exceeded in this case was the exhaust gas temperature at the separate power turbine – Fig. 7d.

In unsteady processes some short-lived exceeding of the maximum exhaust gas temperature at high-pressure turbine inlet is permissible, but this temperature is definitely not allowed to increase by over 20% of its maximal value referring to the nominal steady-load engine operation (depending on the used constructional materials and applied method of turbine cooling) [3, 6].

The excess rate of the fuel burned in the combustion chamber has led to excessive enrichment of the fuel-air mixture and the decrease of the excess air number  $\lambda$  – Fig. 9. When the critical level was reached ( $\lambda \ll \lambda_{\min}$ ) at a given rotational speed of the exhaust gas generator rotor unit, the phenomenon of so-called „rich” flameout of the combustion chamber (flame breakdown) took place, with further automatic shutting the engine down. But despite this shut-down, the temperature of the flow section components (high pressure turbine blades) was so high that the resultant damages (partial burning, cracks) of the constructional material have eliminated the engine from further operation.

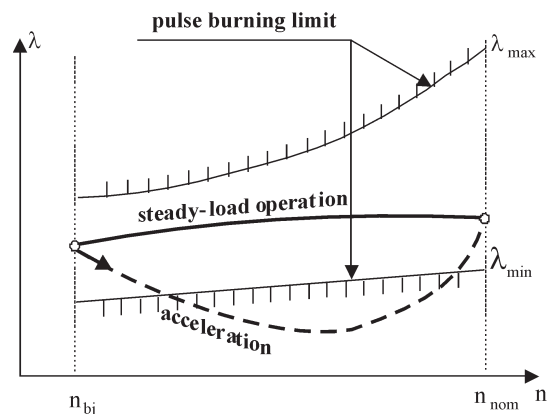


Fig. 9. Relation between the excess air number in the combustion chamber and the rotational speed of the exhaust gas generator rotor unit

## CONCLUSIONS

- The rate of increase of the exhaust gas temperature during the turbine engine start-up and acceleration processes is decisive about engine reliability and lifetime. It is also a basic diagnostic parameter monitored in unsteady processes in order to assess the technical state of the flow section, the fuel and air supply system, and the automatic load control system.
- A key operational problem is adjusting the engine in a way which will simultaneously secure sufficient dynamics of the realised unsteady thermal and flow processes and, on the other hand, protect the engine against exceeding the limits of the exhaust gas temperature and the rate of its increase as possible threats of vast and irreversible damages of the engine flow section.
- Therefore one of basic requirements for the thermal protection system of the engine is maximal reliability of its work during engine operation, which is checked in systematic diagnostic tests.

## BIBLIOGRAPHY

1. Balicki W., Szczeciński S.: *Diagnosing aeronautic turbine engines. Fluid-flow machines* (in Polish). Scientific Library of the Institute of Aviation. Warsaw 2001.
2. Boliński B., Stelmaszczyk Z.: *Aeronautic propulsion systems. Operation of turbine engines* (in Polish). WKiŁ, Warsaw 1981.
3. Cohen H., Rogers G.F.C., Saravanamuttur H.I.H.: *Gas turbine theory*. Longman Scientific & Technical, New York 1987.
4. Dzida M.: *Influence of gas turbine controller adjustment on ship propulsion system behavior in rough sea conditions Part 2. The simulation investigations*. Polish Maritime Research, No 1(39), 2004, Vol.11.

5. Dzida M.: *Simulation of ship propulsion gas turbine dynamics - an educational laboratory model*. Polish Maritime Research, No 4(22), 1999, Vol.6.
6. Hardin J.R. and others: *A gas turbine condition - monitoring system*. Naval Engineers Journal, November, USA 1995.
7. Korczewski Z.: *Method of diagnosing the flow section of a naval turbine engine in operation*. AMW (Ph.D. thesis – in Polish), Gdynia 1992.
8. Korczewski Z.: *Identifying gasodynamic processes in the compressor system of a naval turbine engine for diagnostic purposes* (in Polish) AMW Gdynia 1999.
9. Korczewski Z.: *Endoscopy of marine engines* (in Polish). AMW Gdynia 2008.
10. Orkisz M.: *Selected issues of jet turbine engine theory* (in Polish). ITE, Radom 1995.
11. Pawlak W., Wiklik K., Morawski J.M.: *Synthesis and tests of control systems of aeronautic turbine engines making use of computer simulation methods* (in Polish). Institute of Aviation, Warsaw 1996.
12. Szczeciński S.: *Aeronautic turbine engines* (in Polish). Wydawnictwo MON, Warsaw 1965.
13. *Technical and operating documentation of marine turbine engines GTU6a, DE59, ZORYA of UGT type, General Electric LM2500*.
14. *Reports on diagnostic tests of piston and turbine engines in operation on Polish Navy vessels* (in Polish) – AMW Research Works, Gdynia 1992 ÷ 2008.

---

**CONTACT WITH THE AUTHOR**  
 Zbigniew Korczewski, Assoc. Prof.  
 Faculty of Ocean Engineering  
 and Ship Technology  
 Gdansk University of Technology  
 Narutowicza 11/12  
 80-233 Gdansk, POLAND  
 e-mail: z.korczewski@gmail.com

# Damping of torsional vibrations of ship engine crankshafts – general selection methods of viscous vibration damper

Wojciech Homik, Ph. D.  
Rzeszów University of Technology

## ABSTRACT



*This paper describes causes of torsional vibrations generated in ship engine crankshafts. Means for damping the torsional vibrations as well as general methods for selection of viscous torsional vibration dampers for a given type of engine are also presented. Exemplary results of calculations connected with selection of a viscous torsional vibration damper intended for a six-cylinder engine, are attached.*

**Keywords:** torsional vibrations; torsional vibration damping; torsional vibration dampers; crankshaft; natural vibration frequency

## INTRODUCTION

Crankshafts are applied everywhere it is necessary to convert reciprocating motion into rotational one or inversely. In engines and compressors they are commonly used.

Piston combustion engine in operation generates vibrations which result from occurrence of periodically varying gas and inertia forces. The forces generate the following kinds of vibrations:

- bending vibrations,
- axial vibrations,
- torsional vibrations.

The first two kinds of vibrations occurring in car combustion engines do not constitute any great danger for life time of their crankshafts but for ship large-power engines axial vibrations of crankshafts are a serious problem. Such vibrations cause that the entire system consisted of engine crankshaft, flywheel, shaft line and screw propeller displaces periodically along its axis. Axial vibration amplitude of the system practically depends on a design solution of screw propeller, namely, number of its blades.

However irrespective of an used dynamical engine operation system torsional vibrations are the most dangerous for its crankshaft. Out of many forces acting in the crankshaft-piston system the force T (Fig. 1) tangent to the circle described by crank, makes crankshaft rotating. The force T, one of two components of the force S acting along crankshaft axis, is that periodically changing [8, 9, 11, 12]. Its frequency for two-stroke engines is equal to  $2\pi$ , and for four-stroke ones - to  $4\pi$ . Changes

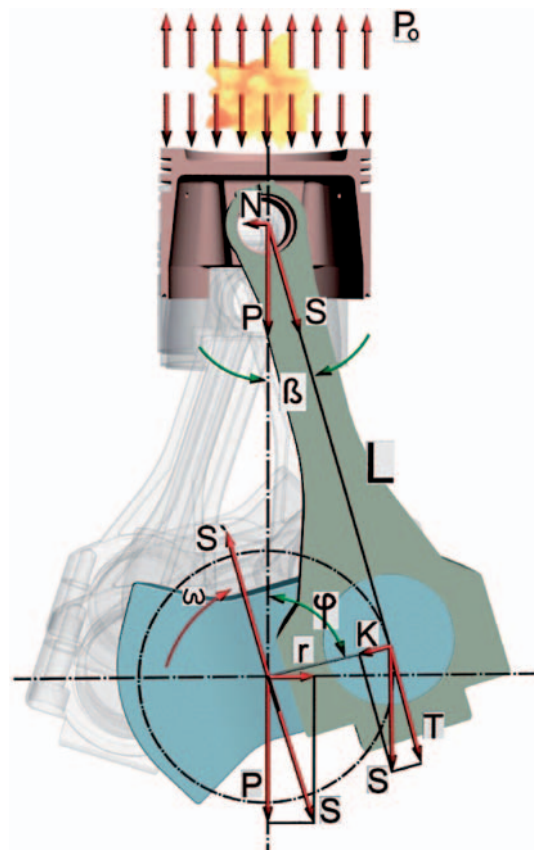


Fig. 1. Distribution of forces in crankshaft - piston system

of the force  $T$  generate accelerations of engine crankshaft rotational motion and in consequence torsional vibrations which change along with changing shaft line rotational speed. Worth mentioning that crankshaft deflection is limited only by shaft line torsional stiffness and torsional vibration amplitude can exceed its permissible values. In the case of lack of damping vibration run curve tends to infinity for any speed which generates a resonance harmonic.

Torsional damage of crankshaft, i.e. one of a changeable stiffness, takes place when the permissible amplitude value (permissible twist angle)  $\varphi_{dop}$  is exceeded (1) [2, 3].

$$\varphi_{rz} > \varphi_{dop} \quad (1)$$

$$\varphi_{dop} = M_s \sum_{i=1}^n \frac{L_i}{GI_{oi}}$$

where:

- $M_s$  – torque,
- $L_i$  – reduced length of shaft segment,
- $G$  – shear modulus,
- $I_{oi}$  – polar moment of inertia.

Many formulae are used for calculating the reduced length of crankshaft, i.e. shaft segment between cylinder axes. Among the most known the following may be numbered:

- Carter formula,
- Ker Wilson formula,
- Tulpin formula.

The formulae may be reduced to the general form as follows (2) [1, 2, 3, 8, 9]:

$$L_i = k_{cg} \frac{I_o}{I_{cg}} + k_{ck} \frac{I_o}{I_{ck}} + k_{rw} \frac{I_o}{I_{rw}} \quad (2)$$

where:

- $I$  – cross-section inertia moments,
- $k$  – set of quantities which account for crank geometry,

and the indices stand for:

- cg – main journal,
- ck – crank journal,
- rw – crank arm,
- o – reduced value.

Importance of the problem in question, i.e. danger of shaft damage due to occurrence of torsional vibrations in propulsion systems of floating objects resulted in that Polish Register of Shipping (PRS) issued a specialty rule publication entirely devoted to the calculating of crankshafts of combustion-ignition engines [10]. One of its sections contains guidelines and conditions to be abide by crankshaft designers.

## DAMPING OF TORSIONAL VIBRATIONS OF CRANKSHAFTS OF SHIP ENGINES

For many years for the damping of torsional vibrations of ship engine crankshafts the following kinds of dampers have been used:

- frictional dampers,
- rubber dampers (Photo 1),
- viscous dampers (Photo 2),
- spring dampers (Photo 3).

Among the above mentioned group of dampers the viscous one is most popular and successfully used for controlling vibration level of ship large-power medium-speed engines [4, 5].



Photo 1

Photo 2

Photo 3

## GENERAL METHODS OF SELECTION AND DESIGN OF VISCOUS DAMPERS OF TORSIONAL VIBRATIONS

In advance of commencing design of a viscous torsional vibration damper its designer should obtain, from engine producer, an appropriate set of necessary data [6].

The data should contain the information on:

- kind of fuel (petrol, diesel oil),
- number of cylinders,
- type of engine (two-stroke, four-stroke),
- minimum rotational speed of engine,
- maximum rotational speed of engine,
- range of operational speed of engine (if not constant),
- ignition sequence,
- main journal diameter,
- crank journal diameter,
- cylinder diameter,
- mean indicated pressure,
- total weight of masses in reciprocating axial motion,
- torsional stiffness of shaft between cylinders,
- permissible value of twist angle of shaft,
- limitations for damper gabarites.

The above specified data make it possible to form, for real propulsion system, a substitute vibrating system which enables to calculate:

- its natural frequency  $\Omega$  [rad/s] (3),
- resonance rotational speeds:

$$n_{wh} = \frac{60 \Omega_w}{2\pi h} \quad (3)$$

where:

- $\Omega_w$  – natural vibration frequency of w-form,
- w – vibration form number,
- h – harmonic's order; for two-stroke engines:  
 $h = 1, 2, 3, 4, \dots$ ;
- for four-stroke engines:  
 $h = 0.5, 1, 1.5, 2, 2.5, 3, 3.5, 4, \dots$

- relative torsional vibration amplitudes  $\Theta_i$  of particular masses of the system (Fig. 2), as well as:
- range of harmonics in the area where calculations have to be performed (4):

$$h_{\max} = \frac{60 \Omega_w}{2\pi n_{\min}}$$

$$h_{\min} = \frac{60 \Omega_w}{2\pi n_{\max}} \quad (4)$$

For the so determined range of harmonics, values of the tangent force  $T_h$  are calculated with accounting for the mean indicated pressure. Despite that the determined range of harmonics may be very wide it is sufficient, basing on multi-year experience, to take into account, in the performed analysis,

only a certain number of harmonics of the tangent force T. It is usually 12 ÷ 18 harmonics, because higher-order harmonics of wide ranges and small amplitudes are of low impact on vibrations.

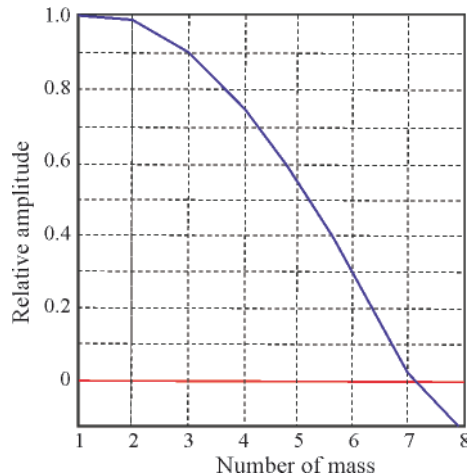


Fig. 2. Exemplary diagram of relative amplitudes calculated for a six-cylinder engine; 1) damper, 2 ÷ 7) crankshaft- piston system, 8) flywheel

As the following is known:

- values of relative amplitudes of masses,
- range of harmonics,
- values of tangent forces,
- values of rotational speed, which correspond to a given harmonic,

torsional vibrations of crankshaft free end can be calculated. First of all the calculations are performed without accounting for torsional vibration damper in the system, but with taking into account screw propeller and elastic coupling (if applied). Value of torsional vibration amplitude of engine crankshaft free end is described by the following formula (5):

$$\Theta_1 = \frac{90 A \sum_{i=1}^c \Theta_i}{2B + 2C + 2D} \quad (5)$$

where:

$$A = D^2 R T_h,$$

$$B = S_c \sum_{i=1}^c \Theta_i^2 \Omega_w,$$

$$C = S_p \Theta_p^2 \Omega_w,$$

$$D = \frac{k_s \Theta_s^2}{M},$$

- $\Theta_1$  – torsional vibration amplitude of crankshaft free end,
- D – cylinder diameter,
- R – crank radius,
- $T_h$  – tangent component of exciting harmonic,
- $\Theta_i$  – relative amplitude of i-th mass,
- $\sum \Theta_i$  – geometrical sum of relative amplitude vectors,
- c – number of cylinders,
- $S_e$  – engine structural damping coefficient,
- $S_p$  – screw propeller damping coefficient,
- $k_s$  – coupling torsional rigidity,
- M – coupling dynamic amplification (specified by coupling producer).

In order to obtain full image of crankshaft loading resulting from torsional vibrations, value of torsional stresses is

calculated, which can be analyzed by using diagrams prepared on the basis of the performed calculations.

The determination of values of twist angles of crankshaft free end and torsional stresses closes the first phase of damper selection after which preliminary calculations of the mass moment of inertia of damper inertia ring,  $I_p$ , are performed.

The mass moment of inertia of damper inertia ring,  $I_p$ , for a selected (designed) damper, has to comply with the following condition (6):

$$0.4 < \frac{I_d}{\sum_{i=1}^c \Theta_i^2 I_i} < 1 \quad (6)$$

where:

$\sum_{i=1}^c \Theta_i^2 I_i$  – the so called equivalent inertia of engine.

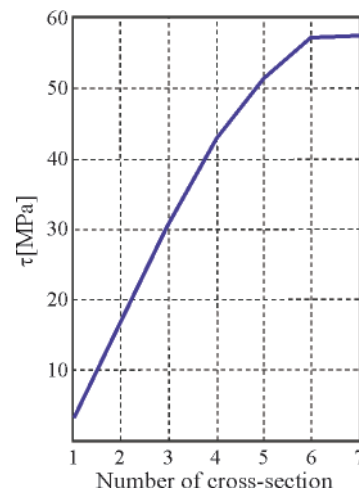


Fig. 3. Diagram of changes of torsional stresses in function of shaft cross-section, for a selected harmonic; exemplary results of calculations for a 6-cylinder engine

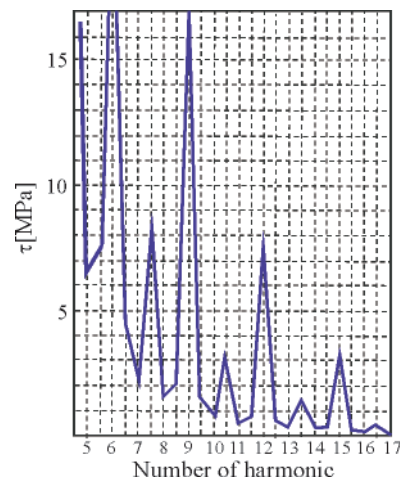


Fig. 4. Diagram of changes of torsional stresses in function of harmonic, for a selected vulnerable cross-section of shaft; exemplary results of calculations for a 6-cylinder engine

From the above given equation unambiguously results that for further analysis it is possible to obtain practically a set of „i” dampers whose effective mass moments of inertia are expressed as follows (7):

$$I_{ef_i} = I_{o_i} + \frac{I_{d_i}}{2} \quad (7)$$

where:

$I_{o_i}$  – mass moment of inertia of i-th damper casing.

Now, having the preliminarily selected set of „i” dampers, one performs identical calculations as for the system without damper but extended by the effective mass moment of inertia  $I_{ef}$ .

For every i-th system equipped with i-th damper the following is determined:

- system natural frequency,
- range of harmonics,
- resonance speeds,
- values of relative amplitudes (Fig. 5),
- values of twist angles of crankshaft free end,
- values of torsional stresses (Fig. 6).

Comparative analysis of the obtained results makes it possible to select, from the set of „i” dampers, that most effective in a given dynamic system.

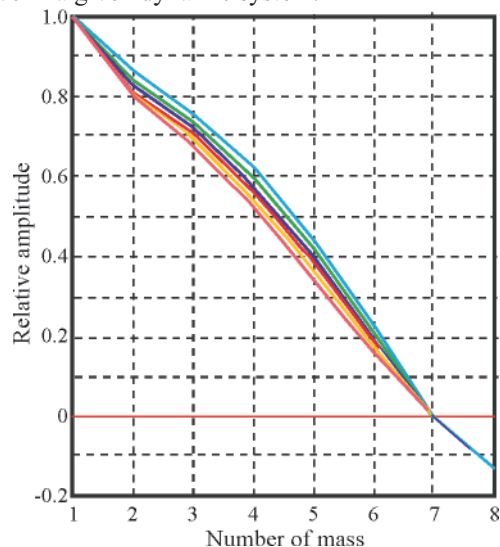


**Fig. 5.** Diagrams of relative amplitudes of particular equivalent systems for the whole set of preliminarily selected dampers; exemplary results of calculations for a 6-cylinder engine

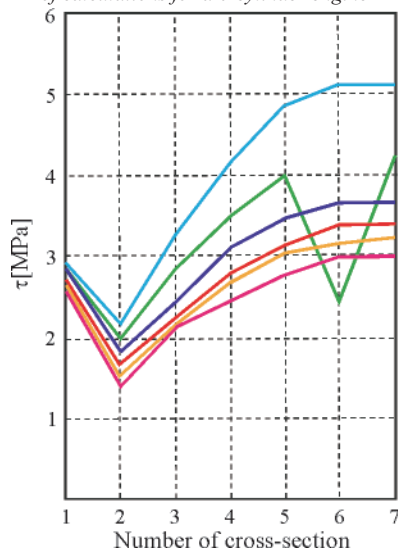


**Fig. 6.** Diagrams of torsional stresses in function of the most loaded cross-sections of shaft for the whole set of preliminarily selected dampers; exemplary results of calculations for a 6-cylinder engine

Viscous torsional vibration damper is that to which the fluid friction phenomenon is applied to effect vibration damping [7]. Therefore also value of friction moment resulting from friction forces acting on working surfaces of damper ring and casing, decides on its effectiveness.

The total value of friction moment which appears on damper inertia ring may be expressed as follows (8):

$$M_{tp} = M_{tpz} + M_{tpw} + M_{tpb} \quad (8)$$

and, that of friction moment on working surfaces of damper casing (9):

$$M_{to} = M_{toz} + M_{tow} + M_{tob} \quad (9)$$

where:

$M_t$  – friction moment,

and the indices stand for:

p – ring,

o – casing,

z – outer surface,

w – inner surface,

b – side surface.

Value of the friction moment does not depend only and solely on the geometrical parameters of damper but also on the fluid kinematic viscosity (10):

$$\nu = \frac{\eta}{\rho} \quad (10)$$

where:

$\eta$  – dynamic fluid viscosity,

$\rho$  – fluid density.

During selection of fluid viscosity intended for damper it should be remembered that the viscosity changes along with temperature changing.

As already mentioned, the vibration damping in the designed device is effected due to friction, hence energy dissipated by damper is transformed into heat. The heat generated in damper during the initial phase of its work is transferred mainly to the environment and partly used for heating the damper. It so long proceeds until the damper obtains the so-called saturation temperature.

After reaching the saturation temperature by the damper a justified concern arises that it may become seized due to its overheating resulting not only from the transformation of dissipated energy into heat but also its operation in an elevated environmental temperature (operation of damper in engine chamber) (Photo 4).



**Photo 4.** Image of an overheated and seized viscous torsional vibration damper, acc. tests made by the DAMPOL

In practice the detrimental phenomenon makes that the damper, instead to damp vibrations, starts to excite them. The damper, if correctly designed, should operate reliably for 20000 ÷ 30000 h in negative temperatures and first of all higher temperatures even as high as 120°C. Laboratory tests performed on viscous torsional vibration dampers demonstrated that events of seizing the dampers occurred when their working temperature values exceeded by 60°C the temperature for which they were designed.

Satisfactory effects of damper operation are reached when it operates within the temperature range from 75° ÷ 90°C in continuous cycle of work.

In view of damper operation effectiveness it is recommended to keep the specific power dissipated by damper lower than 8.6 [KM/m<sup>2</sup>] (counted per total surface area of its inertia member).

The range of heat flow within damper depends on:

- working conditions (a.o. engine rotational speed)
  - damper size,
  - damper design (of screw bolted casing or cold shut one)
- and is expressed as follows (11):

$$H = h \cdot A_p \quad (11)$$

where:

H – permissible heat flow rate [J/h],

A<sub>p</sub> – total surface area of inertia member,

h = 18 ÷ 22 [MJ/m<sup>2</sup>/h] – for instantaneous operation at critical speed,

h = 9 ÷ 11 [MJ/m<sup>2</sup>/h] – for dampers used for small high-speed engines intended for continuous operation at critical speeds, such as those applied to cars,

h = 4.5 ÷ 5.5 [MJ/m<sup>2</sup>/h] – for dampers of large low-speed engines intended for continuous operation at critical speeds, such as those used in ships.

**Note: The paper has been financially supported by the National Science Centre - Research Project No N N509 547440.**

#### BIBLIOGRAPHY

1. Brun R.: *High-speed combustion-ignition engines* (in Polish). WKiŁ (Transport and Communication Publishers), 1973
2. Dąbrowski Z.: *Machine shafts* (in Polish). PWN (State Scientific Publishers), 1999

3. Dąbrowski Z. Maksymiuk M.: *Shafts and axles* (in Polish). PWN, 1984
4. Homik W.: *Diagnostics, maintenance and regeneration of torsional vibration dampers for crankshafts of ship diesel engines*. Polish Maritime Research, No 1/2010
5. Homik W.: *Assessment criteria of merits of viscous torsional vibration damper for combustion engine crankshaft*. Western Scientific Centre of Ukrainian Transport Academy - Transportna Akademia Ukraini. Praci Zachodnowo Naukowo Centrum, NR 19 str 90-94, 2009,
6. Homik W.: *Designing viscous torsional vibration dampers* (in Polish). Przegląd Mechaniczny No.10/2007
7. Homik W.: *Torsional vibrations of crankshaft of engine without damper and that fitted with viscous torsional vibration damper* (in Polish). Przegląd Mechaniczny No. 9/2008
8. Jędrzejowski J.: *Mechanics of car engine crank systems* (in Polish). WKiŁ, 1986
9. Niewiarowski K.: *Piston combustion engines* (in Polish). WKiŁ, 1973
10. Polish Register of Shipping: *Calculation of crankshafts of compression-ignition engines* (in Polish). Publication No. 8/P, Gdańsk, 2007
11. Wajand J. A., Wajand J. T.: *Medium - and high - speed piston combustion engines* (in Polish). PWN, 1984
12. Wajand J.A.: *Self ignition engines* (in Polish). WKiŁ, 1973.

#### CONTACT WITH THE AUTHOR

Wojciech Homik, Ph. D.

Rzeszów University of Technology

The Faculty of Mechanical Engineering and Aeronautics

Al. Powstańców Warszawy 8,

35-959 Rzeszów, POLAND

tel.: 17 865 1100 w 1637, 17 865 1637

e-mail: whomik@prz.edu.pl

e-mail: whomik@interia.pl

# Operating and economic conditions of cooling water control for marine steam turbine condensers

**Andrzej Błaszczuk**, Assoc. Prof.  
Technical University of Lodz  
**Jerzy Głuch**, Assoc. Prof.  
Gdansk University of Technology  
**Andrzej Gardzilewicz**, Prof.  
Polish Academy of Science, Gdansk

## ABSTRACT

*The article presents the operational and economic analysis of controlling the cooling water flow in marine steam turbine power plants. The analysis bases on selected designs of the main condenser cooling water pumps and makes use of the results of investigations performed in inland power plants. Special attention was focused on marine aspects of the operation of those systems.*

**Keywords:** steam turbines; turbine operation; marine power plants; marine pumps; circulating pumps

## INTRODUCTION

One of basic components of the steam turbine power plant is the condenser in which the steam condenses after passing its heat to the cooling water. In marine power plants the water used for cooling the steam is taken from the outside, i.e. from the water area in which the ship sails. In the majority of power plants the condenser cooling water pumps work at constant mass flow rate, but recently a more and more frequently analysed problem is an attempt to control this parameter, especially when the turbine works under changing load conditions. The main reason for applying control systems in inland turbine power plants is an attempt to save the water, the consumption of which is extremely high during steam power plant operation [1, 5, 8, 12]. Marine turbine power plants also reveal remarkable load changes. Although turbine driven tankers for transporting liquid oil-based chemicals have not been built any longer in recent years, a number of such tankers for transporting liquefied gas were launched. Therefore the economic analysis of cooling pump operation in marine power plants is fully justified, especially in case of tankers, which sail with the cargo in forward trip and return only loaded with the ballast. The above situation considerably differentiates ranges of power required by the ship propulsion system. Moreover, ships with unlimited sailing region, which are, as a rule, designed for least favourable conditions of power plant operation in the tropical zone, also sail in more moderate zones, which needs adapting the operating conditions

of their cooling systems to current ambient temperatures. Another argument justifying the interest in analysing the above problem is the appearance of opinions suggesting the need for reconstruction of the global fleet of liquefied fuel tankers based on new standards [17] due to the exploitation of new deep-sea oil development areas. We can expect that in the nearest future new tankers with both engine and turbine propulsion systems will be built.

Until recently, attempts to decrease the power used by the auxiliary devices have been almost unprofitable, which was connected with the loss of turbine unit power due to the pressure increase in the condenser caused by the reduced mass flow rate of the cooling water at lower loads. It was partially justified, as the efficiency gain resulting from such an approach, which was estimated based on on-line measurements, turned out very inaccurate.

That is why the mass flow rate of the condenser cooling water was controlled rather rarely. This control referred to, for instance, changing the angular position of the blades in the rotors of axial-flow pumps, done in order to reduce the technically unfavourable power limits during pump start-ups rather than for economic and water saving reasons [15, 16].

It should be mentioned here that the "seasonal" rotation of axial-flow pump rotor blades, which was used for years, resulted from the "numerical" water flow optimisation oriented on adapting the system to tropical, moderate, or arctic conditions. The above actions were a source of operating problems connected with blade seizing in these



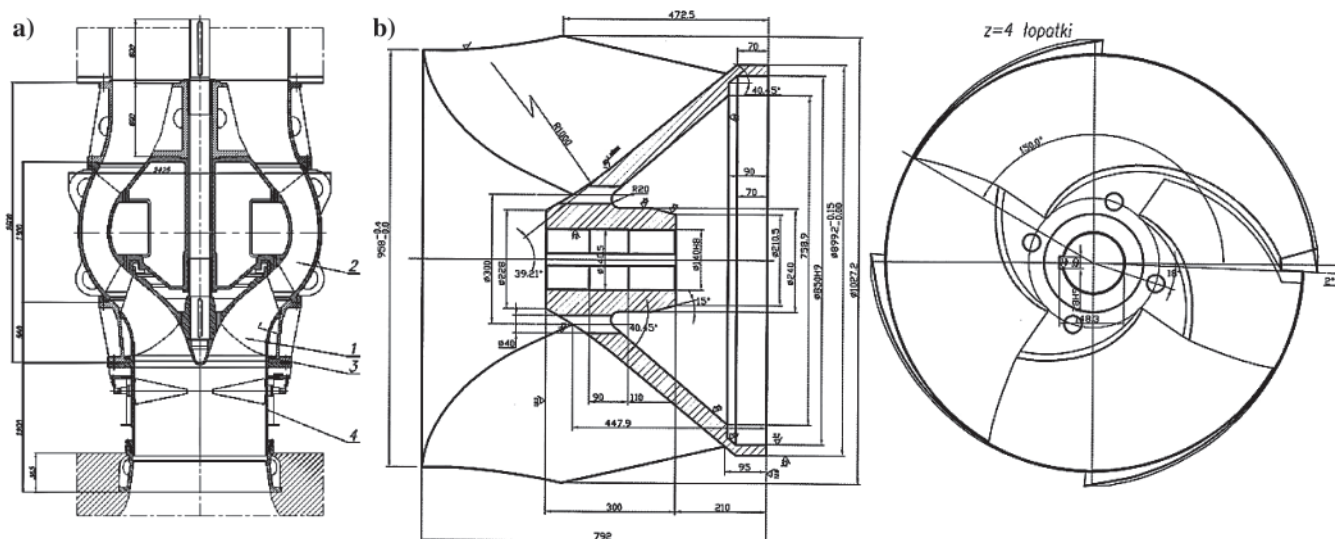


Fig. 1. Designs of cooling water pumps used in inland 360 MW steam turbine power plants (a) and their rotors used in 200 MW power plants (b) [2, 3]

pumps. Pumps of other types have no practical possibilities to control the water flow via changing the geometry of the rotating elements.

The article presents a comprehensive evaluation of the effect of controlling the mass flow rate of the water pumped by the diagonal pumps for cooling the condenser on the economy of operation of the entire power plant. The analysis takes into account, on the one hand, the reduction of the power needed for driving the cooling water pumps at their reduced capacity, but also, on the other hand, power losses of the main turbines resulting from the lower-quality vacuum in the condenser due to smaller rate of the cooling water. Operating aspects of such solutions which are specific for marine applications are also discussed.

### PROPOSED DESIGNS OF COOLING WATER PUMPS

Controlling the cooling water mass flow rate started to be the subject of discussion when the turbine blocks in inland steam turbine power plants were to be modernised. Old pumps in those blocks were subject to failures during block operation, as they frequently worked in cavitation areas. Consequently, they did not guarantee preserving the required parameters in the repaired blocks. Castings of their rotors were made carelessly of carbon steel, which considerably affected their lifetime. Modern design and technological procedures and methods have made it possible to design new rotors which remarkably improved the efficiency of pumping and provided opportunities for better adjustment of the operation of these pumps to changing load conditions. The designs of the cooling water pumps for inland large-power turbines are shown in Fig. 1 [2, 3].

Tests of the new pumps have revealed remarkable advantages of their designs, which can be observed when comparing the operating characteristics of the old and new pumps cooperating with one turbine, see Figs. 2 and 3, [7]. The efficiency gains after modernisation amounted to over 10%, at simultaneous increase of the elevation head and water mass flow rate.

Positive tests were the motivation for designing water control systems for those pumps to adapt their operation to changing power loads and environmental conditions. The technical analysis performed for the existing configurations of the cooling systems has revealed that the best way to control the water mass flow rate is the use of guide vanes.

Introducing guiding blades at the impeller pump inlet turned out operationally stable, cheapest, and very efficient when the control range was not excessively high [14]. An inlet guide vane designed and installed in the cooling water pump working in the 360 MW turbine system is shown in Fig. 4 [4]. By changing the guide blade setting angle  $\alpha$  the cooling water flow could be changed with high efficiency by even as much as 30% reduction of the nominal mass flow rate, what can be seen on the experimentally determined operating characteristics, Figs. 2 and 3. This method turned out much better than throttling, which was used in the past for pumps cooperating with turbines and cooling towers [1].

It also turned out that the inlet guide vanes can be set with “negative” angles with respect to the direction of rotor rotation, thus introducing an opposite angular momentum of the water flow onto the rotor blades. Such an approach enabled increasing the mass flow rate of the condenser cooling water over the nominal level for unchanged pump construction. Indeed, this effect is occupied by increased power taken by the motor used for driving the pump, but it makes it possible to decrease the steam condensing pressure when the temperature of the cooling water is extremely high. This pump operation control is only possible when the (usually electric) motor used for driving the pump has excess power reserve and can be overloaded.

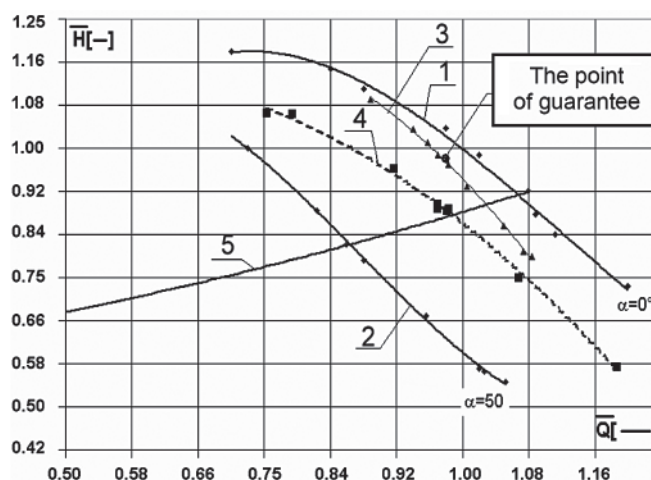


Fig. 2. Generalised flow characteristics of the cooling water pumps installed in an inland power plant: new pump (1 ÷ 3), old pump (4), pipeline (5), [3]

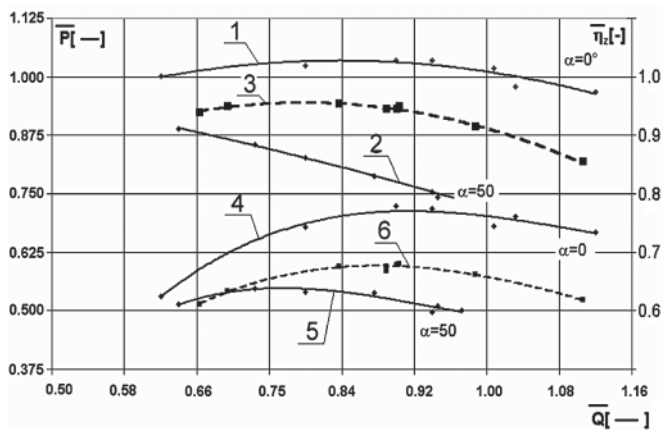


Fig. 3. Efficiency characteristics of the old non-controlled pump (6) and the modernised pump (3), along with the electric power consumption of the cooling water pumps installed in an inland turbine system: old pump (1) and new controlled pump (2, 4, 5) [2, 3]

### COOLING WATER PUMP CONTROL IN SEA CONDITIONS

The operation of the cooling water pumps in marine turbine power plants was performed using the gas tanker driven by the main turbine of an approximate power output of 25000 kW as a sample case. A scheme of this turbine power plant is shown in Fig. 5.

The main condenser is cooled with the sea water using circulating pumps of approximate capacity 8000 m<sup>3</sup>/h (about 2250 kg/s) each. The configuration of the condenser cooling system is given in Fig. 6, while the scheme of cooling water pump connections is shown in Fig. 7.

Since the main turbines work at changing power, it is advisable to use cooling water pumps of changing capacity. For this purpose the control systems described in the previous section which make use of the inlet guide vane can be applied. These systems have already been positively tested and checked in a number of inland power plants. It is noteworthy that the cooling water mass flow rate is controlled by changing the

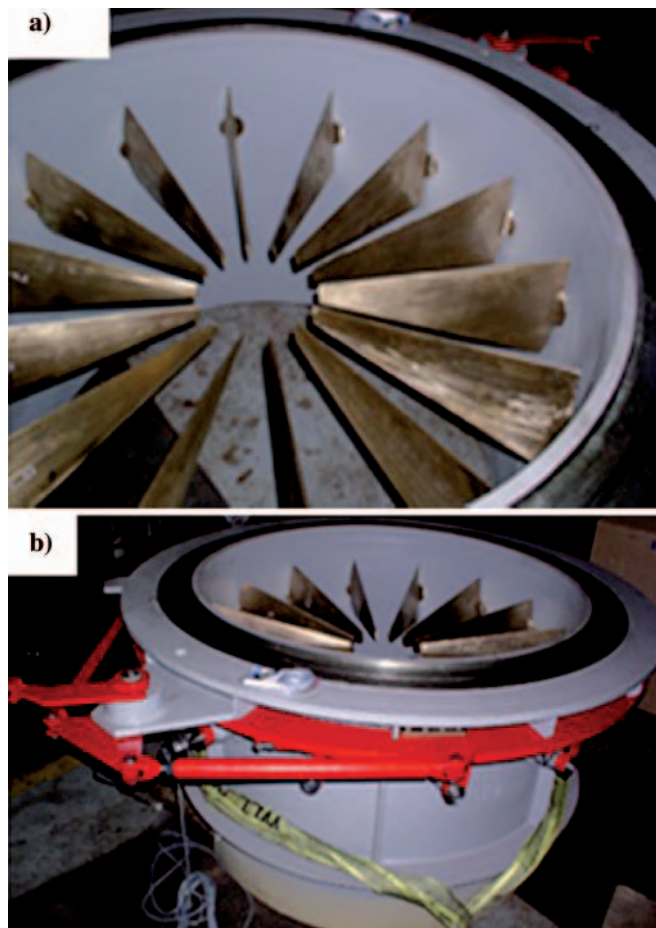


Fig. 4. View of inlet guide vane blades (a) and blade setting mechanism (b)

setting of the inlet guide blades, i.e. the immovable element. In inland condition, no traces of seizing of the setting mechanism of the guide vane blades were recorded during the pump operation. The above control method improves operating characteristics as it requires less servicing actions, a factor which is very important in sea conditions.

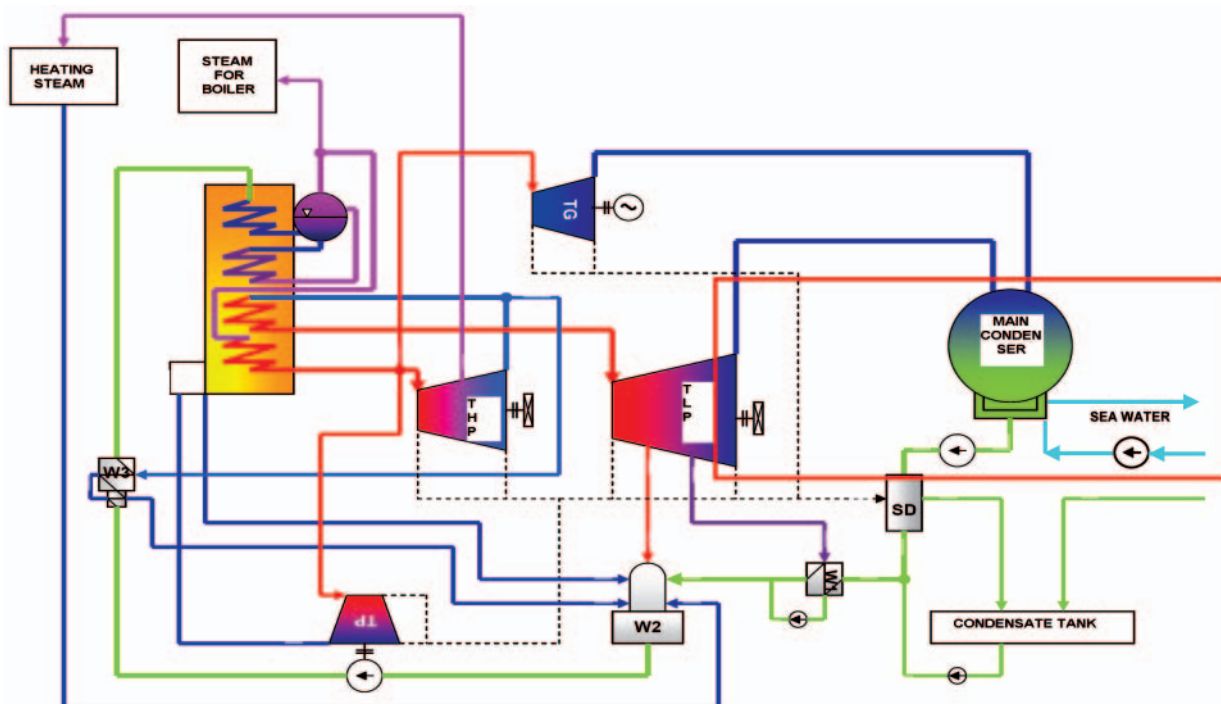


Fig. 5. Scheme of steam turbine power plant of approximate power of 25000 kW in an LNG tanker [17]

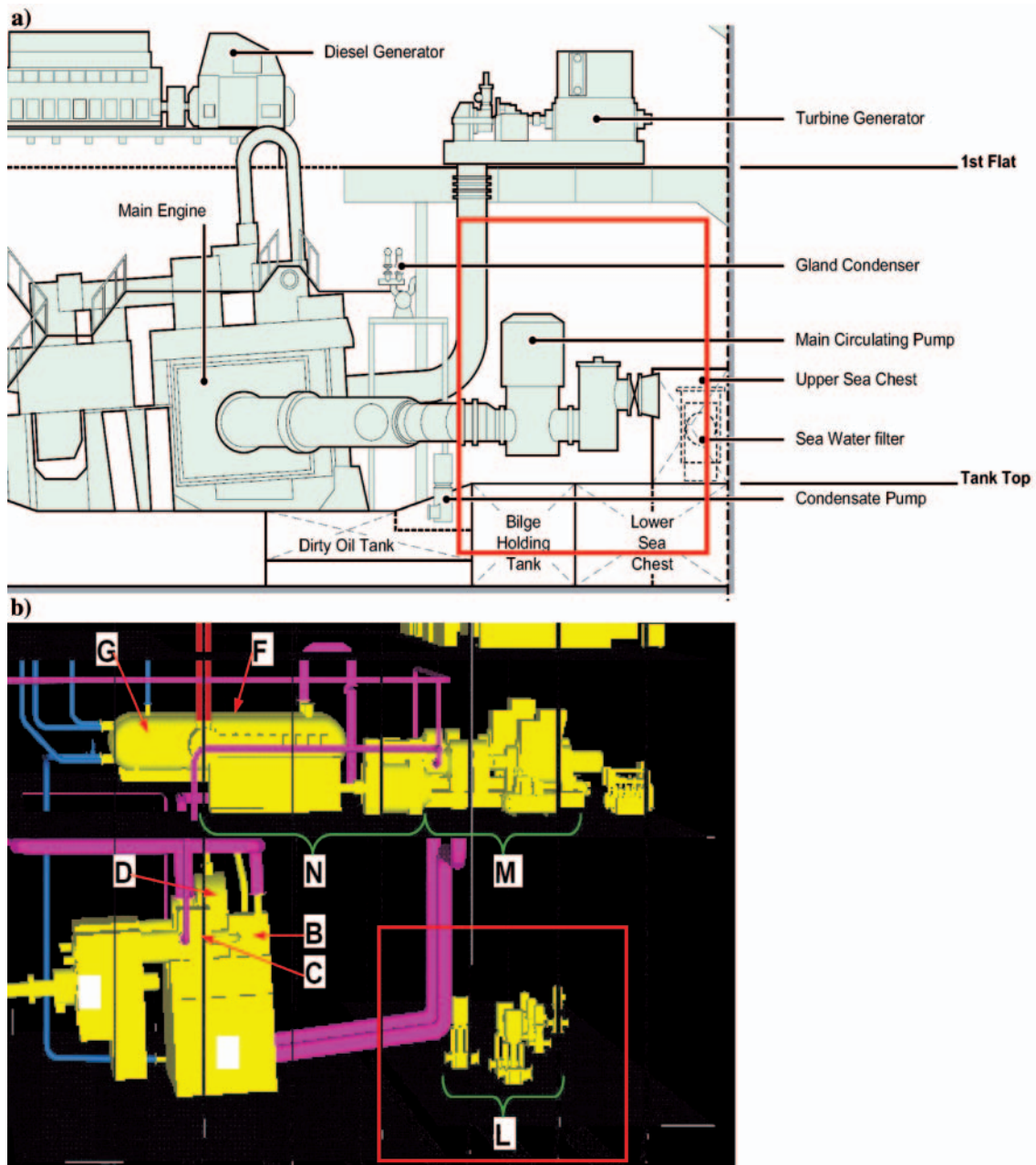


Fig. 6. Configuration of the main condenser cooling system in the steam turbine power plant of an approximate power of 25000 kW in an LNG tanker [17]; a) cross section; b) view.

A system feature which should be mentioned here is the possibility to increase the mass flow rate of the condenser cooling water by introducing the negative angular momentum at water inlet using a negative setting angle of the inlet vane blades. This solution can be profitable for the marine power plants operating in extreme tropical conditions. Another way of using this control method may consist in assuming lower sea water temperatures than those for tropical conditions when designing power plants of the ships with unlimited sailing region.

### ECONOMIC AND TECHNICAL ANALYSIS OF THE USE OF COOLING WATER CONTROL

For the time being, the economic and technical analysis of the use of cooling water control systems in steam turbines to follow turbine load changes was only possible based on detailed design calculations taking into account the turbine geometry,

see for instance the study by Dzierzgowski [6]. This situation originated from the fact that evaluating possible gains of such control should take into account the entire thermal cycle of the turbine set, with very accurate evaluation of the operation of so-called “cold end” apparatuses including: low pressure turbine, condenser, pumps, and the cooling water system. It was a rather difficult task as the gains resulting from the use of this control were very small compared to the turbine power output, while the physical description of thermal and flow phenomena accompanying this process, necessary for performing the above calculations, were extremely complicated.

This situation was the reason why the advantage of water control could not be uniquely evaluated, even based on warranty thermal measurements performed in steam turbine power plants [8, 12]. In inland conditions this inability was checked on 200 MW blocks, where the gains calculated using the nomogrammes obtained from the producers and describing the operation of these apparatuses [7] were at the level of calculating errors.

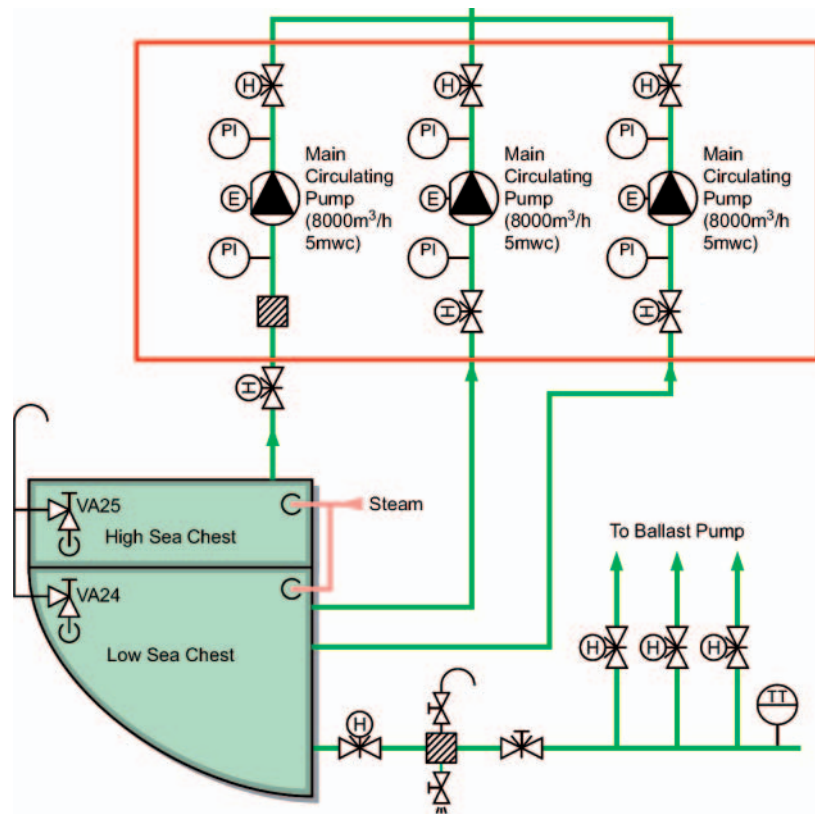


Fig. 7. Connections of main condenser cooling water pumps in the steam turbine power plant of an approximate power of 25000 kW in an LNG tanker [17]

In this article, the water control effects are proposed to be evaluated using the code DIAGAR [9] which was successfully used in thermal diagnostics including repair prognoses for individual apparatuses in 200 MW turbine systems in inland power plants [10, 11]. High accuracy of calculations done using this code results from the fact that the balances obtained from the measurements are currently verified by the calculations making use of detailed description of the geometry of individual apparatuses in the thermal cycle. The performed investigations have proved that this numerical “calibration” of the results of the measurements done by DCS systems in power plants provides opportunities for evaluating the operation of individual apparatuses at the accuracy level below  $\pm 30$  kW [10]. The above methodology has made it possible not only to evaluate precisely the efficiency of particular apparatuses, follow the course of their degradation, and prepare a reasonable repair plan, but also to analyse possible modernisation and improvement variants, including the evaluation of advantages of particular cooling water control systems.

A numerical test of the above described cooling water pump control system was performed for a selected inland power plant turboset and for a marine power plant shown in Fig. 5. The apparatuses in the frame in Fig. 5 represent the “cold end” of the turbine and in the examined case were the subject of detailed control.

The initial version of the diagnostic calculations performed for the thermal cycles of the inland and marine power plants had omitted cooling water system components [12]. For the purpose of the present analysis these components were included in the calculations, along with relevant data about their operation, which made it possible to calculate their energy parameters in changed operating conditions. Beside pumps and pipelines, the delivered information also referred to low-pressure turbine and condenser components which had been modernised in the inland turboset. The calculated characteristics of the power plant turboset were verified by comparing them with the results

of the measurements done on a real block [3, 11]. The obtained results are shown in successive figures, with labels facilitating their interpretation, to illustrate advantages of the discussed control method.

The pump characteristic shown in Fig. 3 refers to electric power and efficiency changes as a function of the water mass flow rate. In this case the gains connected with the reduction of the mass flow rate result directly from the savings of the electric power needed for driving the pumps. This was not so clear for old pumps, whose characteristics (1, 6) obtained from measurements are given in Fig. 3, for the case of throttle governing. The operating characteristics recorded for the control performed by changing the blade settings, which are shown in this figure, have been recorded in model tests [2, 3].

The characteristic of the low-pressure turbine part shown in Fig. 8 reveals that the load change, which is here equivalent to the change of the volumetric steam flow rate ( $G_p \cdot v_k$ ), can result in efficiency changes equalling even as much as 5%. For the given turboset power and the assumed steam mass flow rate  $G_p$ , the efficiency gains (or losses) result from specific volume  $V_k$  at the controlled mass flow rate  $G_w$  of the cooling water. The quantity  $V_k$  is stabilised for new conditions in the condenser as a result of pressure changes behind the turbine:  $V_k = f(p_k)$ . These parameters can be determined directly from the condenser characteristics, which for the tested turbine are shown in Fig. 9. They are given in the form of  $p_k = f(G_w)$  for different mass flow rates and constant inlet temperature of the water.

The same efficiency changes, in percents, were assumed for the analysis of the marine power plant.

Based on the curves shown in the figures, which correspond to turbine and condenser operation at nominal and changing loads, it is difficult to evaluate precisely gains resulting from the cooling water control. It only becomes possible after the calculations of the entire thermal cycle, done by the code DIAGAR which makes use of the above operating characteristics

of the cold end apparatuses. The results of these calculations, which include the evaluation of power gains and the specific heat consumption of the entire thermal cycle as a function of the load with and without cooling water control, are shown in Figs. 10 and 11. They are given in the form of  $\Delta N$ ;  $\Delta q = f(N/N_0)$  for inlet water temperatures equal to 15°C and 30°C which corresponds to winter and summer conditions of turboset operation. The diagrams take into account the assumed 15% reduction of the water mass flow rate with respect to the nominal rate, which was assumed here at the level of 25000 m<sup>3</sup>/h.

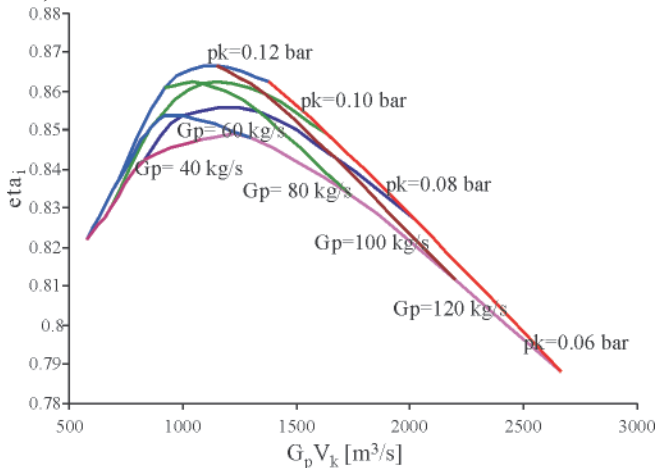


**Fig. 8.** Efficiency of the modernised low part of the inland turbine vs. volumetric flow rate of steam for different mass flow rates of steam and different condenser pressures  
 $T_{w1} = 15 [^{\circ}C]$

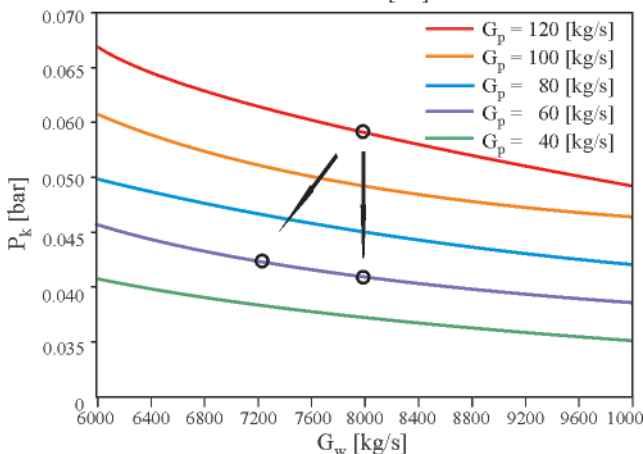


**Fig. 9.** Condenser pressure changes vs. cooling water mass flow rate for different mass flow rates of steam at the assumed inlet water temperature

The presented diagrams reveal that the 15% reduction of the water flow in winter ( $t_w = 15^{\circ}C$ ) brings gains practically within the entire operating range. At 50% load these gains exceed 300 kW (about 0.2% of the turboset power). It is noteworthy that the water flow control for low loads eliminates supercooling of the condensate in the condenser, see Fig. 10. This is a positive

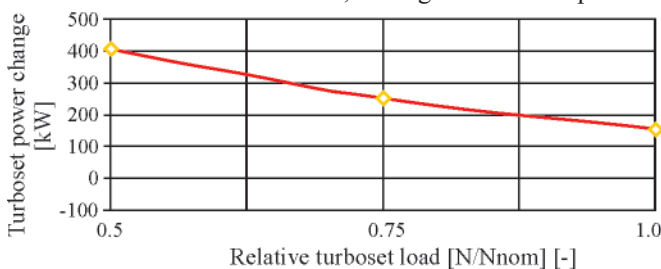


**Fig. 10.** Increase of turboset power (specific heat consumption) vs. load for the cooling water mass flow rate reduced by 15% for winter conditions ( $t_w = 15^{\circ}C$ )

feature as the supercooling effect is unfavourable for the turboset efficiency. At the same time in the summer, at high inlet water temperatures ( $t_w \sim 30^{\circ}C$ ) the control brings gains only when the load decreases below 50%, while the loss at nominal load and 15% water flow reduction reaches 400 kW! In this case the cooling water flow should be increased rather than reduced. Therefore it is advisable to evaluate precisely once again the nominal cooling water mass flow rate in the cooling pumps for each turboset after its modernisation.

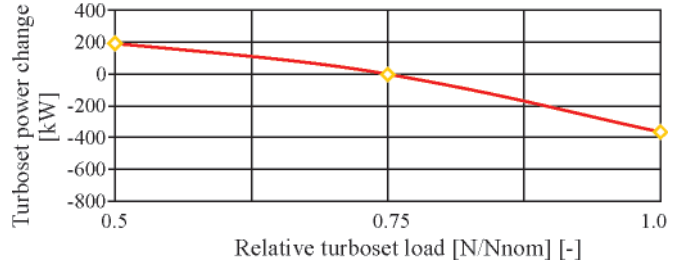


**Fig. 11.** Increase of turboset power (specific heat consumption) vs. load for the cooling water mass flow rate reduced by 15% for summer conditions ( $t_w = 30^{\circ}C$ )

## TECHNICAL ASPECTS OF COOLING WATER CONTROL IN MARINE POWER PLANTS

Preliminary calculations performed for the marine power plant, see fig. 5, with the aid of the code DIAGAR confirmed the opinion that the nature of efficiency changes and power gains resulting from the control of the mass flow rate of the water cooling the condenser is similar to that recorded in inland turbine power plants. However, in case of the marine power plants there are more uncertainties concerning the temperatures of the seawater taken for cooling purposes. Nevertheless we can conclude that the percent changes of power and efficiency observed in inland and marine power plants are close to each other.

That means that in the moderate and tropical zones the characteristics realised by the marine power plants will be similar to those of the inland power plants working in comparable conditions. In particular, in the moderate zone at a reduced power plant power we can expect the maximal power gains within the limits up to 0.2% of the nominal power for the entire thermal cycle, taking into account both the reduced power needs for driving the pumps, and the power loss resulting from the lower-quality vacuum in the condenser. For the marine steam turbine power plant with the main turbines of the approximate nominal power of 25000 kW it gives about 50 kW of the reduction of the ship's power plant load. Assuming that the specific fuel consumption in this power plant is approximately equal to 200 g/kWh, we can expect the reduction of the fuel consumption by about 240 kg per 24 hours. The above assessment refers to the moderate zone. The expected gains will be much higher when sailing close to the arctic zone.

In extreme conditions in the tropical zone we should increase the mass flow rate of the condenser cooling water to reach the deepest possible vacuum. We can easily obtain this effect by generating a negative angular momentum via turning the guide vane blades.

In marine conditions axial pumps can be used, as the elevation head, measured in mwc, needed for cooling the condenser is relatively small. These pumps can also be controlled using inlet guide vanes. The power and efficiency gains expected in this case can be even larger than for diagonal pumps [2].

## CONCLUSIONS

- The presented analysis has proved that it is advisable to control the cooling water mass flow rate in steam turbine power plants to follow turbine load changes. Possibility of this control is provided in the designs of cooling water pumps installed in recently modernised large-power blocks [2, 3]. These pumps reveal cavitation-free operation and higher efficiency. Water flow changes can be realised in these pumps by changing the angular settings of the inlet guide vane blades, to response to accurately measured changes of the electric power of the turboset and the inlet temperature of the cooling water, or (alternatively) the pressure in the condenser. However, these signals are to be correlated with the calculations of the turboset thermal cycle, which can be done online using the data recorded by the power plant measuring system and a relevant computer code [13].
- Preliminary calculations making use of the results of measurements performed in inland power plants have revealed that in winter for the 200 MW blocks, power gains can be obtained within the entire range of turbine operation when the mass flow rate of the cooling water is reduced by 15% with respect to the nominal value. When the load is reduced by 50%, these gains can even reach 400 kW i.e. 0.2% of turboset power, which is equivalent to the decrease of the specific heat consumption by 15 kJ/kWh. In the summer these gains are smaller, for higher load ranges when the temperature of the cooling water exceeds 30°C it is advisable even to increase the flow of the cooling water with respect to the nominal mass flow rate, which can be done using the inlet guide vanes.
- Similar gains can be expected in case of steam turbines working in marine power plants. When the ship sails in the moderate zone and at reduced driving power we can expect the reduction in power plant fuel consumption amounting approximately to 240 kg per 24 hours. At the same time, the control making use of adjustable guide vane blades provides good opportunities for increasing the cooling water mass flow rate to obtain deeper vacuum in the condenser in the tropical zone.

## NOMENCLATURE

- $\eta_i$  – efficiency of turbine Low Pressure (LP) part [-],  
 $G_p$  – steam mass flow rate [kg/s],  
 $G_w$  – cooling water mass flow rate [kg/s],  
 $H$  – pump outlet pressure [m of H<sub>2</sub>O or MPa],  
 $N$  – power of power unit [kW],  
 $\Delta N$  – change of power of power unit [kW],  
 $Q$  – volumetric flow rate [m<sup>3</sup>/s],  
 $p_k$  – condenser pressure [kPa],  
 $P$  – power of pump motor [kW],  
 $t_{in}$  – inlet temperature of cooling water [°C],  
 $v_k$  – specific volume of condensing steam [m<sup>3</sup>/kg].

## BIBLIOGRAPHY

1. Bilkowski E., Olszowiec R., Szybalski K.: *Production of electric energy in the Belchatow power plant in the aspect of water pump operation in its technological systems* (in Polish), Proceedings of the 10-th Forum of Pump Users, Bełchatów 2004.
2. Błaszczuk A., Popierski A., Staniszewski J.: *Modernisation of 160 D30/HP cooling water pumps* (in Polish), Proceedings of the 7-th Scientific and Technical Conference, Słok 2005.
3. Błaszczuk A., Popierski A., Najdecki A., Staniszewski: *Modernization of the hydraulic system of the 120D40 cooling water pumps*, (in Polish), Proceedings of the 7-th Scientific and Technical Conference, Słok 2007.
4. Błaszczuk A., Staniszewski J., Kuźba G., Woźniak D.: *Control of the 160D30 cooling water pump*, (in Polish), Proceedings of the 7-th Scientific and Technical Conference, Słok 2007.
5. Dzida M.: *Problems of steam condensers cooling water flow control in case of turbine partial loads*, (in Polish), Proc. 2-nd Scientific and Technical Conference on Power Plants, Słok 1995.
6. Dzierzgowski J.: *Technical analysis of designing steam turbine condensers*, (in Polish), Ph.D. thesis, Faculty of Ocean Engineering & Ship Technology, Gdansk University of Technology, Gdańsk 1992.
7. Energopomiar Gliwice, *Recommendations after the control of the operation of steam turbine condensers*, (in Polish) Publications of the Ministry of Mining and Energy, Warsaw, Gliwice 1986.
8. Gardzilewicz A., Błaszczuk A., Głuch J.: *Advantages of Condenser Cooling Water Control in Large Steam Power Units*, Proc. European Conference on Turbomachinery ETC'2009, Graz 2009.
9. Gardzilewicz A., Głuch J., Bogulicz M., Jankowski T., Uziębło W.: *Code package DIAGAR for steam turbine thermal diagnostics calculations*, (in Polish), Report of DIAGNOSTYKA MASZYN, Gdańsk 1995-2009.
10. Gardzilewicz A. Głuch J., Bogulicz M., Walkowiak R., Najwer M., Kiebdój J.: *Experience in Application of thermal Diagnostics in the Turów Power Station*, Proc. ASME IJPGC, Atlanta 2003.
11. Gardzilewicz A., Marcinkowski S., Kurant B.: *Thermal and Flow Investigations in LP of Turbine Blade System*, Proc. Turbomachinery, Workshop, Gdańsk 2006.
12. Głuch J.: *Selected Problems in Determining an Efficient Operation Standard in Contemporary Heat and Flow Diagnostics*, Polish Maritime Research S1/2009, Gdańsk 2009.
13. Głuch J., A. Gardzilewicz A.: *The analysis of performance of the turbine condenser with prognosis of repair*, Proc. ASME IJPGC, Baltimore, 1998.
14. Łojek A.: *Pre-rotational and extractive control of impeller pumps*, (in Polish), Ph.D. thesis, Institute of Fluid-Flow Machinery, PAS, Gdańsk 1987.
15. Marczewski J. et al.: *Modernisation of the control system for the cooling water pumps of 200 MW turbine sets in the Połaniec power plant*, (in Polish), Internal report of the Połaniec power plant, 2001-2003.
16. Sadowski A., Łojek A., Klein M., Szerucki J.: *Modernisation of the control system for the cooling water pumps of 500 MW turbine sets in the Kozienice power plant*, (in Polish), Pompy i pompowanie.
17. Sienica K.: *A preliminary project of the steam turbine power plant for the ship transporting the liquid natural gas*, (in Polish), M.Sc. thesis, Faculty of Ocean Engineering & Ship Technology, Gdansk University of Technology, supervisor: Krzysztof Kosowski, Gdańsk 2005.

## CONTACT WITH THE AUTHORS

Andrzej Błaszczuk, Assoc. Prof.  
Institute of Fluid-Flow Machinery,  
Technical University of Lodz, Stefanowskiego 15,  
90-537 Lodz, POLAND  
email: akblaszc@p.lodz.pl

Jerzy Głuch, Assoc. Prof.  
Faculty of Ocean Engineering & Ship Technology,  
Gdansk University of Technology,  
Narutowicza 11/12,  
80-233 Gdansk, POLAND  
email: jgluch@pg.gda.pl

Andrzej Gardzilewicz, Prof.  
Institute of Fluid-Flow Machinery,  
Polish Academy of Science,  
Fiszera 14,  
80-952 Gdansk, POLAND  
email: gar@imp.gda.pl

# Influence of hydraulic oil viscosity on the volumetric losses in a variable capacity piston pump

Jan Koralewski, M. Sc.  
Gdańsk University of Technology

## ABSTRACT



*The variable capacity piston pumps are elements of the great power and highest energy efficiency hydrostatic drives. They are used in the drive systems of ship equipment such as deck cranes, steering gears, main propulsion of smaller vessels. The laboratory and simulation investigations of the influence of liquid viscosity on the variable capacity displacement pump energy losses have not been so far performed.*

*The paper presents results of the investigations of impact the hydraulic oil viscosity has on the volumetric losses in a piston pump operating in the full range of its capacity and oil pressure.*

**Key words:** hydrostatic drive; displacement pumps; estimation of energy losses; impact of the oil viscosity on losses

## INTRODUCTION

A hydraulic system with variable capacity pump, as a structure allowing to change the motor speed, is a hydrostatic drive solution with the highest energy efficiency. It is used in the great power systems, in the situations of prolonged system operation, wherever the energy saving is preferred even with more expensive investment and greater operation requirements. Examples of the ship applications are the drive and control solutions of a deck crane, steering gear and main propulsion of smaller vessels.

It is important to know the transmission energy efficiency in the nominal conditions but also in the whole range of the operating conditions (hydraulic motor load and speed, hydraulic oil viscosity), particularly in the most often occurring or most prolonged operating conditions.

A hydraulic drive system designer or user has at his disposal, provided only by some manufacturers, results of the energy efficiency tests of machines in the systems, tests performed with a selected oil viscosity. The efficiency of a hydraulic motor and its driving pump as elements of a hydrostatic transmission system should be determined as a function of the motor shaft speed and torque.

There is no tool allowing to perform full energy analysis of the hydrostatic transmission as a whole composed of any different set of machines. The transmission system efficiency should be presented as dependent on the hydraulic motor speed and load, with a possibility of evaluating the impact of volumetric, pressure and mechanical losses, different in various types and sizes of the machines used an also evaluation of the impact of pressure losses in the system conduits.

All those losses are also a function of current motor operating parameters and of the oil viscosity changing during the system operation.

So widely understood simulation investigations require a suitable model of the variable capacity pump losses and energy efficiency, and also a model of the system efficiency with such pump. In order to verify the models, it is necessary to carry out carefully prepared laboratory investigations of the pump, hydraulic motor and the whole system. Such investigations, with the constant recommended oil viscosity  $\nu_n = 35\text{mm}^2\text{s}^{-1}$  were performed by M. Czyński [1].

**The laboratory and simulation investigations of the impact of liquid viscosity on the variable capacity displacement pump energy losses have not been performed yet.**

## MATHEMATICAL MODELS OF THE DISPLACEMENT MACHINES LOSSES AND ENERGY EFFICIENCY

Assessment of the capability of energy savings in the hydrostatic drive system operation requires the system losses to be defined.

The simulation determination of the system energy efficiency may be used for the purpose in the system design and operation process [2]. The following factors in the simulation model should be taken into account:

- the hydraulic motor speed control system structure,
- energy losses in the system elements,
- the pump driving motor speed decrease,
- the system control element characteristics,

- load and speed of the controlled hydraulic motor,
- hydraulic oil viscosity, changing in the system operation process due to change of the oil temperature.

In order to make the transmission system efficiency determination method easily applicable, it is necessary to:

- 1) use the computer programs for the mathematical models, allowing to analyse the hydraulic system efficiency as a function of the decisive parameters (hydraulic motor speed coefficient  $\bar{\omega}_M$  and load coefficient  $\bar{M}_M$ , ratio  $v/v_n$  of the hydraulic oil viscosity  $v$  to the reference viscosity  $v_n$ ),
- 2) determine the values of energy loss coefficients for the pump, rotational hydraulic motor or hydraulic cylinder. Those coefficients should be clearly defined and precisely determined for a given displacement machine.

The mathematical model of the displacement machine losses allowing to fulfil the conditions given in points 1 and 2 above should take into account:

- a) the form and simplicity of the description, deciding of the possible use of that description in the system efficiency model, with maintaining the system efficiency precise assessment,
- b) description of the displacement machines volumetric losses, allowing to evaluate the impact of hydraulic oil kinematic viscosity changing with oil temperature,
- c) separate treatment of the mechanical and pressure losses in the machine. These losses increase the required torque on the machine (pump) shaft but the losses are of different character and depend on the same parameter (viscosity coefficient  $v/v_n$ ) but in a different way.

It is necessary to perform the laboratory and simulation investigations in the displacement machine real operating conditions. The investigations should allow to verify the proposed models of:

- machine volumetric losses,
- machine pressure losses,
- machine mechanical losses,

in the full range of working pressure up to nominal pressure  $p_n$ , in the wide range of pump capacity up to theoretical capacity  $Q_{Pt}$  and in wide range of the hydraulic oil kinematic viscosity  $v$ , and also to determine the  $k_i$  coefficients of specific losses.

## MODEL OF THE DISPLACEMENT PUMP VOLUMETRIC LOSSES

Volumetric losses require an increase of the pump geometrical capacity, are connected first of all with the working liquid leaks through slots between displacement elements and the working chamber walls, distributor (if it exists) elements and are also effect of the liquid compressibility, change of the pump working volume and change of the slot height due to changes of pressure and temperature.

The model of volumetric losses presented by Z. Paszota in [2, 3, 4] meets the requirements given in chapter 2. The author assumes the conditions and simplifications of the impact of certain factors on those losses and that impact is reflected in a coefficient and in power exponents describing the dependence of losses on  $\Delta p_{Pi}$  and  $v$ .

**The theoretical pump working volume  $q_{Pt}$**  (theoretical capacity  $q_{Pt}$  for one pump shaft revolution) – the geometrical difference between the maximum and minimum volume of working chambers – is a characteristic value of a pump. It is determined at the pressure value  $p_{Pi} = 0$  in the pump working chambers during their filling and at the increase  $\Delta p_{Pi} = 0$  of the indicated pressure in the chambers.

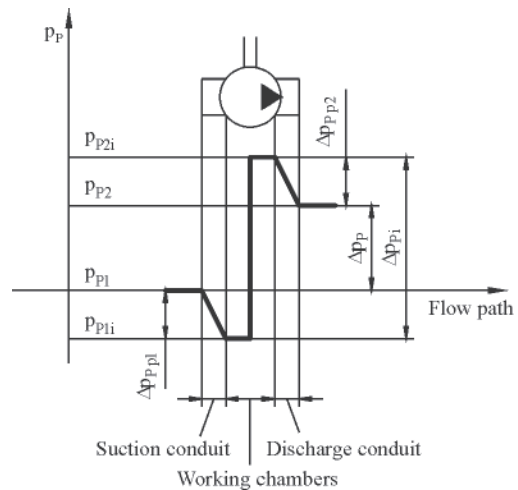


Fig. 1. Approximate changes of the working fluid pressure along the flow in the pump

Under the pressure and temperature, the geometric working volume  $q_{Pg}$  of the pump changes slightly compared with  $q_{Pt}$ . It is assumed (in order to simplify the description of volumetric loss intensity  $Q_{Pv}$  in the pump) that the theoretical pump working volume  $q_{Pt}$  is constant and equal to the geometrical working volume  $q_{Pg}$  determined at the working liquid temperature corresponding to the recommended kinematic viscosity  $v_n = 35 \text{ mm}^2\text{s}^{-1}$ :

$$q_{Pt} = q_{Pg} \begin{cases} p_{Pi}=0 \\ \Delta p_{Pi}=0 \\ v_n \end{cases} \quad (1)$$

and the change of geometric working volume  $q_{Pg}$  during the system operation will be taken into account in the values of loss coefficients in the pump.

The theoretical capacity  $Q_{Pt}$  of a constant capacity pump is given by the formula:

$$Q_{Pt} = q_{Pt} n_{p0} \quad (2)$$

where:

- $n_{p0}$  – the rotational shaft speed of an unloaded pump ( $\Delta p_{Pi} = 0$ ).

**The intensity  $Q_{Pv}$  of the pump volumetric losses** is described by a simulation model:

$$Q_{Pv} = k_{Pv35} \frac{q_{Pt}}{\rho_n v_n} \Delta p_{Pi} \left( \frac{v}{v_n} \right)^{-0.8} \quad (3)$$

where:

- $k_{Pv35}$  – dimensionless constant of volumetric losses in the pump, determined experimentally at the reference viscosity  $v_n = 35 \text{ mm}^2\text{s}^{-1}$ ,
- $q_{Pt}$  – theoretical working volume of a constant capacity pump,
- $\rho_n$  – reference mass density of the working medium (hydraulic oil) determined at the temperature corresponding to the kinematic viscosity  $v_n$  and pressure  $p = 0$  (atmospheric pressure),
- $\Delta p_{Pi}$  – indicated pressure increase in the pump working chambers,
- $v$  – kinematic viscosity of the working medium (hydraulic oil) used for calculation of the volumetric losses  $Q_{Pv}$  and determined at the pump inlet,
- $v_n$  – reference kinematic viscosity of the working medium (hydraulic oil)  $v_n = 35 \text{ mm}^2\text{s}^{-1}$ , determined at the pressure  $p = 0$  (atmospheric pressure),



$(v/v_n)^{-0.8}$  – approximate description of the impact of liquid viscosity  $v$  on the volumetric losses in a displacement rotational machine.

The value -0.8 of the exponent takes into account first of all two types of volumetric losses in the pump – dominating leaks of the laminar flow, proportional to  $(v/v_n)^{-1}$  and leaks of the not fully developed turbulent flow, proportional to  $(v/v_n)^{-0.14}$ . Therefore, the -0.8 exponent may be replaced by a different value in a more precise description of the intensity  $Q_{pv}$  of volumetric losses in specific pump.

The value of that exponent must be determined experimentally for each type of a displacement pump.

The pump capacity  $Q_p$  is described by the expression:

$$Q_p = q_{pt}n_p - k_{pv35} \frac{q_{pt}}{\rho_n v_n} \Delta p_{pi} \left( \frac{v}{v_n} \right)^{-0.8} \quad (4)$$

where: the speed  $n_p$  lower or equal to  $n_{p0}$ , depends on the characteristic of the pump driving motor ( $n_p$  decreases when the torque  $M_p$  required by the pump increases).

Coefficient  $k_1$  of the volumetric losses  $Q_{pv}$ , determined during one shaft revolution of a constant or variable capacity pump, at the pressure increase  $\Delta p_{pi}$  equal to the hydraulic system nominal pressure  $\Delta p_{pi} = p_n$  and at the viscosity  $v_n$ , the losses related to the pump theoretical working volume  $q_{pt}$ , is described by the formula:

$$k_1 = \frac{Q_{pv} \left| \frac{q_{pt}}{\Delta p_{pi} = p_n} \frac{1}{v_n} \right.}{n_p \left| \frac{q_{pt}}{\Delta p_{pi} = p_n} \frac{1}{v_n} \right.} \quad (5)$$

The relation between coefficient  $k_1$  and the constant value  $k_{pv35}$  of the volumetric losses in the pump is the following:

$$k_1 = k_{pv35} \frac{p_n}{\rho_n v_n n_p \left| \frac{q_{pt}}{\Delta p_{pi} = p_n} \frac{1}{v_n} \right.} \quad (6)$$

The relation between coefficient  $k_{1|v}$  calculated at the oil viscosity  $v$  changing during the drive system operation and coefficient  $k_1$  is the following:

$$k_{1|v} = k_1 \left( \frac{v}{v_n} \right)^{-0.8} \quad (7)$$

It results from the presence of two types of volumetric losses in the pump: dominating leaks of the laminar flow and leaks of not fully developed turbulent flow.

Using the volumetric loss coefficient  $k_1$ , the following formula for the intensity  $Q_{pv}$  of volumetric losses is obtained:

$$Q_{pv} = k_1 q_{pt} n_p \left| \frac{q_{pt}}{\Delta p_{pi} = p_n} \left( \frac{\Delta p_{pi}}{p_n} \right)^1 \left( \frac{v}{v_n} \right)^{-0.8} \right. \quad (8)$$

and the pump capacity  $Q_p$  formula:

$$Q_p = q_{pt} n_p - k_1 q_{pt} n_p \left| \frac{q_{pt}}{\Delta p_{pi} = p_n} \left( \frac{\Delta p_{pi}}{p_n} \right)^1 \left( \frac{v}{v_n} \right)^{-0.8} \right. \quad (9)$$

The use of coefficient  $k_1$  of volumetric losses for description of the relation of  $Q_{pv}$  intensity to the indicated increase  $\Delta p_{pi}$

of pressure in the pump working chambers allows to describe that relation by an exponential function with the exponent not necessarily equal to 1. The use of  $k_{pv35}$  constant to the description of  $Q_{pv}$  required an assumed proportionality of  $Q_{pv}$  to  $\Delta p_{pi}$ .

The expressions describing the variable capacity pump capacity takes the form:

$$Q_p = b_p q_{pt} n_p - k_{pv35} \frac{q_{pt}}{\rho_n v_n} \Delta p_{pi} \left( \frac{v}{v_n} \right)^{-0.8} \quad (10)$$

or:

$$Q_p = b_p q_{pt} n_p - k_1 q_{pt} n_p \left| \frac{q_{pt}}{\Delta p_{pi} = p_n} \left( \frac{\Delta p_{pi}}{p_n} \right)^1 \left( \frac{v}{v_n} \right)^{-0.8} \right. \quad (11)$$

The expressions (10, 11) assume, that change of the pump capacity setting  $b_p$  (change of the pump capacity) does not influence the intensity of pump volumetric losses  $Q_{pv}$ .

In the expressions (9, 11) the value 1 of exponent describing the impact of the  $\Delta p_{pi}/p_n$  ratio and also the value -0.8 of exponent describing the impact of the  $v/v_n$  ratio on the intensity  $Q_{pv}$  of pump volumetric losses should take into account all the factors influencing the volumetric losses (character of the flow in slots, change of the slots cross-section with pressure and temperature, liquid compressibility, change of the liquid viscosity in slots etc.).

The value 1 of exponent describing the impact of the  $\Delta p_{pi}/p_n$  ratio and also the value -0.8 of exponent describing the impact of the  $v/v_n$  ratio on the intensity  $Q_{pv}$  of pump volumetric losses must be verified experimentally for each pump type.

## RESULTS OF THE LABORATORY INVESTIGATIONS

Laboratory investigations of an axial piston variable displacement pump of bent axis design (BOSCH REXROTH A7V58RD type) were carried out on a test stand in the Chair of Hydraulics and Pneumatics of the Gdańsk University of Technology Mechanical Engineering Faculty.

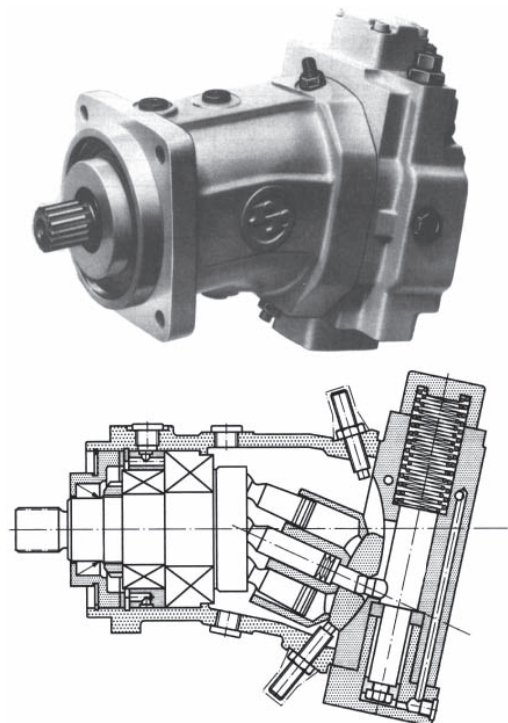


Fig. 2. Axial piston variable displacement pump of bent axis design (BOSCH REXROTH A7V58RD type)

- The investigations were performed with:
- 8 temperatures of hydraulic oil (oil kinematic viscosity  $\nu$ ):  
 $\nu = 20^\circ\text{C}$  ( $\nu = 120.40 \text{ mm}^2\text{s}^{-1}$ ),  $\nu = 24^\circ\text{C}$  ( $\nu = 91.16 \text{ mm}^2\text{s}^{-1}$ ),  
 $\nu = 30^\circ\text{C}$  ( $\nu = 65.37 \text{ mm}^2\text{s}^{-1}$ ),  $\nu = 36^\circ\text{C}$  ( $\nu = 47.05 \text{ mm}^2\text{s}^{-1}$ ),  
 $\nu = 43^\circ\text{C}$  ( $\nu = 34.68 \text{ mm}^2\text{s}^{-1}$ ),  $\nu = 50^\circ\text{C}$  ( $\nu = 26.41 \text{ mm}^2\text{s}^{-1}$ ),  
 $\nu = 60^\circ\text{C}$  ( $\nu = 18.77 \text{ mm}^2\text{s}^{-1}$ ),  $\nu = 68^\circ\text{C}$  ( $\nu = 14.53 \text{ mm}^2\text{s}^{-1}$ ),
  - 8 values of the increase  $\Delta p_p$  of pump pressure:  
 $\Delta p_p = 1.6 \text{ MPa}$ ,  $\Delta p_p = 3.2 \text{ MPa}$ ,  $\Delta p_p = 6.3 \text{ MPa}$ ,  
 $\Delta p_p = 10 \text{ MPa}$ ,  $\Delta p_p = 16 \text{ MPa}$ ,  $\Delta p_p = 20 \text{ MPa}$ ,  
 $\Delta p_p = 25 \text{ MPa}$ ,  $\Delta p_p = 32 \text{ MPa}$

- 7 values of pump capacity coefficient:  
 $b_p = 0.227$ ;  $b_p = 0.361$ ;  $b_p = 0.493$ ;  
 $b_p = 0.623$ ;  $b_p = 0.752$ ;  $b_p = 0.880$ ;  $b_p = 1$ .

The selected method of determination of the geometrical (variable) capacity  $q_{p_{gv}}$  per one pump shaft revolution and theoretical capacity  $q_{p_t}$  per one shaft revolution was based on the extrapolation of linear functions  $q_p = f(\Delta p_{p_i})$ , in the range of small increases  $\Delta p_{p_i}$  of pressure in the pump working chambers (Fig. 3).

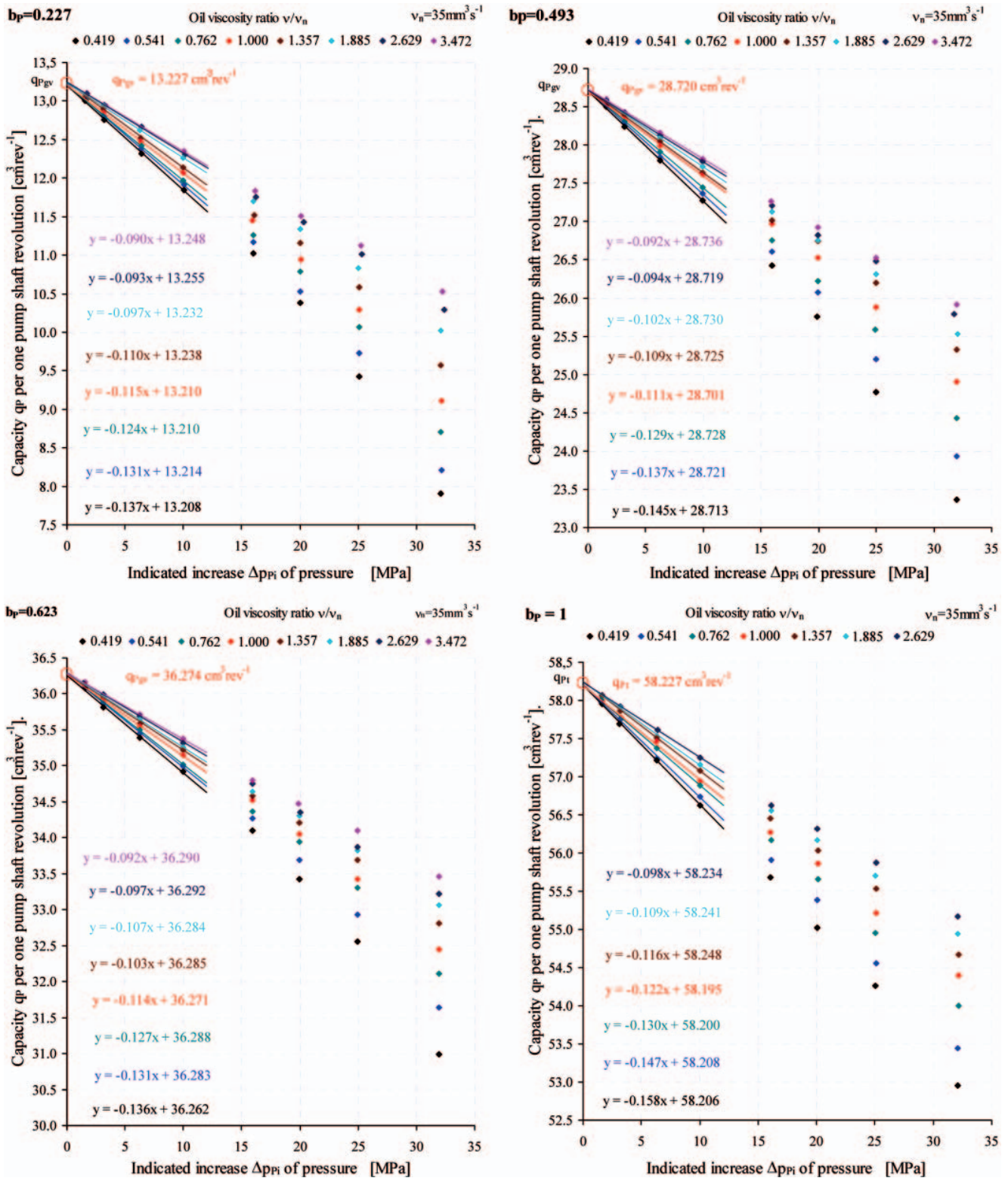


Fig. 3. Determination of the geometrical (variable) capacity  $q_{p_{gv}}$  ( $q_{p_{gv}} = b_p \cdot q_{p_t}$ ) per one shaft revolution and of the value of the pump capacity coefficient  $b_p$  from the relation of the pump capacity  $q_p$  per one shaft revolution to the indicated increase  $\Delta p_{p_i}$  of pressure in the pump working chambers at different values of the oil viscosity ratio  $v/v_n$ ; examples for four choices of different pump capacity settings  $b_p = 0.227 \div 1$

Description of  $q_p = f(\Delta p_{pi})$ , with those linear functions in the range of small pressure increases  $\Delta p_{pi}$ , allowed to determine  $q_{p_{gv}}$  ( $q_{pt}$ ) with the accuracy of an order of 1 per mille (0.001). Approximation, instead with a linear function in the whole

range of the increase  $\Delta p_{pi}$  of pressure (up to 32 MPa) or a second degree polynomial or an exponential function in the whole or a small range of  $\Delta p_{pi}$  allowed to determine  $q_{p_{gv}}$  ( $q_{pt}$ ) with much less accuracy.

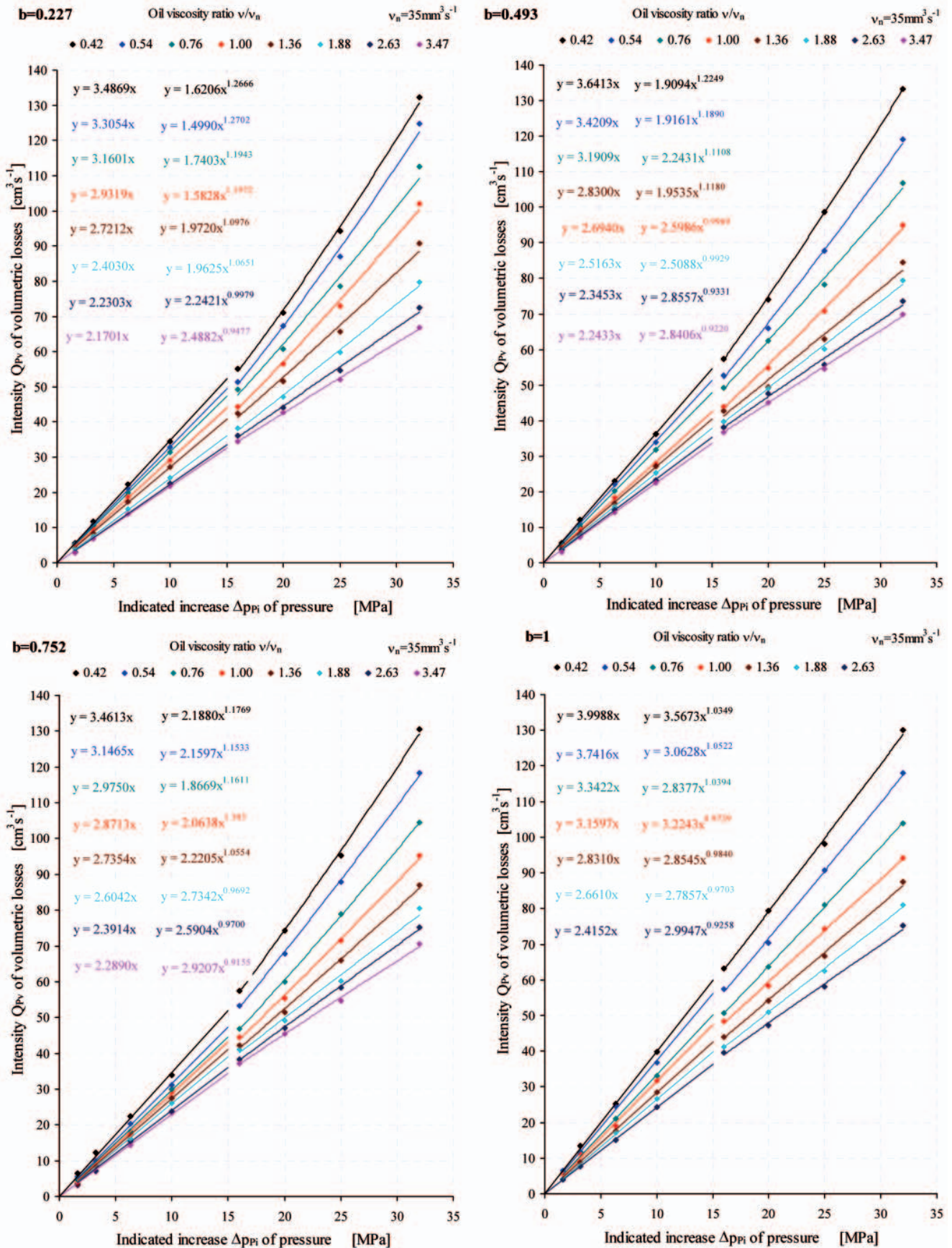


Fig. 4. Relation of the intensity  $Q_{pv}$  of volumetric losses to the indicated increase  $\Delta p_{pi}$  of pressure in the pump with different values of the oil viscosity ratio  $v/v_n$ ; examples for four chosen values of the pump capacity coefficient  $b_p = 0.227 \div 1$ . In the range up to  $\Delta p_{pi} = 16$  MPa, the  $Q_{pv}$  intensity is most precisely described by the linear functions, in the  $\Delta p_{pi} = 16 \div 32$  MPa range, the  $Q_{pv}$  intensity is described by exponential functions

The figure 4 demonstrates a complex impact on  $Q_{pv}$  of the flow character in the slots and of the changes of slot cross-section and the hydraulic oil viscosity under the influence of pressure and temperature.

Choice of the functions (Fig. 5) assumes the best conformity with the measurement results at  $\Delta p_{pi} = p_n$ . A consequence of the choice of such functions is worse conformity with the measurement results at lower  $\Delta p_{pi}$  values.

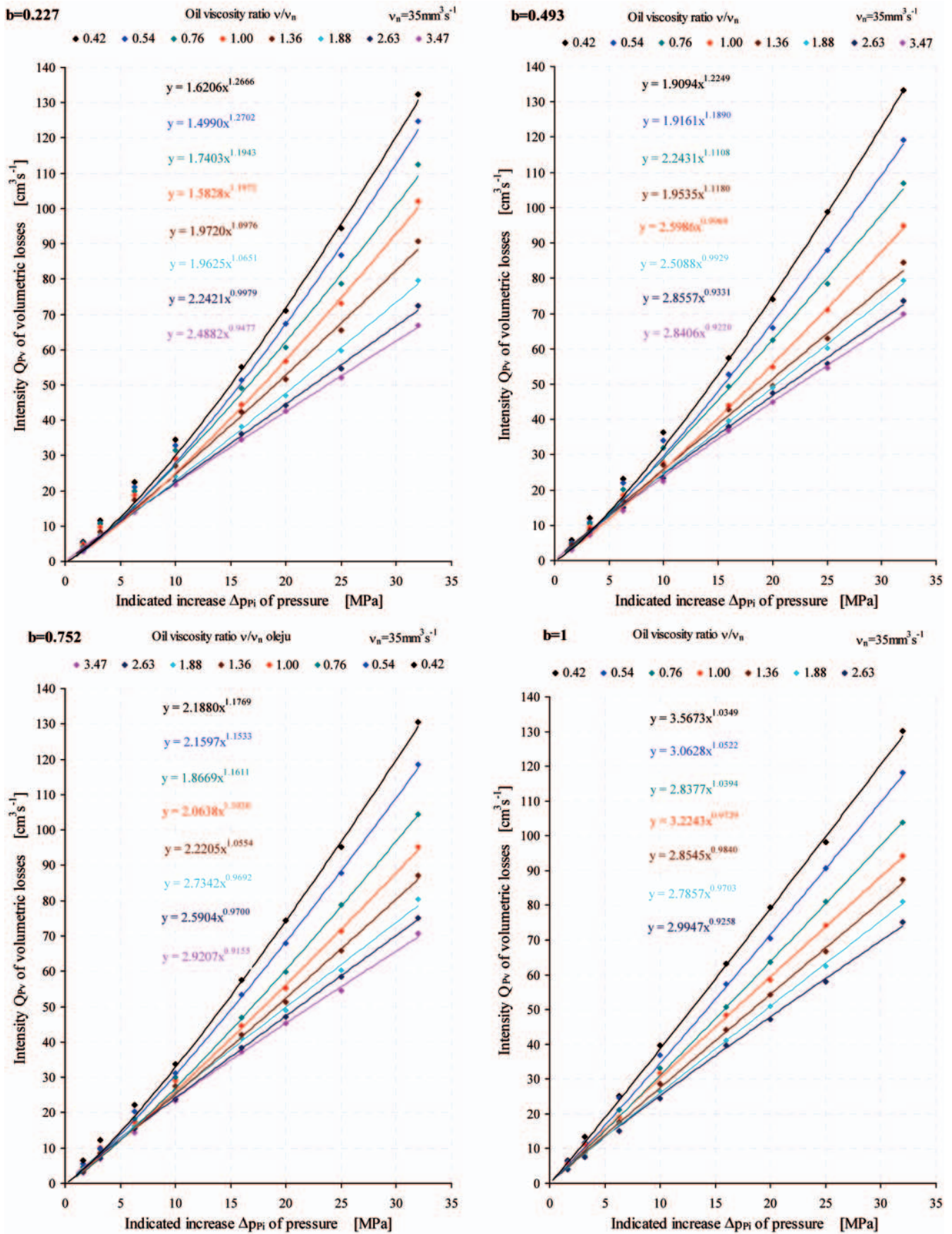


Fig. 5. Relation of the intensity  $Q_{pv}$  of volumetric losses to the indicated increase  $\Delta p_{pi}$  of pressure in the pump, described by exponential functions in the whole range of pressure; examples for four chosen pump capacity coefficients  $b_p = 0.227 \div 1$

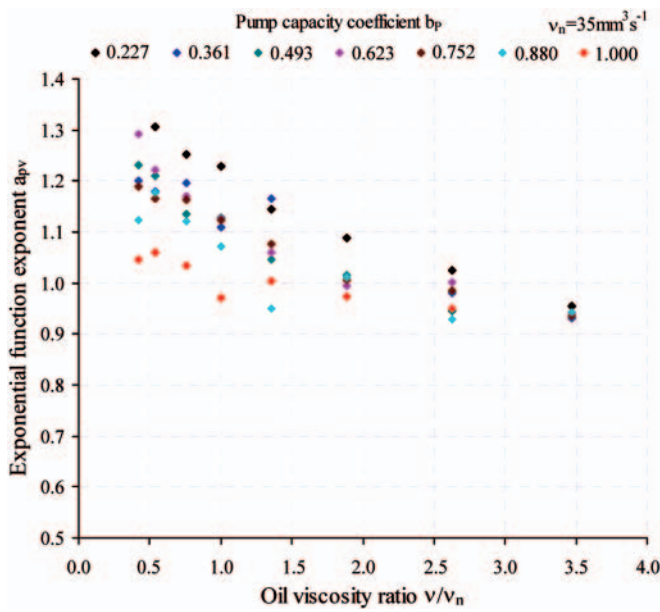


Fig. 6. Value of the  $a_{pv}$  exponent (in the exponential function describing the relation of the intensity  $Q_{pv}$  of volumetric losses to the indicated increase  $\Delta p_{pi}$  of pressure in the pump) at changing pump capacity coefficient  $b_p$  for different oil viscosity ratios  $v/v_n$

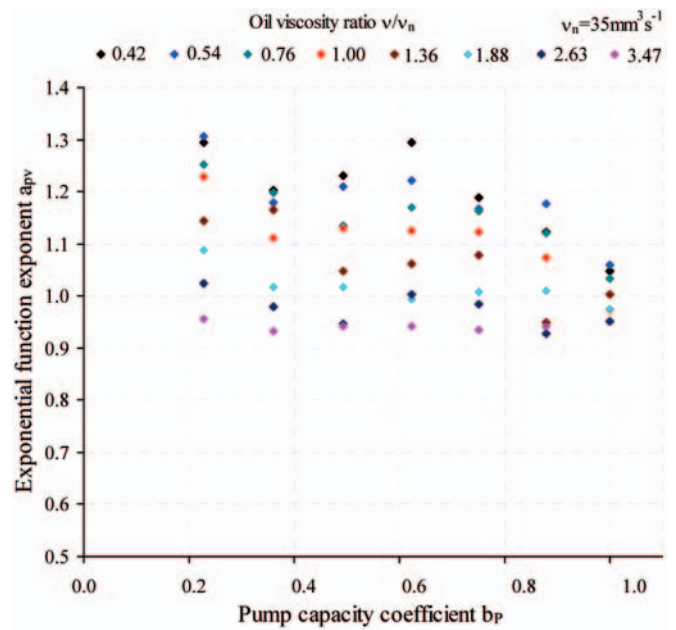


Fig. 7. Value of the  $a_{pv}$  exponent (in the exponential function describing the relation of the intensity  $Q_{pv}$  of volumetric losses to the indicated increase  $\Delta p_{pi}$  of pressure in the pump) at changing oil viscosity ratio  $v/v_n$  for different pump capacity coefficients  $b_p$

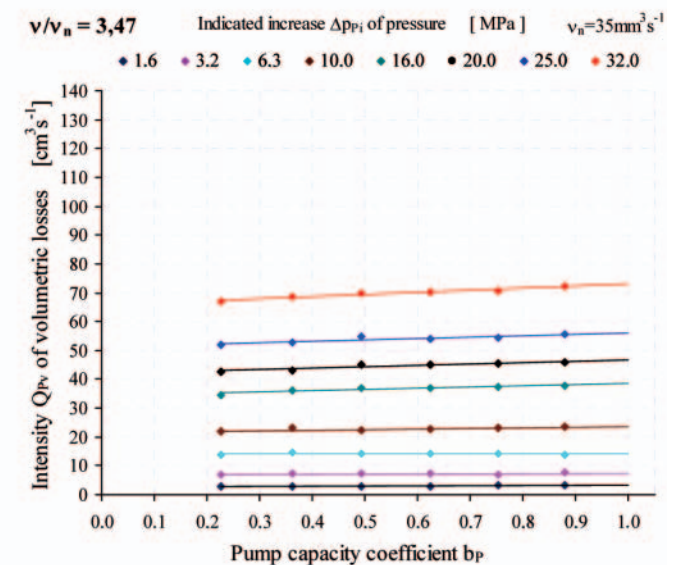
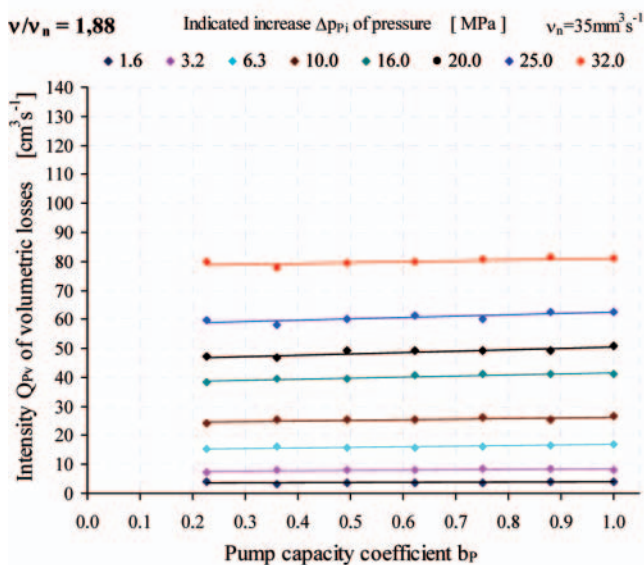
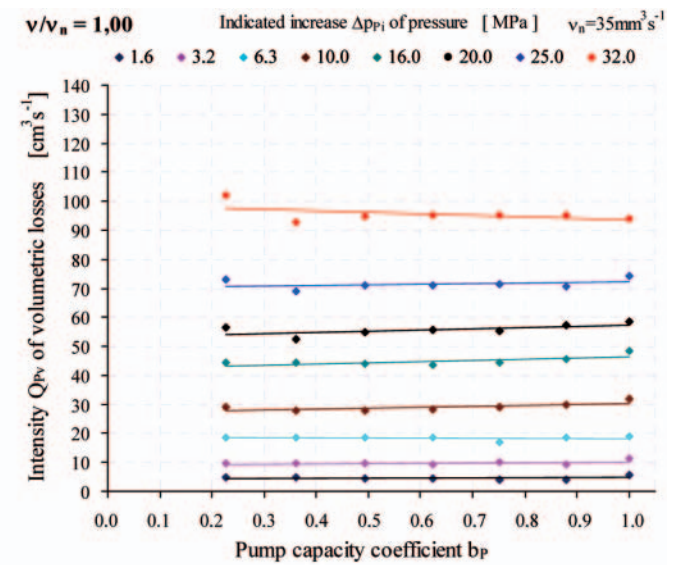
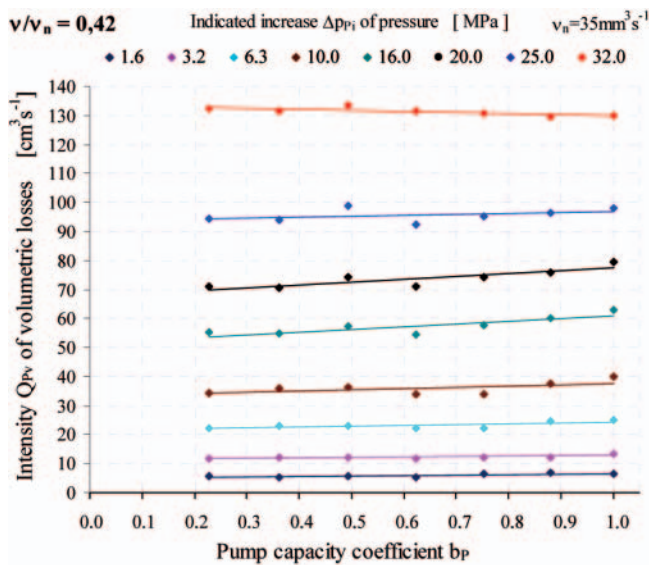


Fig. 8. Relation of the intensity  $Q_{pv}$  of volumetric losses to the pump capacity coefficient  $b_p$  at different values of indicated increase  $\Delta p_{pi}$  of pressure in the pump working chambers and at different  $v/v_n = 0.42 \div 3.47$  ratios of oil viscosity

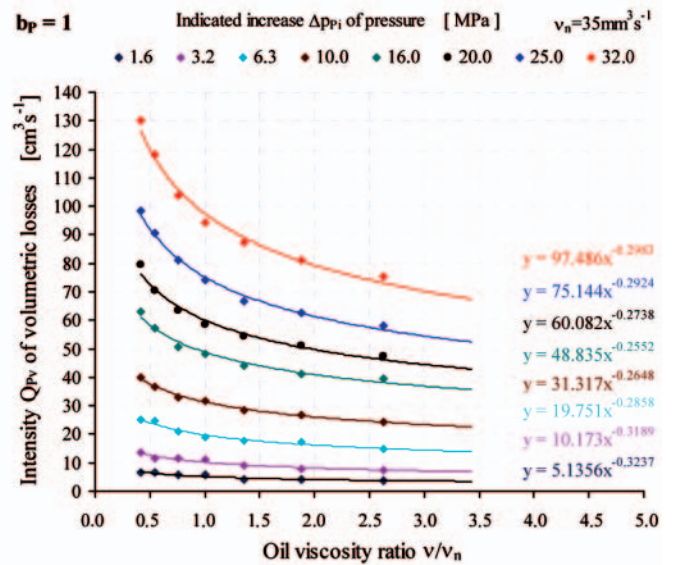
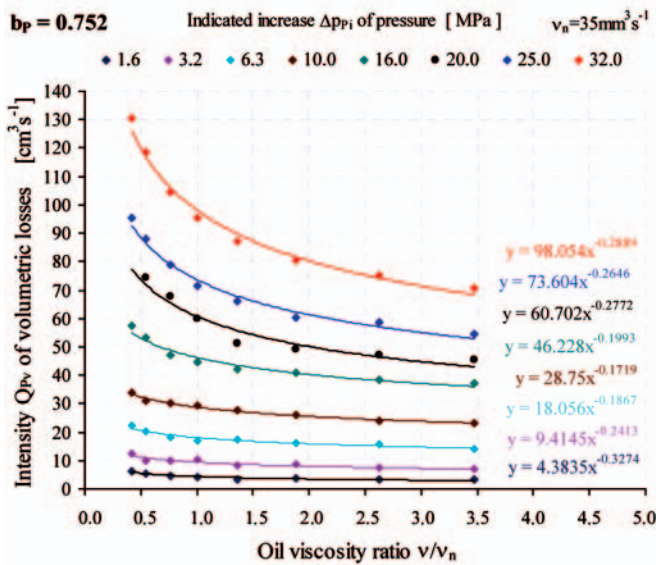
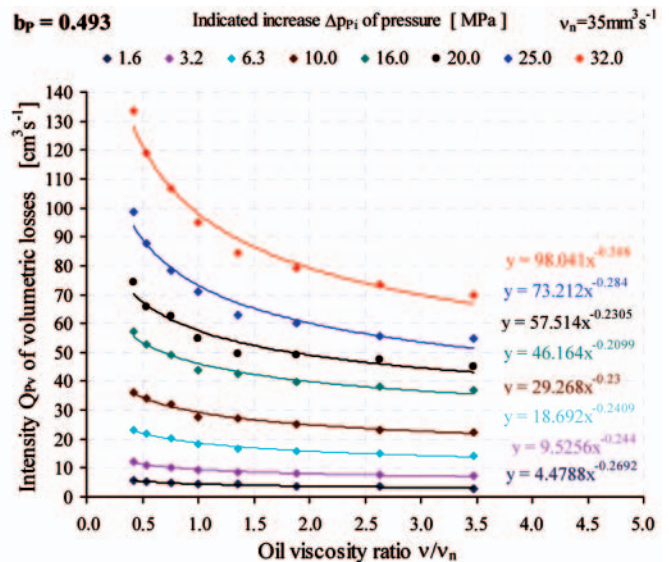
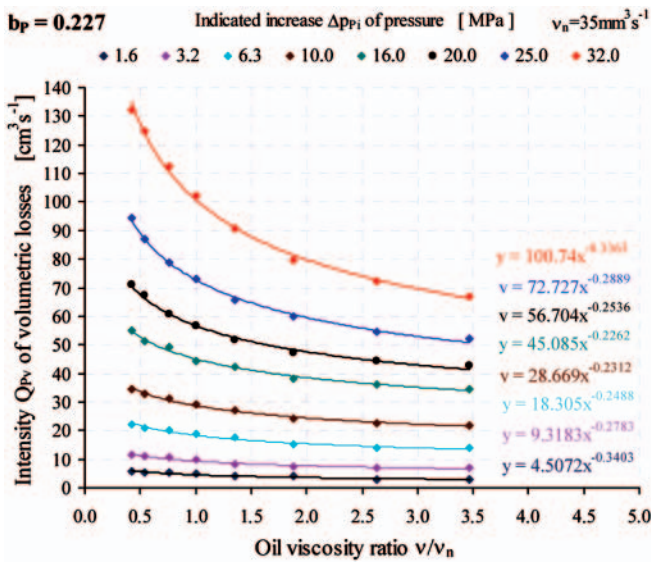


Fig. 9. Relation of the intensity  $Q_{pv}$  of volumetric losses to the oil viscosity ratio  $v/v_n$  at different values of indicated increase  $\Delta p_{pi}$  of pressure in the pump working chambers and at different values of the pump capacity coefficient  $b_p = 0.227 \div 1$

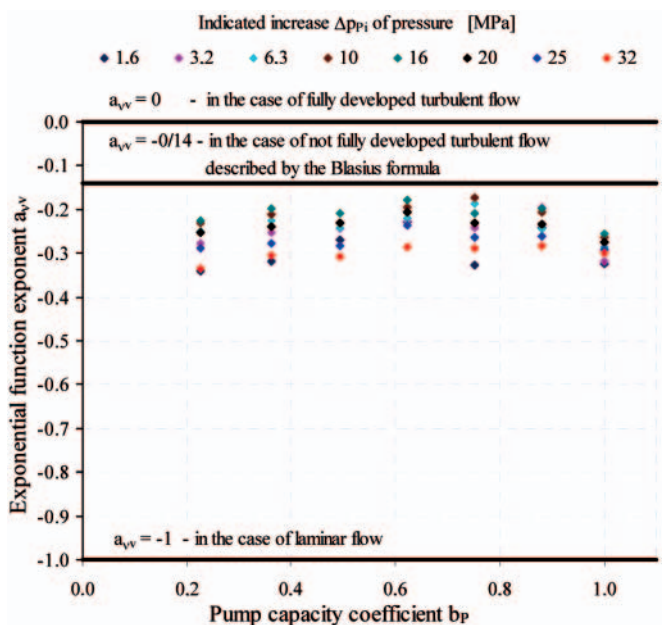
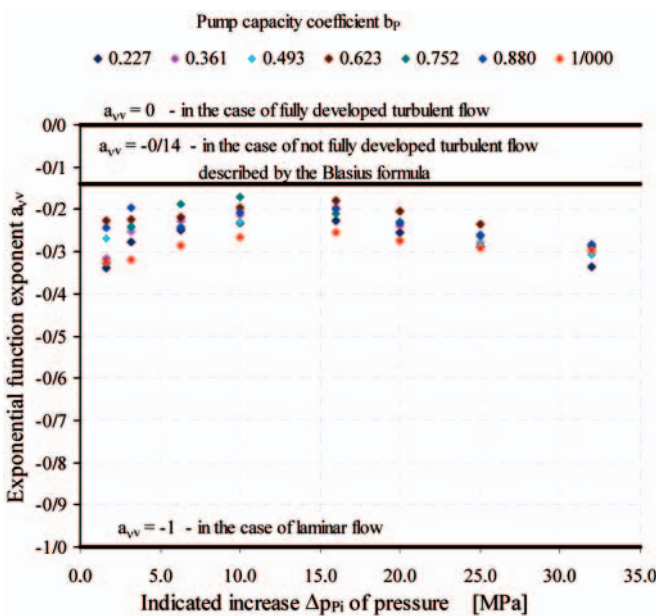


Fig. 10. Value of the  $a_{vv}$  exponent (in the exponential function describing the relation of the intensity  $Q_{pv}$  of volumetric losses to the oil viscosity ratio  $v/v_n$ ) at changing indicated increase  $\Delta p_{pi}$  of pressure in the pump for different values of the pump capacity coefficient  $b_p$

Fig. 11. Value of the  $a_{vv}$  exponent (in the exponential function describing the relation of the intensity  $Q_{pv}$  of volumetric losses to the oil viscosity ratio  $v/v_n$ ) at changing pump capacity coefficient  $b_p$  and for different values of the indicated increase  $\Delta p_{pi}$  of pressure in the pump

Values of the  $a_{pv}$  exponent, in the exponential function describing the relation of the intensity  $Q_{pv}$  of volumetric losses to the indicated increase  $\Delta p_{pi}$  of pressure in the pump, presented in figures 6 and 7, are within the  $0.91 < a_{pv} < 1.31$  range. This range is limited to  $0.91 < a_{pv} < 0.96$  at the oil viscosity ratio  $v/v_n = 3.47$ .

The exponent values  $a_{pv} < 1$  obtained at the highest oil viscosity allow to conclude that in the whole range of viscosity  $v$  the flow in slots is of a not fully developed turbulent character (with increasing turbulence at decreasing viscosity). Increase of the  $a_{pv}$  exponent above 1 at decreasing viscosity  $v$  indicates an impact of the slot increase upon the intensity  $Q_{pv}$  of volumetric losses as an effect of temperature increase.

The pump capacity coefficient  $b_p$  has practically no impact on the intensity  $Q_{pv}$  of volumetric losses in the pump working chambers (Fig. 8).

Values of the  $a_{vv}$  exponent in the exponential function describing the relation of the intensity  $Q_{pv}$  of volumetric losses to the oil viscosity ratio  $v/v_n$ , presented in figures 9, 10 and 11, in the  $a_{vv} = -0.20 \div -0.35$  range indicate the domination of not fully developed turbulent flow over laminar flow in the pump slots.

## VERIFICATION OF THE MATHEMATICAL MODEL OF PUMP VOLUMETRIC LOSSES

In order to verify the mathematical model described by formula (8), it was replaced by a mathematical expression taking into account the relations, obtained during the investigations, of the intensity  $Q_{pv}$  of pump volumetric losses to the indicated

increase  $\Delta p_{pi}$  of pressure in the pump working chambers (to the  $\Delta p_{pi}/p_n$  ratio) and also to the oil viscosity ratio  $v/v_n$ :

$$Q_{pv} = k_1 q_{pt} n_p \left| \frac{q_{pt}}{\Delta p_{pi} = p_n} \frac{v_n}{p_n} \right| \left( \frac{\Delta p_{pi}}{p_n} \right)^{a_{pv}} \left( \frac{v}{v_n} \right)^{a_{vv}} \quad (12)$$

Assumed was (Fig. 12) the value of exponent  $a_{pv} = 0.97$  in the formula (12) determined with the pump capacity coefficient  $b_p = 1$ , the oil viscosity ratio  $v/v_n = 1$  and the coefficient of volumetric losses  $k_1 = 0.065$  calculated from formula (5).

Assumed was (Fig. 13) the value of exponent  $a_{vv} = -0.30$  in the formula (12) determined with the pump capacity coefficient  $b_p = 1$ ,  $\Delta p_{pi}/p_n = 1$  ratio and the calculated coefficient of volumetric losses  $k_1 = 0.065$ .

The obtained values of the coefficient  $k_1 = 0.065$  of intensity  $Q_{pv}$  of volumetric losses, exponent  $a_{pv} = 0.97$  of the relation of intensity  $Q_{pv}$  of the volumetric losses to the ratio  $\Delta p_{pi}/p_n$  of the pressure increase, exponent  $a_{vv} = -0.30$  of the relation of intensity  $Q_{pv}$  of the volumetric losses to the  $v/v_n$  ratio of oil viscosity, have made it possible to present the mathematical model of the intensity  $Q_{pv}$  of pump volumetric losses in the form:

$$Q_{pv} = 0.065 q_{pt} n_p \left| \frac{q_{pt}}{\Delta p_{pi} = p_n} \frac{v_n}{p_n} \right| \left( \frac{\Delta p_{pi}}{p_n} \right)^{0.97} \left( \frac{v}{v_n} \right)^{-0.30} \quad (13)$$

Model (13) describes precisely the intensity  $Q_{pv}$  of volumetric losses in the nominal conditions of the pump operation, i.e. at the pump capacity coefficient  $b_p = 1$ , the pressure increase ratio  $\Delta p_{pi}/p_n = 1$  and the oil viscosity ratio

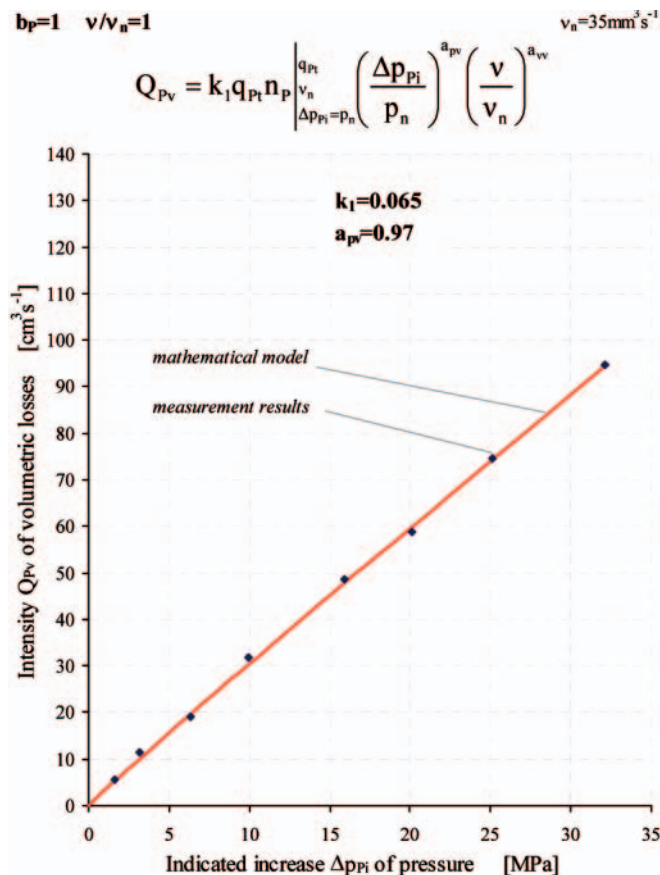


Fig. 12. Determination of the  $a_{pv}$  exponent in the mathematical model describing the relation of the intensity  $Q_{pv}$  of volumetric losses to the indicated increase  $\Delta p_{pi}$  of pressure in the pump working chambers; pump capacity coefficient  $b_p = 1$ , the oil viscosity ratio  $v/v_n = 1$ . From formula (5), the value of coefficient  $k_1 = 0.065$  of volumetric losses is determined. The value of  $a_{pv} = 0.97$  exponent is obtained

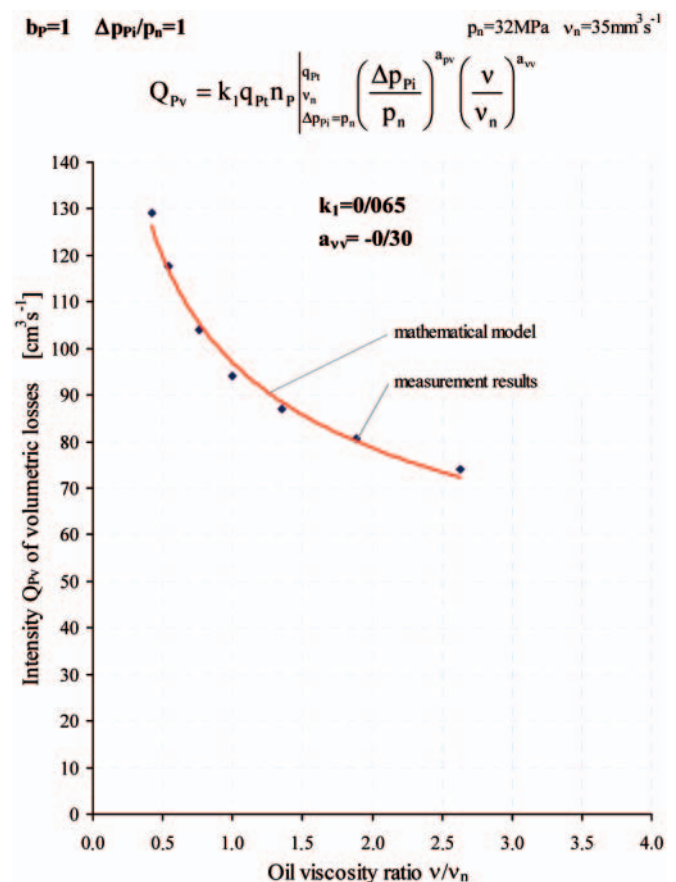


Fig. 13. Determination of the  $a_{vv}$  exponent in the mathematical model describing the relation of the intensity  $Q_{pv}$  of volumetric losses to the oil viscosity ratio  $v/v_n$ ; pump capacity coefficient  $b_p = 1$ , indicated increase  $\Delta p_{pi} = p_n = 32$  MPa of pressure in the pump working chambers, coefficient  $k_1 = 0.065$  of volumetric losses. The value  $a_{vv} = -0.30$  of the exponent is obtained

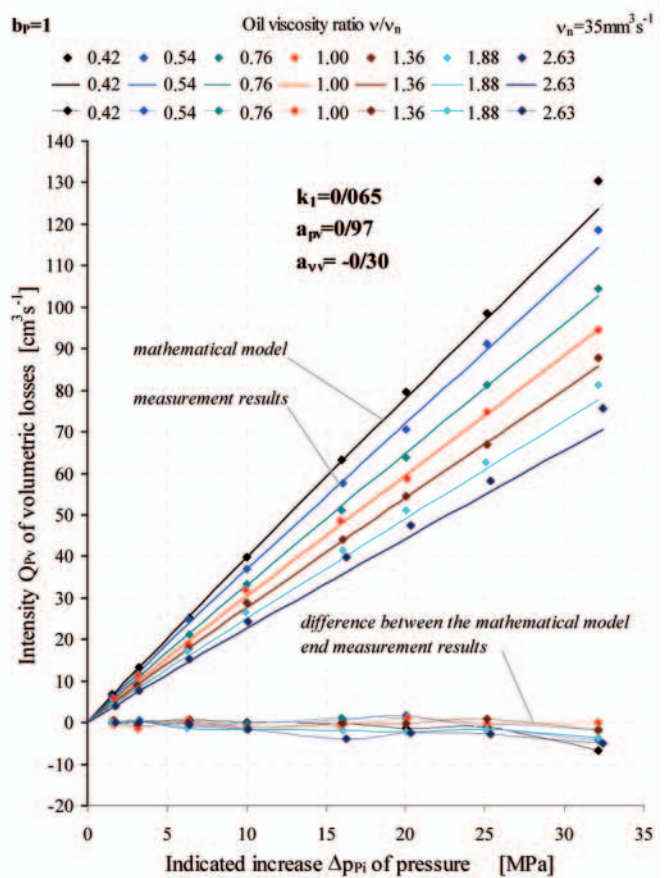
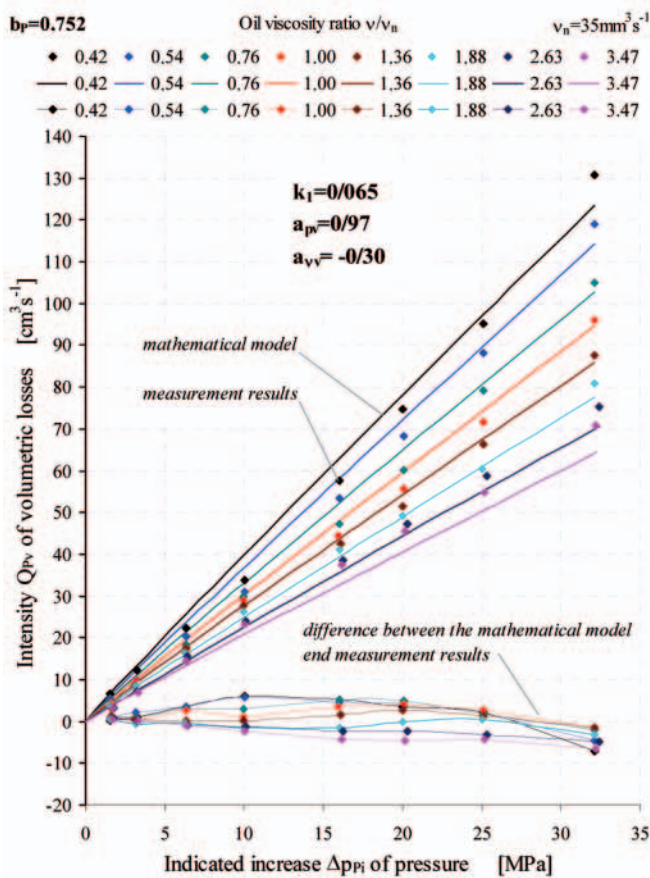
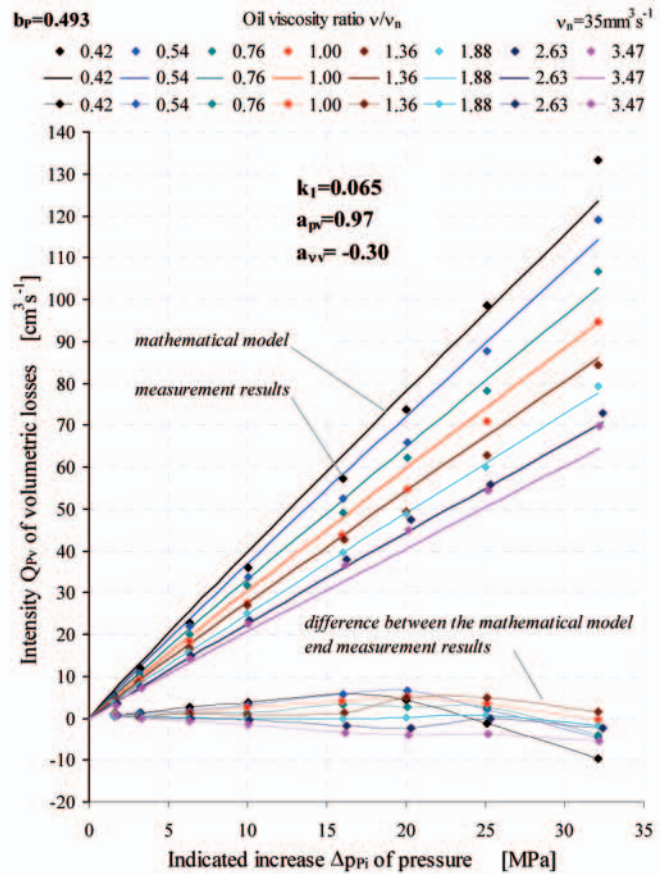
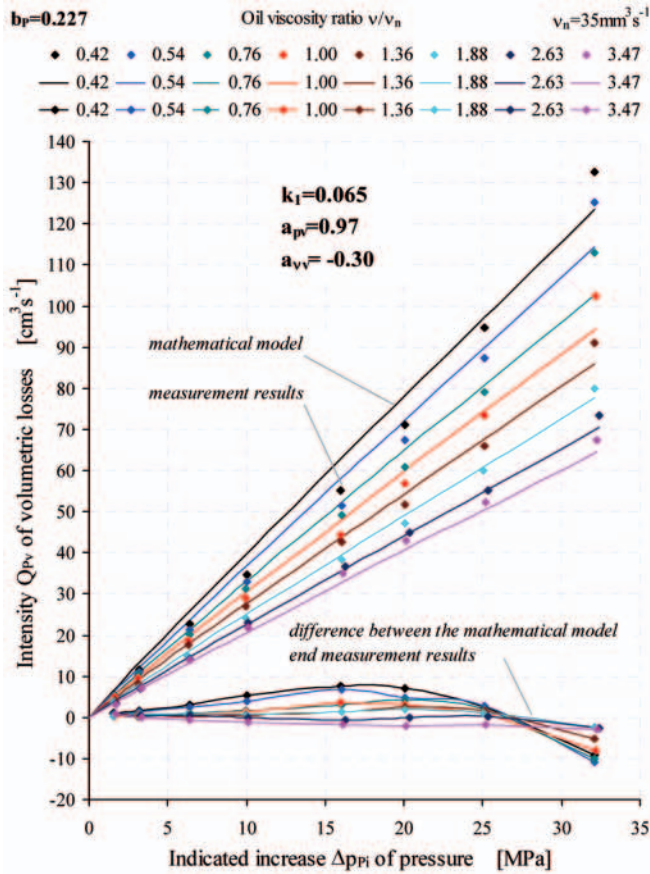


Fig. 14. Comparison of the intensity  $Q_{pv}$  of volumetric losses described by the mathematical model (13) with the laboratory investigation results and the absolute difference between the mathematical model values and the laboratory investigation values; assumed were: the coefficient  $k_1 = 0.065$  of volumetric losses, exponent  $a_{pv} = 0.97$ , exponent  $a_{vv} = -0.30$ ; examples for four chosen values of the pump capacity coefficient  $b_p = 0.227 \div 1$



$v/v_n = 1$ . At the same time this model is a simulation formula describing the change of intensity  $Q_{pv}$  of volumetric losses with the change of the pressure increase ratio  $\Delta p_{pi}/p_n$  and the oil viscosity ratio  $v/v_n$  (the change of pump capacity coefficient  $b_p$  has practically no impact on the change of intensity  $Q_{pv}$  of volumetric losses).

Figure 14 presents a comparison of the intensity  $Q_{pv}$  of volumetric losses described by the mathematical model (13) with the results of laboratory investigations, supplemented by the information about the absolute difference between the values from the mathematical model (13) and results of laboratory investigations. Examples are given for four selected values of the pump capacity coefficient  $b_p$ .

Differences between the simulation and experimental values of the intensity  $Q_{pv}$  of volumetric losses, determined in the whole range of the pressure increase ratio  $\Delta p_{pi}/p_n$ , oil viscosity ratio  $v/v_n$  and pump capacity coefficient  $b_p$  are mainly caused by the change of  $a_{pv}$  exponent describing the relation of the intensity  $Q_{pv}$  of volumetric losses to the pressure increase ratio  $\Delta p_{pi}/p_n$  in the situation of using in the mathematical model the value  $a_{pv} = 0.97$  determined at  $b_p = 1$  and  $v/v_n = 1$ .

## CONCLUSIONS

1. The purpose of the investigations was experimental verification of the mathematical model (8) [2, 3, 4], describing the volumetric losses in a variable capacity displacement pump used in hydrostatic transmissions. Model (8) allows to describe the losses and the energy efficiency of the pump and hydrostatic drive as a function of the drive speed and load and also the hydraulic oil viscosity.
2. Model (8) allows a simple and precise determination of the pump volumetric losses by determining the coefficient  $k_1$  of volumetric losses (5) in the nominal conditions of pump operation – at  $\Delta p_{pi} = p_n$ ,  $b_p = 1$ ,  $v/v_n = 1$ .
3. Model (8) allows also to determine the impact of the ratio  $\Delta p_{pi}/p_n$  of pressure increase, the hydraulic oil viscosity ratio  $v/v_n$  on the intensity  $Q_{pv}$  of volumetric losses in the whole range of the pump capacity coefficient  $b_p$ .
4. The investigations were carried out with an axial piston variable displacement pump of bent axis design, commonly used in hydrostatic transmissions.
5. In order to verify the mathematical model (8), it was replaced by formula (12) for investigating the exponent  $a_{pv}$  in the expression  $Q_{pv} \sim (\Delta p_{pi}/p_n)^{a_{pv}}$  and exponent  $a_{vv}$  in the expression  $Q_{pv} \sim (v/v_n)^{a_{vv}}$ .
6. The chosen method of determining the pump geometrical working volume  $q_{p_{gv}}$  and theoretical working volume  $q_{p_{ti}}$  was based on extrapolation of linear functions  $q_p = f(\Delta p_{pi})$  within the range of small pressure increases  $\Delta p_{pi}$  in the working chambers. This allows to determine  $q_{p_{gv}}$  ( $q_{p_{ti}}$ ) with the accuracy of an order of 1 per mille (0.001).
7. A complex impact on the intensity  $Q_{pv}$  of volumetric losses was found of the character of flow in slots as well as the impact on  $Q_{pv}$  of the change of slot cross-sections and hydraulic oil viscosity  $v$  due to the change of pressure and temperature. Up to  $\Delta p_{pi} = 16$  MPa, the intensity  $Q_{pv}$  was best described with linear functions, in the  $\Delta p_{pi} = 16 \div 32$  MPa range the intensity  $Q_{pv}$  is described by exponential functions. For description of the  $Q_{pv}$  to  $\Delta p_{pi}$  relation in the whole range of the pressure increase, the exponential functions giving the best agreement with the measurement results in the  $\Delta p_{pi} = p_n$  area were chosen.
8. The values of exponent  $a_{pv}$  in the expression  $Q_{pv} \sim (\Delta p_{pi}/p_n)^{a_{pv}}$  are in the  $0.91 < a_{pv} < 1.31$  range narrowing to the  $0.91 < a_{pv} < 0.96$  range at the oil viscosity ratio  $v/v_n = 3.47$ .

9. It has been found out that the pump capacity coefficient  $b_p$  has practically no impact on the intensity  $Q_{pv}$  of pump volumetric losses.
10. The values of exponent  $a_{vv}$  in the expression  $Q_{pv} \sim (v/v_n)^{a_{vv}}$  are in the  $-0.35 < a_{vv} < -0.20$  range and show the domination of not fully developed turbulent flow over the laminar flow in the pump slots in the whole range of investigation parameters.
11. The value  $k_1 = 0.065$  of the coefficient of the volumetric losses in the pump working chambers was calculated at the pump capacity coefficient  $b_p = 1$ , the pressure increase ratio  $\Delta p_{pi}/p_n = 1$  and the oil viscosity ratio  $v/v_n = 1$ . The so determined value of  $k_1$  coefficient allows the quantitative and qualitative evaluation of the pump volumetric losses.
12. The value  $a_{pv} = 0.97$  of the exponent in the expression  $Q_{pv} \sim (\Delta p_{pi}/p_n)^{a_{pv}}$  was determined at the pump capacity coefficient  $b_p = 1$  and the oil viscosity ratio  $v/v_n = 1$ .
13. The value  $a_{vv} = -0.30$  of the exponent in the expression  $Q_{pv} \sim (v/v_n)^{a_{vv}}$  was determined at the pump capacity coefficient  $b_p = 1$  and the pressure increase ratio  $\Delta p_{pi}/p_n = 1$ .
14. In effect, the mathematical model of volumetric losses in the investigated pump takes the form (13):

$$Q_{pv} = 0.065 q_{p_{ti}} n_p \left( \frac{\Delta p_{pi}}{p_n} \right)^{0.97} \left( \frac{v}{v_n} \right)^{-0.30}$$

15. Intensity  $Q_{pv}$  of pump volumetric losses described by the mathematical model (13) was compared with the results of laboratory investigations. The absolute difference between the values from the model and from the laboratory experiment did not exceed: at  $b_p = 1 - +2 \div -6$  cm<sup>3</sup>s<sup>-1</sup>, at  $b_p = 0.227 - -8 \div -11$  cm<sup>3</sup>s<sup>-1</sup> compared with the nominal operation value of  $Q_{pv} = 94$  cm<sup>3</sup>s<sup>-1</sup>.
16. It must be underlined, that in the assumed conditions of determination of the  $k_1$  coefficient (conclusion 11), the difference between the value of the intensity  $Q_{pv}$  of volumetric losses from the model and the results of laboratory investigations in nominal conditions ( $b_p = 1$ ,  $\Delta p_{pi}/p_n = 1$ ,  $v/v_n = 1$ ) is equal to zero.

## BIBLIOGRAPHY

1. Czyński M.: *Laboratory investigations of a hydraulic transmission energy efficiency model*. Doctor thesis. Politechnika Szczecińska, Wydział Techniki Morskiej. Szczecin 2005, promotor: Z. Paszota.
2. Paszota Z.: *Model of volumetric losses in the variable capacity displacement pump used in hydrostatic drive*. Materiały „Napędy i Sterowania’2006”. Seminarium Naukowo-Techniczne „TECHNICON’06” Gdańsk, 25.10.2006.
3. Paszota Z.: *Aspects énergétiques des transmissions hydrostatiques*. Monografia, Wydawnictwo Politechniki Gdańskiej, Gdańsk 2002. 293 s., 199 rys. bibliograf. 41 poz. Aspekty energetyczne przekładni hydrostatycznych.
4. Paszota Z.: *Model of the energy losses in the displacement rotational machines for description of efficiency of the hydrostatic drive. Part I. Model of volumetric losses*. Polish Maritime Research. 2000 vol. 7 nr 3, s. 3 – 8, 7 rys., bibliograf. 22 poz. Model strat energetycznych w maszynach wyporowych obrotowych służący opisowi sprawności napędu hydrostatycznego. Część I. Model strat objętościowych.

## CONTACT WITH THE AUTHOR

Jan Koralewski, M. Sc.  
Faculty of Ocean Engineering and Ship Technology  
Gdansk University of Technology  
Narutowicza 11/12  
80-233 Gdansk, POLAND  
e-mail: jkoral@pg.gda.pl  
tel.: (4858) 347 29 19

# Estimation of rolling bearing life with damage curve approach

H. Mehdigholi, Ph. D.  
H. Mirzaei Rafsanjani, Ph. D.  
Behzad, Mehdi, Prof.  
Sharif University of Technology

## ABSTRACT

*The ability to determine the bearing life time is one of the main purposes in maintenance of rotating machineries. Because of reliability, cost and productivity, the bearing life time prognostic is important. In this paper, a stiffness-based prognostic model for bearing systems is discussed. According to presumed model of bearing and fundamental of damage mechanics, damage curve approach is used to relate stiffness of vibratory system and bearing running life. Furthermore, using the relation between acceleration amplitude at natural frequency and stiffness, final relation between acceleration amplitude at natural frequency and running life time according to damage curve approach can be established and the final running time is predicted. Experiments have been performed on self alignment bearing under failures on inner race and outer race to calibrate and to validate the proposed model. The comparison between model-calculated data and experimental results indicates that this model can be used effectively to predict the failure lifetime and the remaining life of a bearing system.*

**Keywords:** Rolling bearing, Prognostic, Damage mechanics, Damage curve approach

## INTRODUCTION

Nowadays, rotating machineries are widely used in mechanical equipments and different industries. The failure of a rolling element of bearing is one of the primary causes of breakdown in rotating machineries. Consequently, development of reliable techniques for the prediction of rotating element failure is more important to facilitate preventive maintenance.

The ability to determine the bearing life time is one of the main purposes in maintenance and condition monitoring of rotating machineries. If remaining life time of bearing be predicted then reliability of bearing will be improved and cost of maintenance will be reduced, so bearing life time prognostics is one of key points of condition monitoring of rotating machineries.

Maintenance of bearing can be categorized in two main group of diagnostic and prognostic. Currently, there are three methods for bearing diagnostic. These methods are vibration analysis [1, 2, 3], statistical study [4, 5] and neural network [6, 7]. The researches in the field of diagnostic of failures of bearings are focused on determination of failures of bearing and do not predict the running life of bearing.

Diagnostic do not estimate the bearing life while prognostic is focused on prediction of bearing life time. The studies of prognostic of remaining life of bearing is categorized in two approaches: Direct approach of fracture mechanics [8, 9, 10],

and indirect approach which is a statistical analysis of vibration signals [11].

The primary researches to estimate the remaining life of bearing was carried out in 90 decay. Li et al., 1999, used the vibration analysis and fracture mechanic to produce a recursive algorithm to predict the remaining life of bearing. These research shows that fracture mechanics can be useful to predict the bearing life. Qiu et al., 2002, used damage mechanics to predict the bearing life. In this research, three approaches of damage mechanics [Linear Damage Rule (LDR), Damage Curve Approach (DCA) and Double Linear Damage Rule (DLDR)] for trend the variation of acceleration amplitude on natural frequency of system were compared. However, the deterministic formula for estimation of remaining life of bearing did not explain. Due to previous studies in the fields of diagnostic and prognostic of bearing remaining life, this is obvious that most of researches are focused on diagnostic of defects of bearing and prognostic of bearing life time is a new branch in the field of condition monitoring and maintenance of bearings.

As a result, there is still a lack of reliable prognostic methods to predict the remaining life of bearing. Reliable and physically meaningful estimation of bearing life under various operating conditions remains a challenging and important aspect for maintenance optimization and catastrophe avoidance. In this paper, a stiffness-based prognostics model for a bearing system based on vibration response analysis and

damage mechanics is developed. The effectiveness of the model has been studied by comparison between estimated life due to model and real running life of experiment, and accuracy of the model is also investigated.

### BEARING DYNAMIC MODEL

A bearing system can be introduced with a self-excitation dynamic system. In this system, two types of loads exist. One type is external loads which affect bearing because of working situation and the other loads are due to defect of bearing such as surface defects, unbalancing, etc. According to the studies of Qiu et al., 2002, bearing system can be simplified as single-dof systems as shown in figure 1.

In this model, the stiffness and damping of system have two parts: undamaged part and damage part. Undamaged part is the part of bearing which is remain safe during test running life and damage part is the part of bearing which is finally cause bearing break down. According to the fracture mechanics, high cycle fatigue is the main reason of bearing failure and during bearing life the two phase of crack (initiation and propagation) are happened. Damage part of bearing in this model is the presumed crack which finally leads to failure and its stiffness reduced during the working life. The total stiffness and total damping of bearing system is summation of stiffness and damping of damaged part and undamaged part, respectively,  $= K_u + K_d$  &  $C = C_u + C_d$ . In this equation u denotes undamaged part and d denotes damaged part.

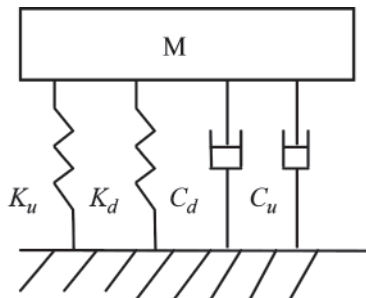


Fig. 1. The dynamic model of bearing system

Because of rotating nature of bearings the forces which are affected on bearing systems are periodic, and we call them  $F(t)$ . Expanding  $F(t)$  by Fourier transform, the acceleration response of system can be obtained as:

$$\ddot{x} = \sum_i \frac{-\Omega_i^2 F_i \sin(\Omega_i t + \alpha_i)}{\sqrt{(K - M\Omega_i^2)^2 + (C\Omega_i)^2}} \quad (1)$$

where:

$\Omega_i$  – the frequency of the  $i$ th harmonic excitation  
 $F_i, \alpha_i$  – the amplitude and phase angle between  $F_i$  and  $x$ .

The amplitude of acceleration response at the natural frequency is:

$$A_n = \frac{\omega_n F_n}{C} \quad (2)$$

Presume proportional damping for system,  $C = aM + bK$  and considering the nature of presumed system, such as no mass enters and no mass comes out of system and the mass of system is constant, then  $a = 0$ . Consequently, damping of system is only a proportion of the system stiffness. With this presumption, equation (2) can be written as:

$$A_n = \frac{c}{\sqrt{K}} \quad (3)$$

where:

$c = F_n / (b\sqrt{M})$  – a parameter which is depend on characteristics of system.

### DAMAGE MECHANICS MODEL OF BEARING

Under the definition of the reference volume element (RVE) in damage mechanics of material [12], and previous studies in this field (Qiu et al., 2002), a damage factor can be generally defined as:

$$D = d \left( 1 - \frac{K_d}{K_{d0}} \right) \quad (4)$$

Where  $d$  is scaling factor [ $d = K_{d0} / (K_{d0} - K_{df})$ ] and  $K_d$  is the stiffness of damage part which is reduce during the working life of bearing and initial and final value of it are  $K_{d0}$  and  $K_{df}$  respectively. Based on damage mechanics, Damage curve approach can be used to relate the running life of bearing with damage factor as below

$$D = \left( \frac{N}{N_f} \right)^q \quad (5)$$

where:

$N$  – the running cycles,  
 $N_f$  – the failure lifetime in cycles,  
 $q$  – a material and structure-dependent factor.

From equations (4) and (5), it can be shown that:

$$\frac{K_d}{K_{d0}} = 1 - \frac{1}{d} \left( \frac{N}{N_f} \right)^q \quad (6)$$

On the other hand, the equation (3) can be written as below:

$$\left( \frac{A_0}{A_d} \right)^2 = \frac{c_0}{c_d} \left( \frac{K_d + K_u}{K_{d0} + K_u} \right) \quad (7)$$

Where  $A_d$  and  $A_0$  are the amplitudes of acceleration response at the natural frequency under damaged and initial conditions, respectively, and  $c_d$  and  $c_0$  stand for coefficient  $c$  in equation (3) under damaged and initial conditions, respectively. Combination of equations (6) and (7), the final equation for estimation of the failure life is obtained as below:

$$\begin{aligned} \left( \frac{A_0}{A_d} \right)^2 &= \frac{c_0}{c_d} \left( 1 - \left( \frac{K_{d0}}{d(K_{d0} + K_u)} \right) \left( \frac{N}{N_f} \right)^q \right) = \\ &= \alpha \left( 1 - \beta \left( \frac{N}{N_f} \right)^q \right) \end{aligned} \quad (8)$$

Where  $\alpha, \hat{\alpha}$  and  $q$  are the coefficients depending on the operating condition, materials and structure of the system. Subscript  $d$  denotes the damaged condition, subscript  $0$  denotes the initial condition and subscript  $f$  denotes the final life time of bearing. For bearings, the failure time represents the time when the vibration signals tend to be infinite. In equation (8),  $\hat{\alpha}$  and  $q$  are constant for each bearing then with substitution  $N_{fe} = \frac{N_f}{q/\beta}$ , equation (8) can be written as below:

$$\left(\frac{A_0}{A_d}\right)^2 = \alpha \left(1 - \left(\frac{N}{N_{fe}}\right)^q\right) \quad (9)$$

It is obvious that if vibration signal tends to be infinite then  $N$  will tend to  $N_{fe}$ . According to equation (9), obviously if unknown parameters,  $\alpha$  and  $q$  be determined, and amplitude of acceleration response at any time of useful life of bearing be measured, then the lifetime of bearing system can be calculated during running life of bearing. To determine the unknown parameters, Recursive Least Square (RLS) parameter estimation algorithm can be used. Following, an experimental test rig is designed to validate the theoretical equation. Using RLS algorithm and experimental data, first the unknown parameters are identified and then accuracy of estimated life of bearing is investigated.

### EXPERIMENTAL TEST RIG

For prognosis bearing life time an experiment test rig is used. The experimental test rig has two parts, electrical and mechanical parts. The electrical part is data acquisition system which is used to acquire the bearing vibration signals. The mechanical part of experimental test rig is shown in Fig. 2. Two supporting bearings, shaft, electromotor and main bearing test are segments of mechanical part of test rig. The shaft was driven by an electromotor with a speed controller.

Supporting bearings are self-alignment spherical roller bearing 22311EXK. These bearings can tolerate the fatigue stresses during fatigue test of bearing and would not fail during the experiment. The main bearing which is studied is a self-alignment ball bearing 1206C3. Defects on inner race and defects on outer race are main defects of this type of bearing, so both of these defects are studied. The operating conditions of the experiment are: shaft speed 1500 rpm and radial load is equal to 9 kN.

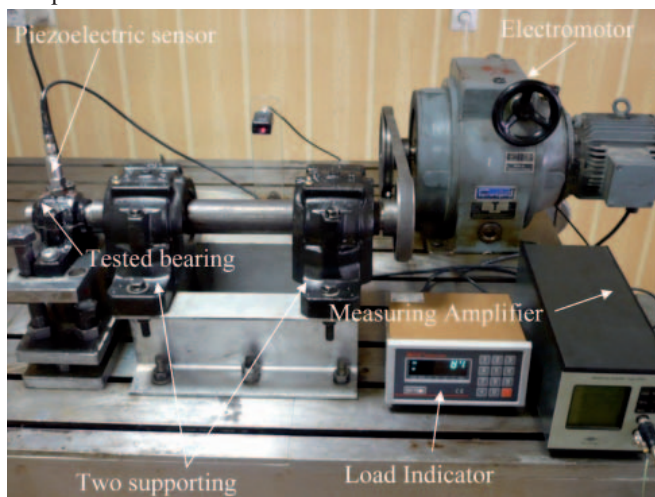


Fig. 2. Experiment test rig

The radial load which is applied to the tested bearing is measured by a load-cell (the load-cell is connected to load indicator which shows the value of load). The manufacturer of Load-cell and load indicator is Bongshin Company, load-cell model is DBBP and load indicator model is BS-7220. In Fig. 3 the loading configuration is shown. As shown in this figure, the loading configuration consists of a lower metal plate (thickness = 20 mm), upper metal plate (thickness = 20 mm), load-cell, 4 machine bolts (M24) and tested bearing housing. In Fig. 3 these parts are shown.

According to Fig. 4, by screwing the nut of 4 machine bolts the lower plate goes down and consequently the load-cell which

is placed between two plates will be tensioned. The tension force leads to a radial force on bearing by bearing housing. In Fig. 4 the radial force is shown. The vibration signal will be measured by piezoelectric sensor. The manufacturer of sensor is ENDEVCO Company and the model of sensor is 2235C. The signal amplifier is made by Brüel & Kjær and its model is 2525. Moreover, AD convertor is made by ADVANTECH and its model is USB4711. In this experiment acceleration of tested bearing is measured.

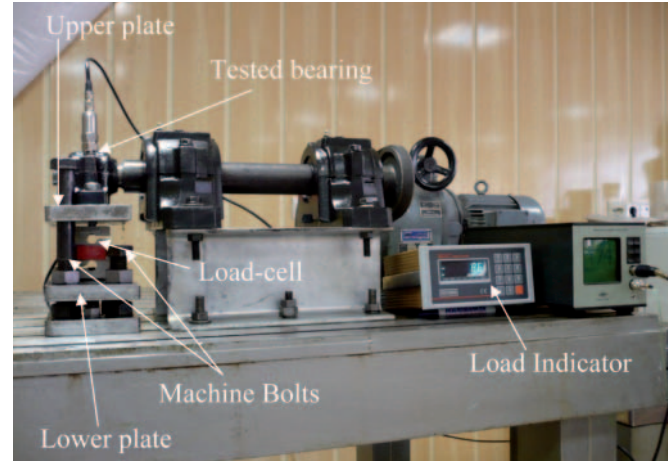


Fig. 3. Loading Configuration

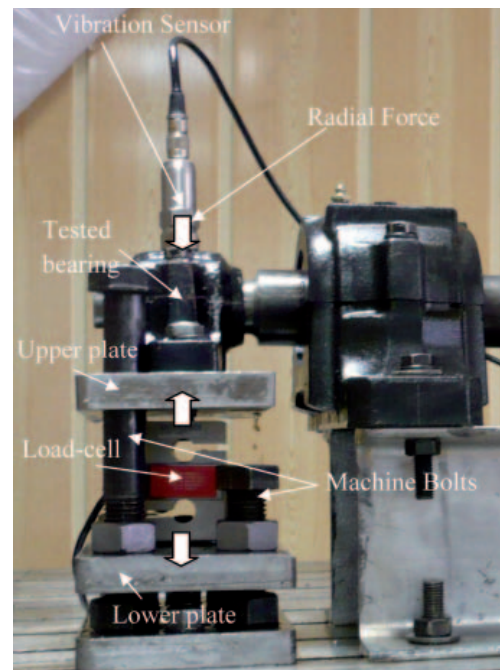


Fig. 4. Loading on tested bearing

### EXPERIMENTAL RESULT ANALYSIS

As mentioned earlier, the equation for estimation of remaining life of bearing has two unknown parameters which must be defined with RLS algorithm. For this reason four primary tests are carried out to calculate these parameters. In test 1 and 2, defect is on outer race and in test 3 and 4 the defect is on inner race of the bearing. After primary tests, the unknown parameters are determined. Equation (9) is rewritten for both defects on the outer race and  $t$  on the inner race, respectively, as follows:

$$\left(\frac{A_{n0}}{A_{nd}}\right)^2 = 1.25 \left(1 - \left(\frac{N}{N_{fe}}\right)^6\right) \quad (10)$$

$$\left(\frac{A_{n0}}{A_{nd}}\right)^2 = 0.9 \left(1 - \left(\frac{N}{N_{fe}}\right)^6\right) \quad (11)$$

Now, two tests are carried out to evaluate the precision of equations (10) and (11). In test 5, defect is on the outer race and in test 6, defect is on the inner race. Equations (10) and (11) can be written as below:

$$N_{fe} = \frac{N}{\sqrt[6]{1 - \frac{\left(\frac{A_{n0}}{A_{nd}}\right)^2}{1.25}}} \quad (12)$$

$$N_{fe} = \frac{N}{\sqrt[6]{1 - \frac{\left(\frac{A_{n0}}{A_{nd}}\right)^2}{0.9}}} \quad (13)$$

In tests 5 and 6, if the acceleration amplitude at natural frequency of each cycle of running life of bearing be calculated and consequently ratio of calculated amplitude acceleration to the initial amplitude  $\left(\frac{A_{n0}}{A_{nd}}\right)^2$  determined, then the remaining life of bearing can be estimated.

Before estimating the life of bearing in tests 5 and 6, the rating life of bearing evaluated. The theoretical life of bearing calculated according to ISO 281:1990 by following equation:

$$L_{10} = \left(\frac{C}{P}\right)^{10/3} \quad (14)$$

The C parameter for tested bearing is equal 15600 N and as mentioned previously the P value is equal 9000 N; consequently, the  $L_{10}$  equals to  $6.25 \times 10^6$  revolutions. The obtained estimations of life of bearings are shown in figures (5) and (6). In figures (7) and (8), error percentage of the estimated life in tests 5 and 6 are shown.

As shown in figures (7) and (8), the final life of bearing estimated precisely during running of bearing. In test 5, during 31 percent of last running life of bearing the error of estimated life of bearing is below 15 percent. Moreover, in test 6, during 37 percent of last running life of bearing the error of the estimated life of bearing is below 15 percent. The final estimation is more precise, error percentage of final estimation of life of test 5 is 0.36 and for test 6 the final error is 1.17 percent. Consequently, damage curve approach can be used for bearing prognostic in an online manner.

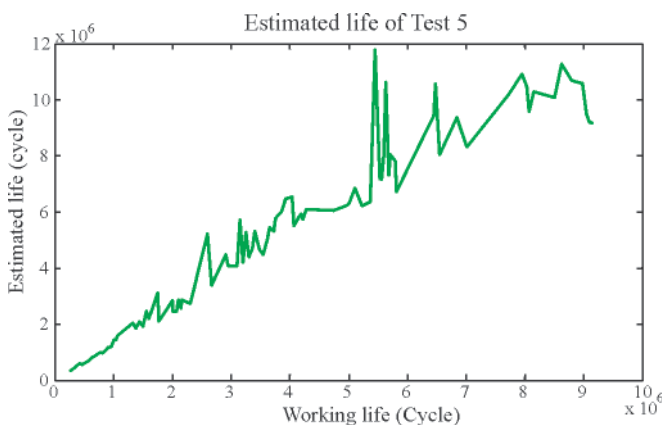


Fig. 5. Estimated life of the ball bearing in Test 5 (defect in outer race)

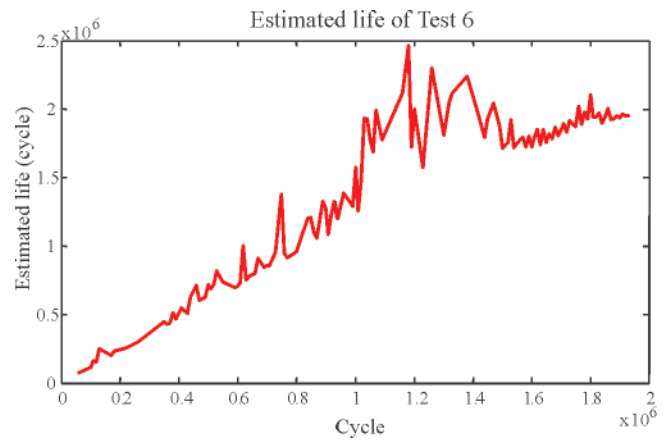


Fig. 6. Estimated life of the ball bearing in Test 6 (defect in inner race)

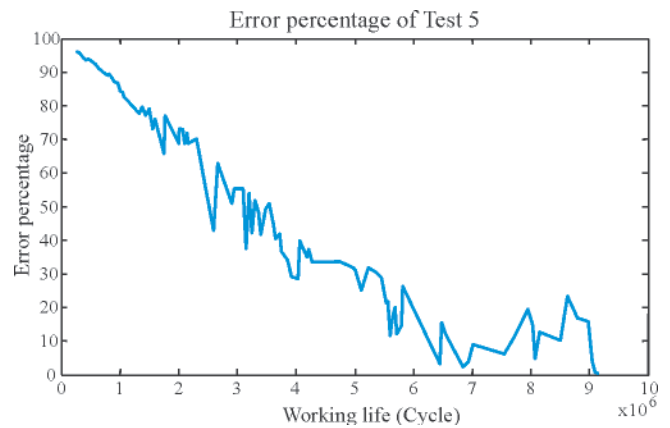


Fig. 7. Error percentage of estimated life in Test 5



Fig. 8. Error percentage of estimated life in Test 6

## CONCLUSION

This paper is used the damage curve approach to estimate the remaining life of bearing. Using damage mechanics and single-dof model for bearing system, the appropriate equation for estimation of final life of bearing is developed. Experiments are carried out to calculate the unknown parameters of theoretical equations by RLS algorithm during four primary tests. After primary tests, the unknown parameters determined. Finally, two tests are carried out to evaluate the precision of equations, and the final life of bearings estimated precisely during running of bearing (defect on inner race and defect on outer race). During last third of running life of bearing the error percent of estimated life is below 15%. Consequently, the damage curve approach can be used to estimate the final

life of bearing in online condition monitoring program. Doing this, firstly, using the DCA and RLS algorithm the predictive mathematical model must be made and then, for the other bearings we can use this mathematical model to estimate the remaining life of bearing precisely.

## BIBLIOGRAPHY

1. Qui H., Lee J., Yu G.: *Robust performance degradation assessment methods for enhanced rolling element bearing prognostics*, Advanced Engineering Informatics, Vol. 17 No. (3-4), pp.127-140, 2003
2. Zhao Y., Zhang G., Du J., Wang G., Vachsevanos G.: *Development of distributed bearing health monitoring and assessing system*, 8<sup>th</sup> International conference on control, Automation, Robotics and Vision, pp. 474-478, 2004
3. Mba D., Al-Ghamd A.M.: *A comparative experimental study on the use of acoustic emission and vibration analysis for bearing defect identification and estimation of defect size*, Journal of mechanical systems and signal processing, Vol. 20 No. 7, pp. 1537-1571, 2006
4. Da Silva V., Fujimoto R.Y., Padovese L.R.: *Rolling bearing fault diagnostic system using fuzzy logic*, 10<sup>th</sup> IEEE International Conference on Fuzzy systems, Vol 3 No. 3, pp. 816-819, 2001
5. Artes M., Del Castillo L. and Perez J.: *Failure prevention and diagnosis in machine elements using cluster*, proceeding of the tenth international congress on sound and vibration, pp. 1197-1203, 2003
6. Gebraeel N., Lawley M., Liu R., Parmeshwaran V.: *Residual life predictions from vibration-based degradation signals: a neural network approach*, IEEE Transactions on Industrial Electronics, Vol. 51 No. 3, pp. 694-700, 2004
7. Liu T., Ordukhani F., Dipak J.: *Monitoring and diagnosis of roller bearing conditions using neural networks and soft computing*, International journal of knowledge-based and intelligent engineering systems, Vol. 9 No. 2, pp. 149-157, 2005
8. Li Y., Billington S., Zhang C., Kurfess T., Danyluk S., Liang S.: *Adaptive prognostics for rolling element bearing condition*, Journal of mechanical systems and signal processing, Vol. 13 No. 1, pp. 103-113, 1999
9. Li Y., Billington S., Zhang C., Kurfess T., Danyluk S., Liang S.: *Dynamic prognostic prediction of defect propagation on rolling element bearings*, Tribology Transactions, Vol. 42 No. 2, pp. 385-392, 1999
10. Qiu J., Seth B. B., Liang S., Zhang C.: *Damage mechanics approach for bearing lifetime prognostics*, Journal of mechanical systems and signal processing, Vol. 16 No. 5, pp. 817-829, 2002
11. Li Y., Kurfess T., Liang S.: *Stochastic prognostics for rolling element bearings*, Journal of mechanical systems and signal processing, Vol. 14 No. 5, pp. 747-762, 2000
12. Lemaitre J., Desmorat R.: *Engineering Damage Mechanics*, Springer-verlag, Berlin, 2005.

---

## CONTACT WITH THE AUTHORS

H. Mehdigholi, Ph. D.  
H. Mirzaei Rafsanjani, Ph. D.  
Behzad, Mehdi, Prof.  
Department of Mechanical Engineering,  
Sharif University of Technology  
11155-9567, Azadi Avenue,  
Tehran, IRAN  
email: m\_behzad@sharif.edu



The Ship Handling Research and Training Centre at Ilawa is owned by the Foundation for Safety of Navigation and Environment Protection, which is a joint venture between the Gdynia Maritime University, the Gdansk University of Technology and the City of Ilawa.

**Two main fields of activity of the Foundation are:**

- Training on ship handling. Since 1980 more than 2500 ship masters and pilots from 35 countries were trained at Ilawa Centre. The Foundation for Safety of Navigation and Environment Protection, being non-profit organisation is reinvesting all spare funds in new facilities and each year to the existing facilities new models and new training areas were added. Existing training models each year are also modernised, that's why at present the Centre represents a modern facility perfectly capable to perform training on ship handling of shipmasters, pilots and tug masters.
- Research on ship's manoeuvrability. Many experimental and theoretical research programmes covering different problems of manoeuvrability (including human effect, harbour and waterway design) are successfully realised at the Centre.

The Foundation possesses ISO 9001 quality certificate.

**Why training on ship handling?**

The safe handling of ships depends on many factors - on ship's manoeuvring characteristics, human factor (operator experience and skill, his behaviour in stressed situation, etc.), actual environmental conditions, and degree of water area restriction.

Results of analysis of CRG (collisions, rammings and groundings) casualties show that in one third of all the human error is involved, and the same amount of CRG casualties is attributed to the poor controllability of ships. Training on ship handling is largely recommended by IMO as one of the most effective method for improving the safety at sea. The goal of the above training is to gain theoretical and practical knowledge on ship handling in a wide number of different situations met in practice at sea.

For further information please contact:

**The Foundation for Safety of Navigation and Environment Protection**

Head office:  
36, Chrzanowskiego Street  
80-278 GDAŃSK, POLAND  
tel./fax: +48 (0) 58 341 59 19

Ship Handling Centre:  
14-200 ILAWA-KAMIONKA, POLAND  
tel./fax: +48 (0) 89 648 74 90  
e-mail: office@ilawashiphandling.com.pl  
e-mail: office@portilawa.com

## GDANSK UNIVERSITY OF TECHNOLOGY

is the oldest and largest scientific and technological academic institution in the Pomeranian region. The history of Gdansk University of Technology is marked by two basic dates, namely: October 6, 1904 and May 24, 1945.

The first date is connected with the beginning of the technical education at academic level in Gdansk. The second date is connected with establishing of Gdansk University of Technology, Polish state academic university. Gdansk University of Technology employ 2,500 staff, 1,200 whom are academics. The number of students approximates 20,000, most of them studying full-time. Their career choices vary from Architecture to Business and Management, from Mathematics and Computer Science to Biotechnology and Environmental Engineering, from Applied Chemistry to Geodesics and Transport, from Ocean Engineering to Mechanical Engineering and Ship Technology, from Civil Engineering to Telecommunication, Electrical and Control Engineering. Their life goals, however, are much the same - to meet the challenge of the changing world. The educational opportunities offered by our faculties are much wider than those of other Polish Technical universities, and the scientific research areas include all of 21st Century technology. We are one of the best schools in Poland and one of the best known schools in Europe – one that educates specialists excelling in the programming technology and computer methods used in solving complicated scientific, engineering, organizational and economic problems.

### THE FACULTY OF OCEAN ENGINEERING AND SHIP TECHNOLOGY

The Faculty of Ocean Engineering and Ship Technology (FOEST) as the only faculty in Poland since the beginning of 1945 has continuously been educating engineers and doctors in the field of Naval Architecture and Marine Technology.

The educational and training activities of FOEST are supported by cooperation with Polish and foreign universities, membership in different international organizations and associations, as well as participation in scientific conferences and symposia. Hosting young scientists and students from different countries is also a usual practice in FOEST.


The activities of Faculty departments are related to: mechanics and strength of structures, hydromechanics, manufacturing, materials and system quality, power plants, equipment and systems of automatic control, mostly in shipbuilding, marine engineering and energetic systems.

FOEST is a member of such organizations like WEGEMT; The Association of Polish Maritime Industries and the co-operation between Nordic Maritime Universities and Det Norske Veritas. The intensive teaching is complemented and supported by extensive research activities, the core of which is performed in close collaboration between FOEST staff and industry. We take great care to ensure that the applied research meet both the long term and short term needs of Polish maritime industry. FOEST collaborates with almost all Polish shipyards. Close links are maintained with other research organizations and research institutions supporting the Polish maritime industry, such as Ship Design and Research Centre and Polish Register of Shipping, where several members of the Faculty are also members of the Technical Board.

The Faculty of Ocean Engineering and Ship Technology is a unique academic structure, which possesses numerous highly qualified and experienced staff in all above mentioned specific research areas. Moreover, the staff is used to effective co-operation and exchange of ideas between specialists of different detailed areas. This enables a more integrated and comprehensive treatment of research and practical problems encountered in such a complicated field of activity as naval architecture, shipbuilding and marine engineering.


The staff of the Faculty has strong international links worldwide, being members or cooperating with international organizations like International Maritime Organization IMO, International Towing Tank Conference ITTC, International Ship and Offshore Structures Congress ISSC, International Conference on Practical Design of Ship and other floating Structures PRADS just to name a few.

GDANSK UNIVERSITY OF TECHNOLOGY  
Faculty of Ocean Engineering and Ship Technology  
11/12 Narutowicza Street, 80-233 Gdansk, Poland  
Tel (+48) 58 347 1548 ; Fax (+48) 58 341 4712  
e-mail: sekoce@pg.gda.pl



# Gdansk University of Technology

## Faculty of Ocean Engineering and Ship Technology



[www.oce.pg.gda.pl](http://www.oce.pg.gda.pl)